INVESTIGATION OF METHODS FOR DETECTING NEEDLE INSERTION INTO BLOOD VESSELS

by

Ehsan Qaium

BS in Mechanical Engineering, Virginia Tech, 2012

Submitted to the Graduate Faculty of

the Swanson School of Engineering in partial fulfillment

of the requirements for the degree of

Master of Science in Mechanical Engineering

University of Pittsburgh

2018

UNIVERSITY OF PITTSBURGH

SWANSON SCHOOL OF ENGINEERING

This thesis was presented

by

Ehsan Bin Qaium

It was defended on

April 19,2018

and approved by

William Clark, PhD, Professor

Jeffrey Vipperman, PhD, Professor

Cameron Dezfulian, MD, Associate Professor

Thesis Advisor: William Clark, PhD, Professor

INVESTIGATION OF METHODS FOR DETECTING

NEEDLE INSERTION INTO BLOOD VESSELS

Ehsan Qaium, M.S.

University of Pittsburgh, 2018

Peripheral intravenous IV (pIV) placement is the mainstay for providing therapies in modern medicine. Although common, approximately 107 million difficult pIV placements each year require multiple attempts to establish IV access. Delays in establishing IV access lead to increased patient pain, delayed administration of life saving medicine, and increased cost to the institution. Current solutions involve using visual vein finders, ultrasounds and a central line if peripheral IV insertion attempts fail. The objective of this study was to investigate methods by which entry into a blood vessel could be detected, and to design and test a novel medical device that increases the likelihood of successful pIV placement on the first attempt.

Two types of measurement methods (static and transient) were investigated in this study. Static measurement involved measurements performed with a multimeter and a Wheatstone bridge. The multimeter measurement was unsuccessful due to the effect of polarization. The results from the Wheatstone bridge produced a separation that was less than desired for accurate measurement. Thus the experiment was repeated with a transient measurement method utilizing the RC time constant of the tissue and an associated electrical circuit. The measured tissue

resistance values using this method were found to be much more in line with those previously reported in the literature.

Further modifications of the transient measurement system were developed and tested to improve discernment between different types of tissue and to reduce the necessary applied current. The results showed that fat and plasma-Lyte A (a surrogate for blood) could be detected using the methods, leading the way for its use in a practical vessel entry detection system in a clinical setting.

TABLE OF CONTENTS

LIST OF TABLES

LIST OF FIGURES

PREFACE

This thesis has been written to fulfill the graduation requirement of Swanson School of Engineering. I have worked on this research project since July 2016. The research goal and questions were formulated together with my advisor Dr. William Clark.

I would like to thank my advisor Dr. Clark for his excellent guidance and support during the course of my research. I would also like to thank Dr. Cameron Dezfulian for being a treasure trove of medical knowledge and for his support and guidance throughout this project. Jeff Speakman, whose help and suggestions played a pivotal part in prototype manufacturing. Matt Criado whose help with electrical circuits was crucial to the success of this project, and Vince Melillo for helping to get the project started.

Ehsan Qaium

Pittsburgh, March 7, 2018

1.0 INTRODUCTION

In modern medicine, when a patient is admitted to the hospital one of the most common procedures performed is the placement of a peripheral intravenous line (PIV). A PIV is a thin bendable plastic tube (catheter; Figure **1-1**) that is inserted into a patient's peripheral vein (e.g. a vein in the arm) to facilitate the delivery of medication.

Figure 1-1: Standard catheters used by most healthcare providers. The sizes range from 14 (left) – 24 (right) gauge.

The standard method for IV placement consists of four steps (**Figure 1-2**) which are described below (Peter Switakowski (2003)).

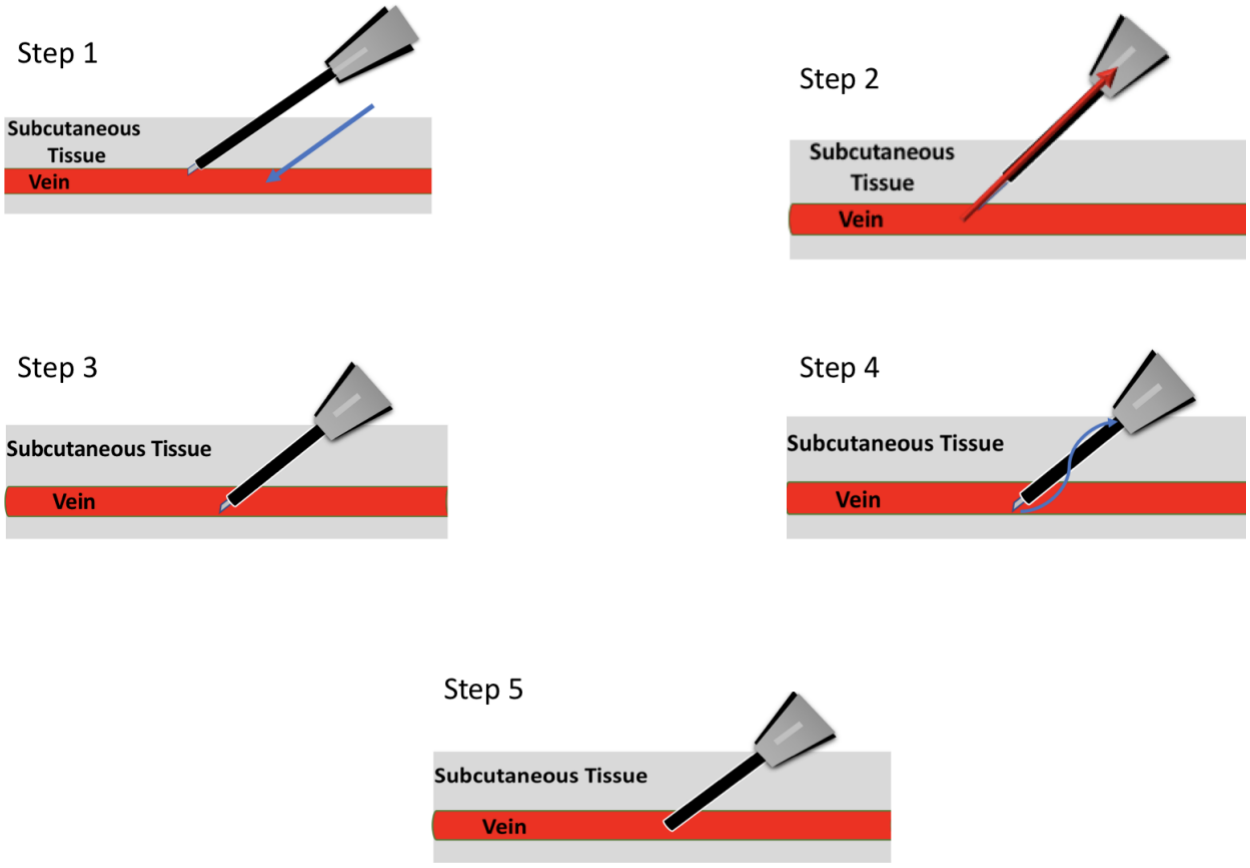

Figure 1-2: Standard technique for peripheral intravenous line (PIV) placement. Step 1) The needle is inserted through the skin into the vein. Step 2) The user watches for blood return (often called the "flash") in the clear chamber of the needle, "the hub", indicating vessel entry. Step 3) The catheter is advanced into the vein. Step 4) Once vessel entry has been detected, the needle is withdrawn. Step 5) The catheter is left in the vein taped in place allowing for the delivery of therapy.

Step 1) The needle is inserted through the skin into the vein.

Step 2) The user watches for blood return (often called the “flash”) in the clear chamber of the needle “the hub” indicating vessel entry.

Step 3) The catheter is advanced into the vein.

Step 4) Once vessel entry has been detected, the needle is withdrawn.

Step 5) The catheter is left in the vein taped in place allowing for the delivery of therapy.

1.1 BACKGROUND AND MOTIVATION

Although routine, PIV placement has a high rate of first-time failures. A study by Lapostolle et al., 2007 found that approximately 26% of the patients undergoing IV placement in an emergency setting require more than one attempt to establish vein access (Lapostolle et al., 2007). Brannam et al., 2004 found that most emergency nurses attempted between one and three blind IV sticks (IV placement attempts without the aid of other technology) (mean 2.2) before trying alternate methods (Brannam, Blaivas, Lyon, & Flake, 2004).

The standard method for IV placements (Figure **1-2**) is reliant upon visualizing a flash of blood into the hub of the catheter. Normal peripheral venous pressure is typically 2-3mm Hg. In difficult patients who are experiencing shock or dehydration, the venous pressure is typically much lower. As a result, the indication from the flash is delayed and many users continue to advance the needle resulting in a "blown vein".

In a standard needle catheter configuration (Figure **1-1**) the catheter is slightly larger than the needle diameter and set further back from the tip of the needle. Thus, it is possible to visualize a flash without the needle fully penetrating the lumen of the vein. When this occurs, the catheter pushes the vein away rather than sliding in over the needle, resulting in a failed IV attempt.

Furthermore, the root causes of first-time IV failures were primarily attributed to obesity, edema, IV drug abuse, renal drug failure, sickle cell anemia and patients with a history of difficult access (Lapostolle et al. (2007); Brannam et al. (2004);Fields, Piela, Au, and Ku (2014); Sebbane et al. (2013); Joing et al. (2012); Gregg, Murthi, Sisley, Stein, and Scalea (2010)). Repeated failures lead to lost time for the hospitals, delays in administering therapies and increased pain for the patient.

To quantify the amount of pain patients experience due to multiple blind attempts, Fields, Piela and Ku 2014 performed an observational study on 729 conscious patients undergoing IV placement.(Fields, Piela, and Ku (2014)) For each subject, the number of IV attempts and the overall patient satisfaction (scale of 1-10) was recorded as part of the study. A ten point-visual analog scale (VAS) was used to quantify the amount of pain a patient experienced while undergoing IV placement. A visual analog scale (Figure ***1-3***) is a measurement instrument used to quantify values that cannot easily be directly measured (Gallagher, Liebman, and Bijur (2001)).

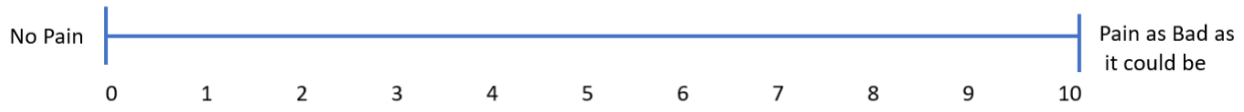

Figure 1-3: Visual analog scale (VAS) employed by physicians to quantify values that cannot easily be measured. Figure re-drawn from Haefeli and Elfering (2006).

When compared to patients with first-time success the results showed that patients who underwent two and three IV placement attempts experienced a pain increase of 1.9 and 3.3 points respectively in the visual analog scale. Furthermore, the patients who endured multiple attempts had a lower overall satisfaction (8.8 vs. 8.4) than those who had first-time success in IV placement (Fields, Piela, and Ku (2014)). The increase in pain level is significant because of a study by Gallagher et al., 2001 determined that an increase in the patient pain level of 1.3 points or higher on the visual analog scale is considered to be clinically significant (Gallagher et al. (2001)).

Abolfotouh et al.,2014 performed an observational study on 359 adult patients in an attempt to determine the type of IV related complications that occur most often (Abolfotouh,

Salam, Bani-Mustafa, White, and Balkhy (2014)). During the study, each patient enrolled was observed by hospital staff and any medical complications related to PIV placement were recorded every twelve hours. Of the 359 patients enrolled, 141 (39.3%) were found to have catheter related complications (Abolfotouh et al. (2014)). These incidents were attributed to phlebitis (inflammation of the vein due to blood clotting (Martin (2010)), pain, infiltration **(**medication leaking to surrounding tissue (Hadaway (2007)), and catheter dislodgement (Abolfotouh et al. (2014)).

Furthermore, results from the study showed a dose-response relationship between the frequency of insertions and incidents of complication (Figure **1-4**). Of the 134 patients who underwent one insertion, 22.39% experienced IV related complications; this rate increased to 50% when compared to those who underwent three insertions and 90% with six insertions (Abolfotouh et al. (2014)).

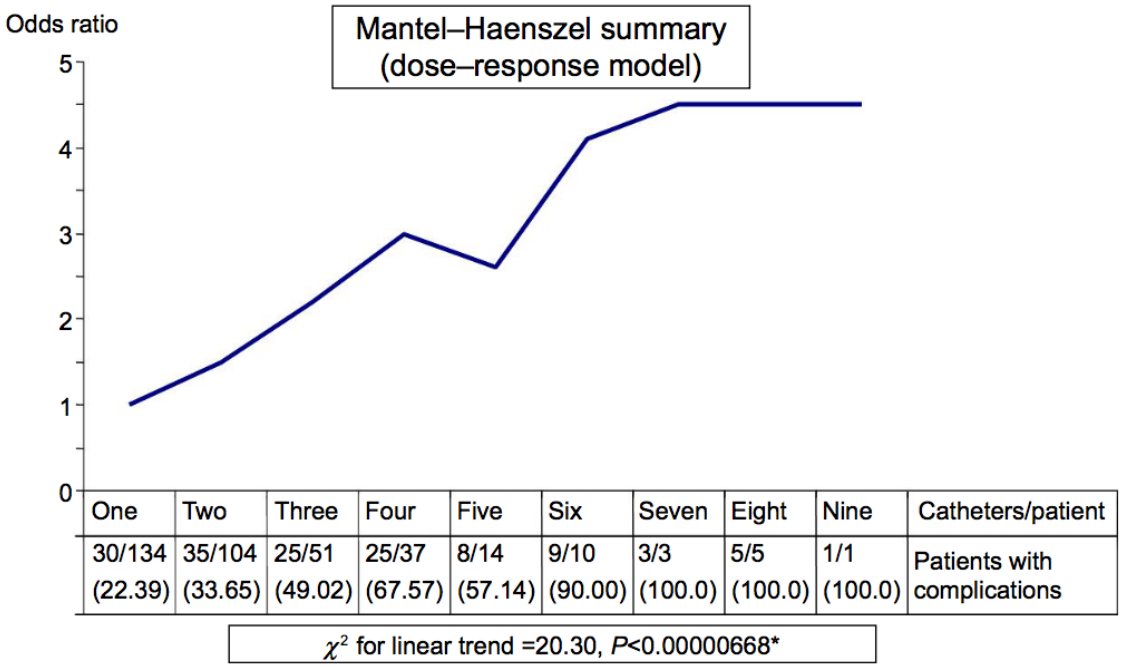

Figure 1-4: Relationship between the frequency of insertions per individual patient and incidence of complications (Numbers in parentheses represent percentages and *indicates significant positive dose-response relationship). Figure from Abolfotouh et al. (2014).

Although the data showed a relationship between the number of insertion attempts and catheter related complications, it should be noted that the study did not mention whether these multiple attempts were due to failed first time IV placements (focus of this thesis) or a patient illness. Patients illness can limit the durability of the catheter leading to additional insertion attempts.

Early identification of potential PIV related complications is crucial to avoid a catastrophic outcome. The current recommended treatment options for infiltrations range from supportive care, manual extraction of the extravasate fluid, use of dispersal agents, (i.e., saline, sodium thiosulfate) and surgical extraction as a last resort (Hadaway (2007)). IV related complications lead to longer hospital stays, increased morbidity, and higher costs for the hospital

and health insurance providers (Hadaway (2007)). When one considers that approximately 1.2 billion catheters are sold worldwide each year, (Alexandrou et al. (2015)) first time PIV placement failures in approximately 26% of the patient population represents a significant problem within the healthcare industry.

This thesis aims to address the problem of failed IV placements by investigating methods by which vein entry may be detected. The results are then used to design a novel medical device. The device consists of a modified single use catheter, a connector cable and a re-usable detector unit about the size of a smartphone. The detector unit alerts the physician to vein entry by providing visual, auditory, or a vibratory signal. The details of the methods tested and the design and bench top testing procedure are described in the chapters to follow.

In the chapters to follow, I will discuss the current solution to failed IV placement attempts by reviewing previous works that served as the inspiration for the catheter insertion device (literature review Chapter 2). Next, I will discuss various measurement methods that have been attempted (static and transient) in relation to the technique employed in this thesis, and their accompanying results (Chapter 3). Lastly, the overall system design and possible variations will be discussed (Chapter 4) followed by a summary of my research findings (Chapter 5).

2.0 LITERATURE REVIEW

In this chapter, I will introduce the background information that was used to develop the novel catheter insertion device. Section 2.1 outlines the current solutions to remedy failed PIV placement. Section 2.2 will discuss previous works on the measurement of biological tissue which contributed to the design of the current device.

2.1 CURRENT SOLUTION

Most often when repeated PIV placement attempts fail, physicians opt for a central line or midline IV to establish venous access. A central line is a large plastic tube that doctors place in the neck, chest, groin, or arm to administer medication (Gregg et al. (2010)). Most often, the Seldinger technique is employed when placing a central line. The Seldinger technique (Figure ***2-1***) comprises six steps which are described below (Busti (2015).

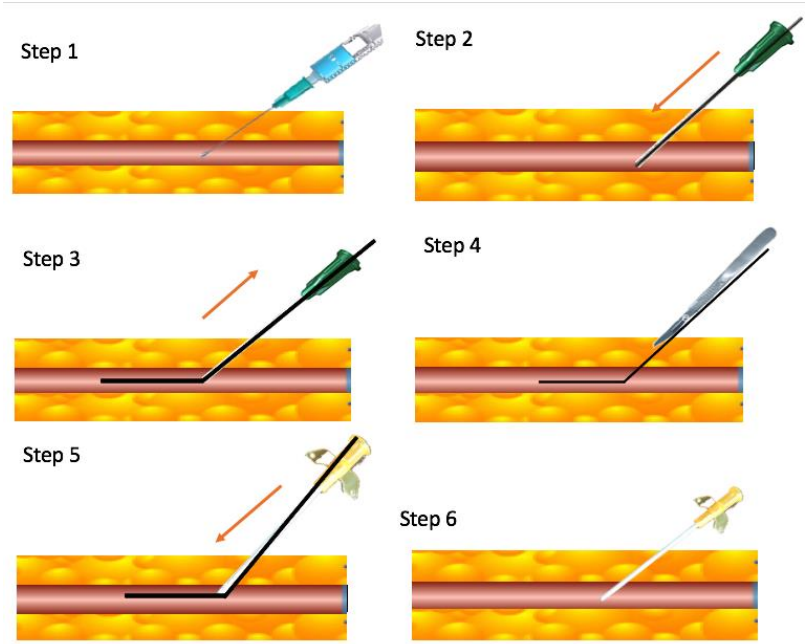

Figure 2-1: Seldinger technique (figure re-drawn from EBMconsult.com). Step 1) the needle is inserted into the skin at a 45°angle, and negative pressure is applied until blood return is visualized inside the syringe. Step 2) the needle is removed, and the guide wire is inserted. Step 3) once guidewire has been advanced to the desired length, the needle is withdrawn. Step 4) Insertion site is enlarged using a scalpel as necessary for large catheters. Step 5) while holding the guidewire, the catheter is advanced into the vein. Step 6) the guidewire is withdrawn, and blood return is sought after to verify catheter placement.

Step 1) the needle is inserted into the skin at a 45°angle, and negative pressure is applied until blood return is visualized inside the syringe.

Step 2) the syringe is removed and the guidewire is inserted into the vein through the needle.

Step 3) once guidewire has been advanced to the desired length, the needle is withdrawn while holding the guidewire.

Step 4) Using a scalpel, the Insertion site is enlarged as necessary for large catheters.

Step 5) the catheter is advanced into the vein using the guide wire.

Step 6) the guidewire is withdrawn, and blood return is sought to verify catheter placement.

The insertion of a central line requires extensive training and setup. This procedure carries additional risk to the standard PIV placement (arterial puncture, hematoma sepsis, pneumothorax, or air embolism (Cameron Dezfulian (2017);Au, Rotte, Grzybowski, Ku, and Fields (2012)) if complications were to arise. In 2002, the cost associated with a single central line-related complication was estimated to be $34,508-$56,000 per incident resulting in an annual cost of $296 million to $2.3 billion nationally (Au et al. (2012)).

To avoid the additional risks associated with central line placement, physicians and nurses turn to ultrasound to facilitate PIV placement. The ultrasound unit employs a high-frequency sound wave through the transducer to capture images inside the human body (Krans (2016)).

Brannam et al., (2004) conducted an observational study where data on IV placement by emergency department nurses was collected over a five-month period (Brannam et al. (2004)). After each procedure, the nurses completed a survey that recorded the reason for ultrasound use, the type of patient, and the associated outcome. Of the 321 surveys collected, ultrasound-guided PIV placement was found to have an 87% overall success rate in difficult patients (Brannam et al. (2004)).

In another study, Arthur et al. (2012) performed an observational study of one hundred patients who underwent ultrasound-guided PIV placement (Au et al. (2012)). The patients were followed for up to seven days to assess the effectiveness of catheter placement. Ultrasound-guided peripheral intravenous line (USGPIV) placement was initially successful in all but twelve patients; at the end of the follow-up period, a total of 15 patients required the placement of a central line. This result represented an 85% overall success rate for USGPIV in patients

classified as high risk (Au et al. (2012)). These patients were slated to undergo central line placement had USGPIV proven to be unsuccessful.

Although ultrasound-guided PIV placement is often advantageous, it is not without its drawbacks. Ultrasound imaging of needle location or vessel entry requires transvere imaging (parallel to the needle) which is technically very challenging. Thus blood return is still utilized as an important step in the placement process (Joing et al. (2012)). Gregg et al. 2010, reviewed ultrasound-guided PIV access over a six-month period between September 2007 and February 2008. Of the 148 PIV lines requested during that time, 29% of patients required multiple attempts to establish access (Gregg et al. (2010)). Additionally, in an observational study on pediatric patients by Oakley and Wong 2010, the overall success rate was 42%. The study also noted that ultrasound-guided placement took a longer time to complete vs. the standard landmark attempts (4 min vs. 2) which the authors noted may present a significant challenge in a clinical environment where time is of the essence (Oakley and Wong (2010)).

An alternative to Ultrasound guided IV placement is the use of vein finders such as VeinViewer, AccuVein, and VascuLuminator (**Figure 2-2**). Vein finders use near-infrared light to aid physicians in visualizing veins that may be invisible to the naked eye (de Graaff et al. (2013)).

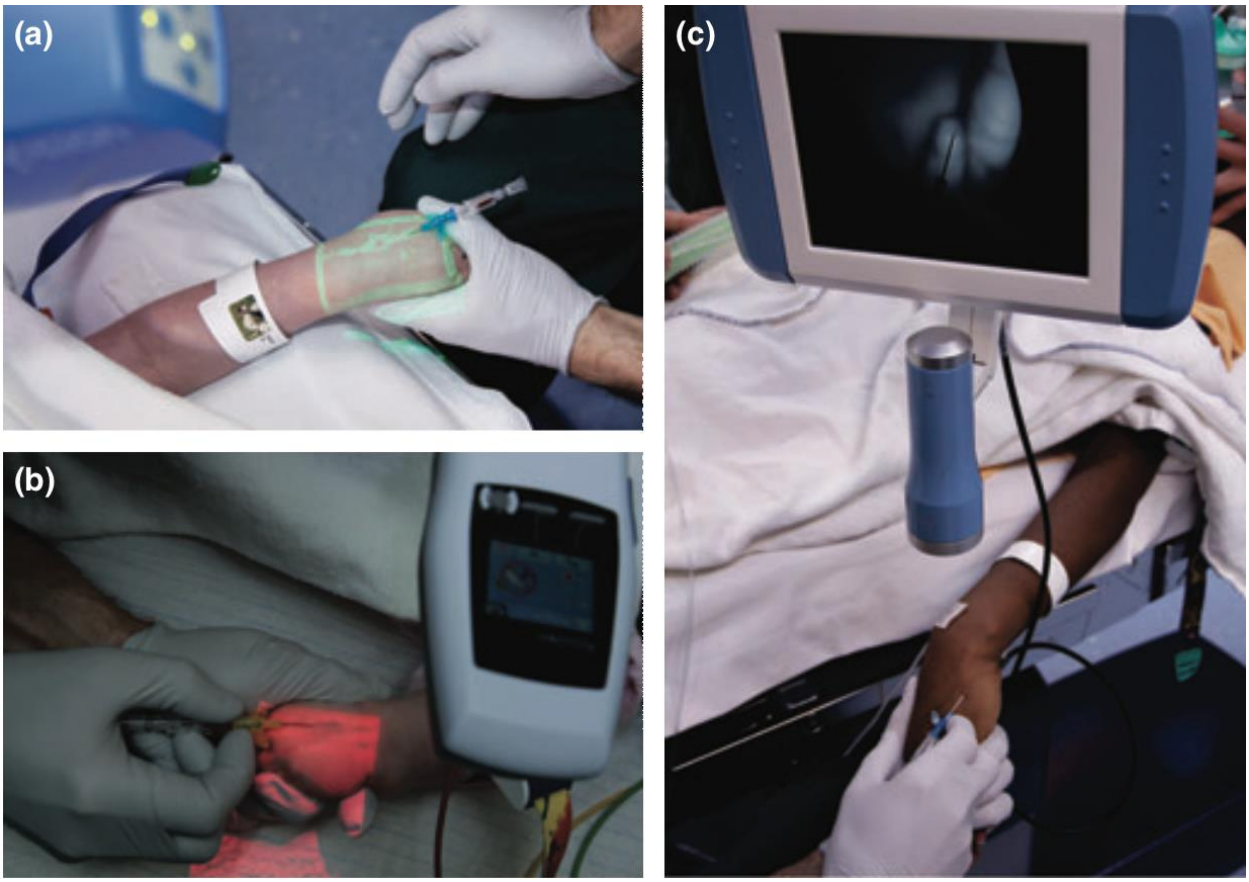

Figure 2-2: Various vein finders used to visualize veins that may be invisible to the naked eye. a) VeinViewer b) AccuVein c) VascuLuminator. Figure obtained from (de Graaff et al. (2013).

Graaf et al. 2013, performed a randomized clinical trial of children undergoing elective surgery to determine the effectiveness of VeinViewer, AccuVein(AV300), and VascuLuminator compared to a control group (de Graaff et al. (2013)). The control group had IV placements attempted by nurses without the guidance of any device. As part of the study, 1913 children under the age of 19 were enrolled and randomly assigned to one of the four study groups. Across all study groups, a suitable vein for cannulation was visible in approximately 87-96% of patients without the aid of any devices (de Graaff et al. (2013)) . The results found that within the sub groups, identifying a suitable vein for cannulation was more easily done with the VeinViewer

(enabled identification of a suitable vein in 95.3% of the cases), followed by AccuVein (94.1%) followed by VascuLuminator vision (89.1%). Within the control group, 95% of the patients had veins that could be easily identified. (de Graaff et al. (2013)). Although vein visibility was enhanced with the aid of visual vein finders, within the study the first time IV placement success ranged from 73.1%- 75%. This indicates that identifying a suitable vein for cannulation is not in and of itself sufficient for a successful catheterization.

Furthermore, the authors noted that since the infrared light was projected onto the skin, it could hamper the detection of blood return. As a result, many physicians chose to make blind IV placement attempts once a suitable vein was identified. These findings led the authors to conclude that "although vein visibility is enhanced, near-infrared devices do not improve cannulation" (de Graaff et al. (2013)).

More often, emergency medical services (EMS) staff are performing intraosseous infusion (IO) over pIV placement in out-of-hospital settings when immediate vascular access is required. (Reades, Studnek, Vandeventer, and Garrett (2011)). Intraosseous infusion is the injection of medications, or fluids into the bone marrow (Hunsaker and Hillis (2013)) . One method for establishing IO access is to employ a spring loaded IO needle gun (Figure **2-3**) which generates enough force to drive a sharp needle into the patient's bone marrow allowing for IV access to be established (Hunsaker and Hillis (2013)).

Figure 2-3: intraosseous infusion (IO) needle guns. Blue (top) is primarily used for adults while the red (bottom) is used for pediatric patients. Figure obtained from (Hunsaker and Hillis (2013)).

Since the mid-1980's the American Heart Association (AHA) and the American Academy of Pediatrics has recommended IO cannulation as a straightforward and efficient mode of establishing IV access in all patients (Hunsaker and Hillis (2013). In one documented case by Hunsaker and Hills (2013) IO placement was performed in a conscious critically ill pediatric patient to establish rapid IV access. The pain experienced by the patient was recorded to be a 6 out of 10 on the FLACC scale (method for measuring pain in children (Voepel-Lewis, Zanotti, Dammeyer, and Merkel (2010)). As a result of the great pain and temporary nature of this form of IV access, intraosseous infusion is reserved strictly for emergency situations such as cardiac arrest.

Reades et al. (2011) performed an out of hospital randomized controlled trial of adult patients experiencing cardiac arrest to determine the effectiveness of tibial intraosseous, humeral intraosseous and peripheral intravenous catheter intervention (Reades et al. (2011)). As part of

the study, 182 patients were enrolled and randomly assigned to one of the three study groups. The results showed that individuals assigned to tibial intraosseous experienced a greater first-time success (91%) than humeral intraosseous (51%) or peripheral intravenous access (43%).

Although tibial IO placement has had a high first-time success rate, the process of puncturing into the bone is extremely painful for the patient. Previous studies have shown that the pain associated with IO placement could be managed through an injection of traditional skin anesthetics such as lidocaine (Hunsaker and Hillis (2013)). Using lidocaine increases the number of needle sticks the patient undergoes, and thus increases the pain associated with the procedure. As a result, IO placement is not a long-term alternative to PIV access due to the amount of pain experienced by the patient.

Alternative attempts at pain management such as skin coolants have had mixed results. A study by Armstrong, young, and McKeown, followed 120 un-pre-medicated patients undergoing gynecological surgery to assess the effectiveness of ethyl chloride (spray on skin anesthetic) vs. lidocaine (applied via injection) (P. Armstrong (1990)). The patients were separated into three groups for this study (control, lidocaine, and ethyl chloride). The patients assessed their perceived pain level (upon anesthetic application, and one minute after the procedure) using a 10-point VAS (Figure ***1-3***). The results found that lidocaine (0.07 points), followed by ethyl chloride (.018 points) performed the best when compared with the control group (0.38 point) that followed standard IV insertion procedure (P. Armstrong (1990)). This finding led Armstrong et al. to recommend the application of ethyl chloride as a skin anesthetic before IV cannulation attempts.

In a subsequent study, Hartstein, and Barry, 2008 tested 1,1,1,3,3-Penta-flouroporopane and 1,1,1,2-tetraflouroethane (skin anesthetics with similar properties as ethyl chloride) to determine their effectiveness as a spray-on anesthetic. For this study, 96 enrolled subjects were randomly placed into two groups: control (individuals not receiving skin anesthetic) and a study group (individual receiving skin anesthetic). As with previous studies, a 10-point VAS was employed to record patients perceived pain levels. The mean pain scores in the study groups were found to be 2.7 points, and 2.8 points in the control group (Hartstein and Barry (2008)). The results left the authors unable to conclude the effectiveness of skin anesthetic in reducing perceived pain levels in patients.

In both of the studies mentioned above, the investigators opted to record the subjects' perceived pain levels after the IV placement procedure. Had the authors recorded the pain levels before and after, both studies potentially could have yielded better outcomes. Although topical skin anesthetics provide an intriguing opportunity, more studies are necessary to definitively judge their success in reducing patient's pain during PIV placement.

2.2 ALTERNATIVE SOLUTION

As mentioned earlier, PIV's are most often placed in veins located below the subcutaneous tissue. Since subcutaneous tissue is comprised of mostly fat cells (Heather Brannon (2017)), (Figure ***2-4***) an alternative approach is to measure the electrical properties of fatty tissue (acting as an insulator) vs. that of blood (acting as a conductor), to establish PIV access in difficult patients.

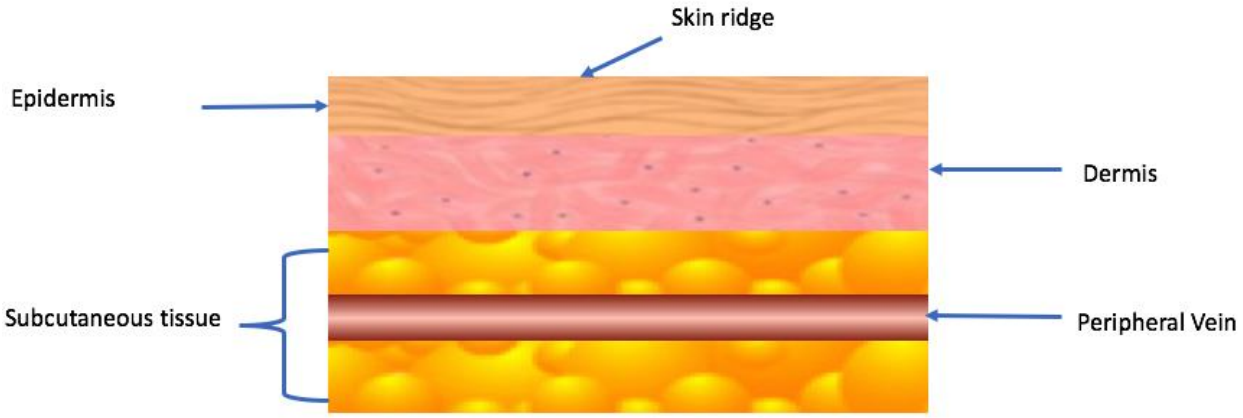

Figure 2-4: Various layers of the skin. (Figure re-drawn from thenakedchemist.com)

The idea of measuring electrical properties in the human body is not new. One of the earliest attempts at measuring the electrical properties of living tissue in situ (in its original place) on anesthetized dogs was performed by Kaufman and Johnson (1943). For their experiment, the authors employed an AC power supply, a modified Jones-Joseph bridge, and two spherical electrodes (platinum wires) to measure the specific resistance of living tissue (Kaufman and Johnston (1943)). The authors employed Mason and Weavers equation (Equation 2-1) to determine the resistance between two spherical electrodes. In the equation, a and b is the radius of the electrodes, l is electrode distance, and T is the specific resistance which was obtained experimentally for various types of tissue.

$$R = \frac{T}{4\pi}\left(\frac{1}{a} + \frac{1}{b} - \frac{2}{l}\right) \tag{2-1}$$

Before the experiment in anesthetized dogs, the electrodes were calibrated by measuring the specific resistance of known liquids such as sodium chloride, and potassium chloride. The electrodes were coated with platinum black to reduce the effects of polarization (accumulation of

ions near the electrode of the cells leading to erroneous results (Analytical (2004)). The results showed that blood has a specific resistance that ranged from 175-235 Ωcm, whereas fat has a specific resistance of 1859-2450 Ωcm. The specific resistance of vital organs such as lungs, heart, liver, and skeletal muscle varied from 744 Ωcm, 216 Ωcm, 506 Ωcm and 643 Ωcm, respectively (Analytical (2004); Kaufman and Johnston (1943)).

Burger and van Millen 1943, performed a subsequent experiment to determine the specific resistance of the human body to direct current. For their research, the authors used a four-electrode system Figure ***2-5*** consisting of two current electrodes (C_1, C_2) two voltage measurement electrodes (M_1, M_2), a 90V DC battery (B) whose current is controlled by a large resistor R_1 (Burger and Milaan (1943)). The potential difference between the two electrodes is sent to a triode voltmeter (dotted frame) which consists of a three-valve cathode follower (G), an accumulator (E), and a galvanometer (D). Once the switch (S) is closed, the change in voltage was displayed by the galvanometer.

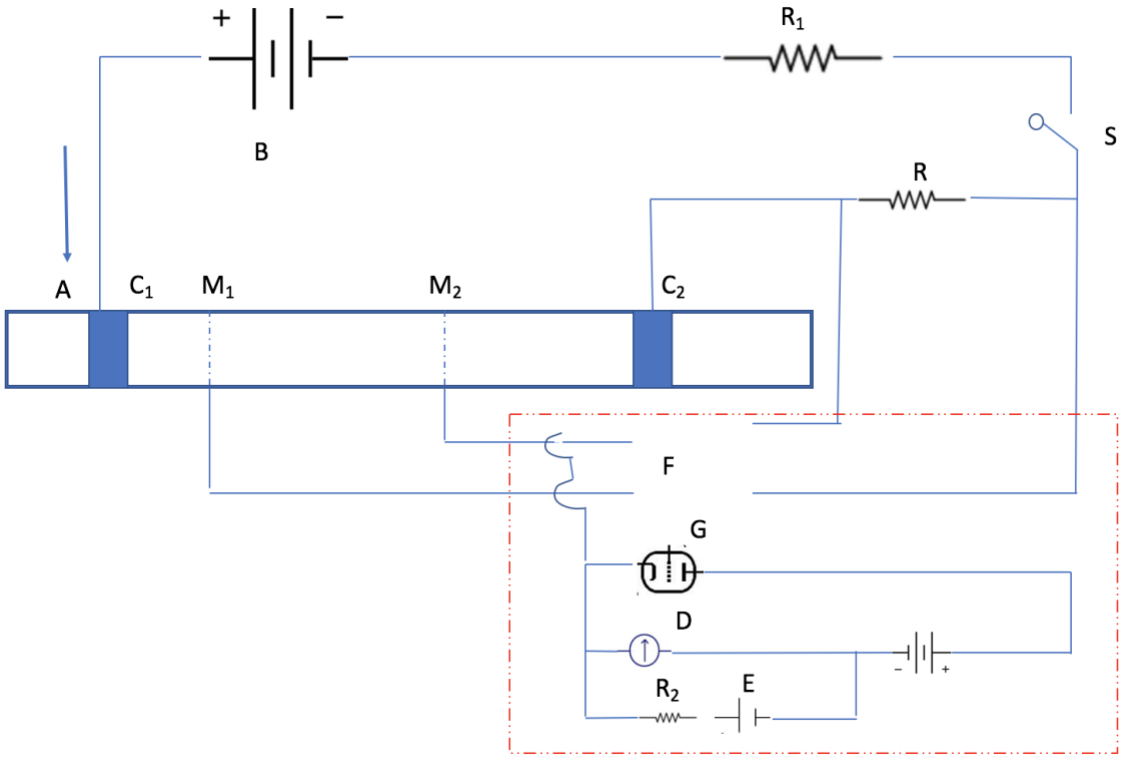

Figure 2-5: Wiring diagram for the resistance measurement in a cylindrical conductor (A) in the human body using four electrodes system in conjunction with a DC power source. (Figure re-drawn from Measurement of the Specific Resistance of the Human Body to Direct Current by Burger and van Milaan). B= battery, R= resistance, C= current electrodes, M = Measurement electrodes. The potential difference from the measurement electrodes is sent to a triode voltmeter (dotted frame) which displays the change on the galvanometer D.

The resistance in the tissue was determined by using Ohms' law (Equation 2-2). In the equation, $(v_1 - v_2)$ is the potential difference between the two measurement electrodes (M_1, M_2), as displayed by the galvanometer, i is current, and R is the resistance.

$$R = \frac{v_1 - v_2}{i} \qquad (2\text{-}2)$$

Subsequently, the resistance was used to calculate the specific resistance (Equation 2-3). In the equation, R is the resistance obtained from Equation 2-2, l is the distance between the electrodes, d is the cross section of the cylinder, and ρ is the specific resistance.

$$R = \frac{l}{d}\rho \tag{2-3}$$

Before collecting data, the measurement methods were tested using pure resistors in place of biological tissue. The results of the experiment showed that blood was found to have a specific resistance of 160 Ωcm at $37°c$; the specific resistance of a dog's torso was found to be 415 Ωcm (Burger and Milaan (1943)). When it came to muscle, the authors measured specific resistance in the transverse direction, situated at an angle with respect to the long axis of the body or organ (Martin (2010)) and longitudinal direction (cross section obtained by slicing in any plane parallel to the vertical axis (Leigh Ann Anderson (2016)) of the arm). The results showed the specific resistance in the transverse and longitudinal direction was found to be 470 Ωcm and 230 Ωcm. The difference in measurement was attributed to the current flowing along the transverse plane encountering a larger number of cells than in the longitudinal direction which subsequently resulted in a larger specific resistance value (Burger and Milaan (1943)) .

After that, Schwan and Kay 1956, performed experiments to measure the specific resistance of tissue of various organs (in situ) in living dogs. As part of the experiment, the dogs were anesthetized, and their chest cavity was opened for measurement. For this experiment, the authors employed two shielded platinum electrodes of various sizes, an AC power supply, and a calibrated Wheatstone bridge (modified Jones Joseph bridge used previously by Kaufman and Johnson) (Schwan and Kay (1956)). The frequency of the AC power supply was from 10–10,000 cycles per second (cps) to observe the effects of frequency on living tissue. The electrodes were

calibrated by measuring the specific resistance of physiological saline solution. During the test in saline solution, the authors noted a 10-15% error at ten cycles per second (cps) and a 3-5% error at 100cps. The values obtained at 10,000 cps matched with the correct specific resistance of the solution (Schwan and Kay (1956)). It was also noted that as the frequency increased, the measured value of the specific resistance of the calibrating solution decreased. During the experiment, measurements were obtained by introducing electrodes directly into the tissue of the desired measurement location. The specific resistivity of blood, lung, muscle, and heart was found to be: 100 Ωcm, 1120 Ωcm, 800Ωcm, and 965 Ωcm respectively; the specific resistance of fat was found to have a value between 1500-5000 Ωcm (Schwan and Kay (1956)).

The variation of specific resistance data between previous works by Burger and van Millen and Schwan and Kay led Burger and van Dongen 1961 to repeat the measurements on various animals (cows, humans, and rabbit), using two and four electrode probes.

The two-electrode probe setup, was part of a Wheatstone bridge circuit (Figure ***2-6***) that consisted of an AC generator of variable frequencies (G), oscilloscope (C), two resistors of known value (R), push-pull amplifier (D), variable resistor and a variable condenser in parallel with the quantity to be measured which was enclosed by a Faraday cage (Burger and Van Dongen (1961)).

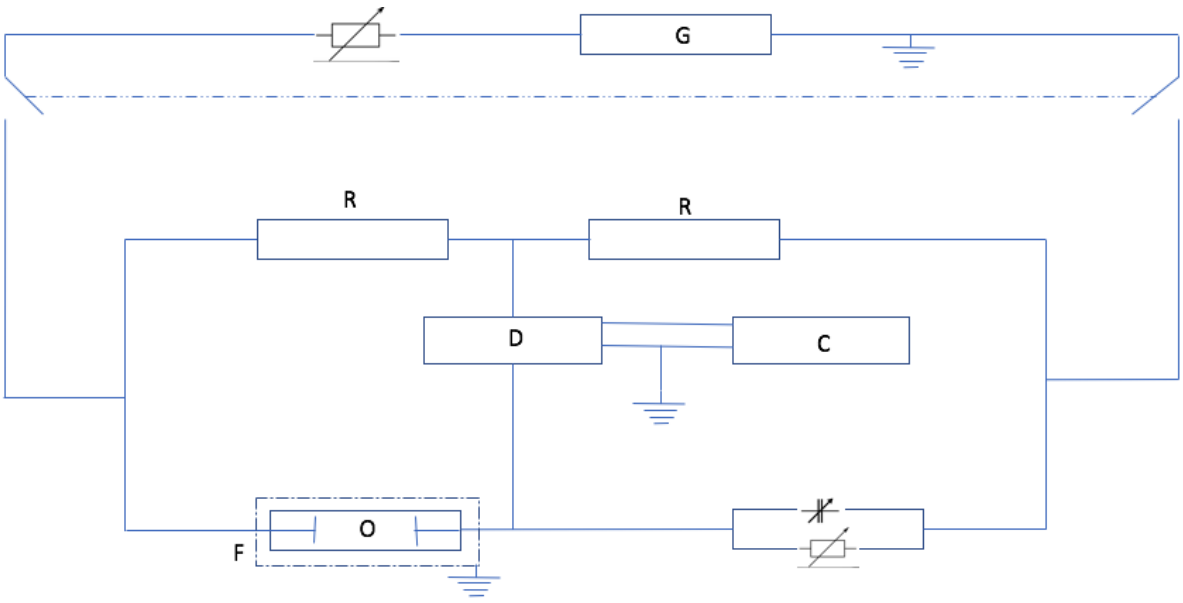

Figure 2-6: Wheatstone bridge circuit for two-electrode setup. (Figure re-drawn from Specific Electric Resistance of Body Tissue by Burger and Van Dongen) G= AC generator, R= resistance, D=push-pull amplifier, C= oscilloscope, O=object to be measured, F= Faraday cage.

The measured resistance was subsequently used to calculate the specific resistance ρ from Equation 2.3. With the two-electrode setup, the authors noted that direct current (DC) could not be used with two electrode system due to the effect of polarization (Burger and Van Dongen (1961)).

The D.C circuit for the four-electrode probe (Figure *2-7*) consisted of a battery, a resistor of known value for comparison, commutator used to reverse the current direction), the unknown object O, and an electronic volt meter (Burger and Van Dongen (1961)).

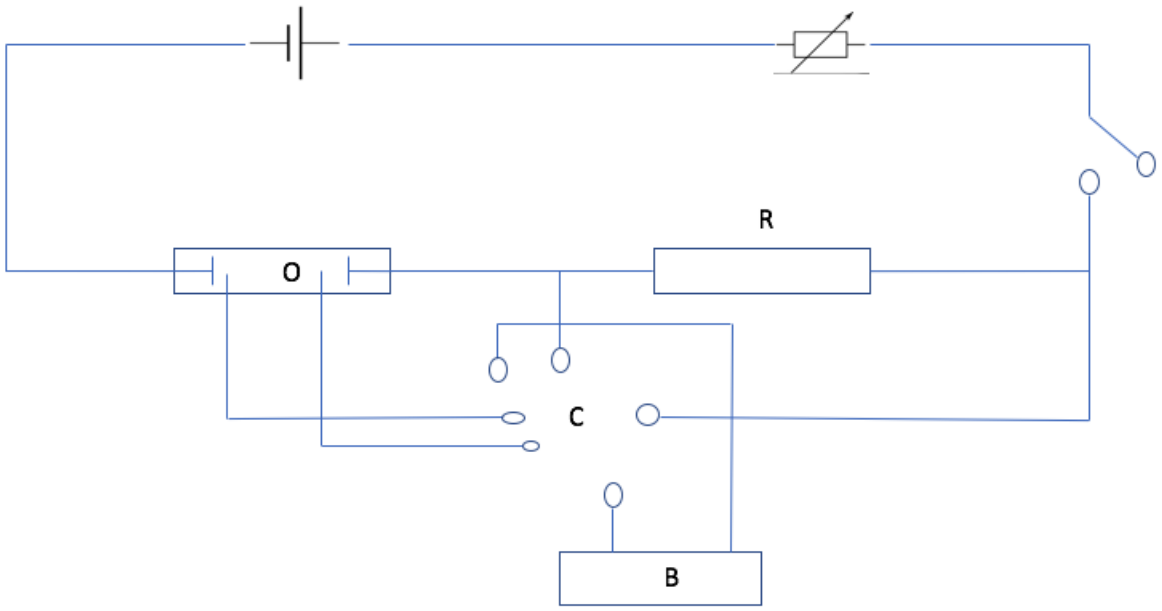

Figure 2-7: D.C circuit for four-electrode setup. (Figure re-drawn from Specific Electric Resistance of Body Tissue by Burger and Van Dongen), R= resistor, C= commutator, O=object to be measured, B= electronic voltmeter.

Within the circuit, two voltage measurement electrodes were placed a known distance between the two current electrodes. The voltage across the two electrodes was then measured and compared with the value of the voltage drop across the resistor. The voltage drop was used to calculate the resistance using Equation 2-2 which was then used to calculate the specific resistance using Equation 2-3.

Both electrode setups were calibrated by measuring a liquid of known specific resistance as was done in previous studies. The specific resistance of cow blood was found to be 166 Ωcm at 10,000 cycles, the specific resistance of human muscle in the leg was found to be 675 Ωcm and 245 Ωcm in the transverse and longitudinal directions respectively (Burger and Van Dongen (1961)). The difference in specific resistance in the longitudinal vs. transverse direction was

attributed to the anisotropy (exhibiting properties with different values when measured in a different direction (Martin (2010)) of biological tissue. The authors also noted the results were independent of frequency which is in direct contrast with the findings of Schwan and Kay. Table 1 displays the resistivity measurements as reported by the authors of the four previous studies. Differences in results between the four studies led Rush et al. (1963) to perform additional measurements on fifty anesthetized dogs ranging in weight from 14-30 kilograms.

Table 1: Mean tissue Resistivity (Ohm-cm) in living animals as reported by the investigators. (table partially re-created from Resistivity of Body Tissue at Low Frequencies by Rush, Abildskov, and McFee)

Tissues	Kaufman and Johnston	Burger and Van Milaan	Schwan and Kay	Burger and Van Dongen
Blood	208	160	100	160
Liver	506		840	
Heart	216		965	
Lung	744		1120	
Fat	2060		1500-5000	
Skeletal Muscle (human or dog)	643	$\rho_h = 470$ $\rho_l = 230$	800	$\rho_h = 675$ $\rho_l = 245$
Skeletal Muscle (rabbit)				$\rho_h = 1800$ $\rho_l = 125$
Dog trunk		415		

For their experiment, the authors employed a four-electrode setup (two current, and two potential measuring electrode) to measure the tissue resistivity in various orientations. The current circuit consisted of a 540-volt battery in series with a 4MΩ resistor operated by a manual

switch (**Figure *2-8***); The switch was closed for 0.1 seconds to generate a pulse during the experiment (Rush, Abildskov, and McFee (1963)).

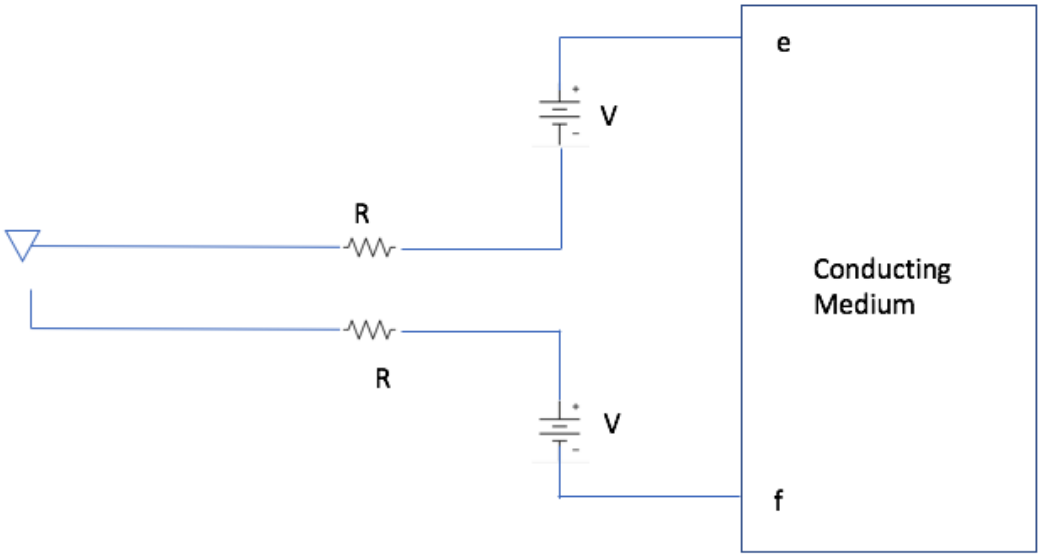

Figure 2-8: The current circuit for the four-electrode setup. (Figure re-drawn from Rush et al. (1963)) R=2 MΩ, v= 270 Volts, e, and f are point electrode through which a fixed amount of current passed through the conductive medium once the switch was closed.

The potential measuring electrodes were connected to a cathode follower (acts as a buffer between input load and the output, where a non-zero output impedance corresponds to the amount of voltage drop (Kuehnel (2009)) whose output was recorded by a Sanborn polyvison unit (Figure ***2-9***). The needles were arranged in various orientations depending on the geometry of the tissue to be measured.

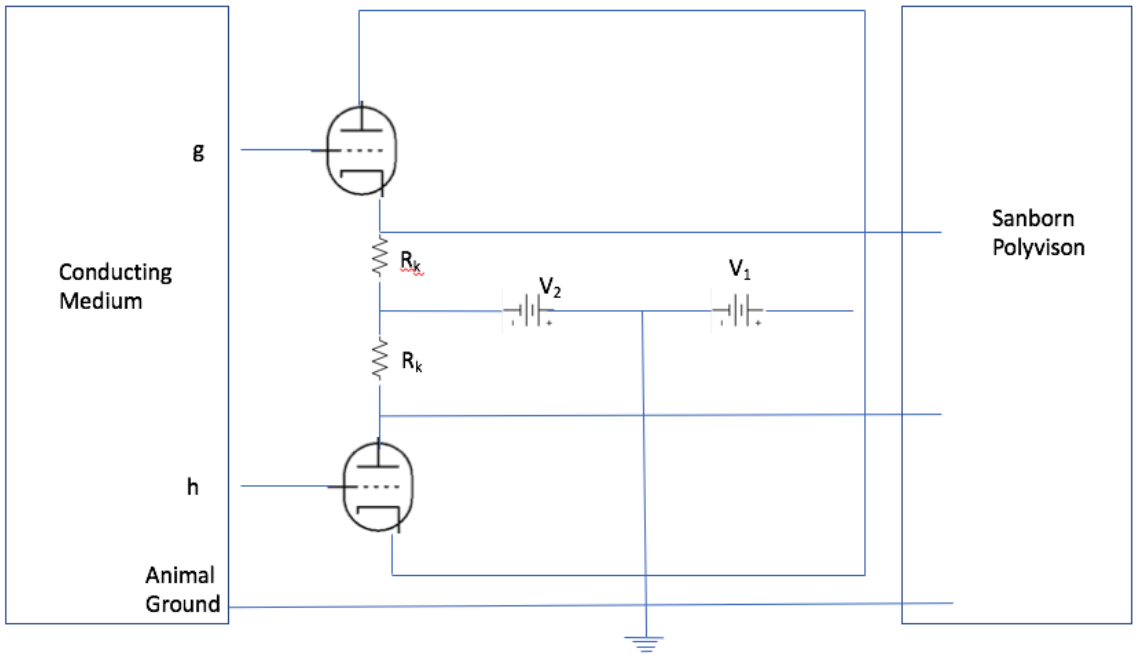

Figure 2-9: Voltage measuring circuit for the four-electrode setup. (Figure re-drawn from Rush et al. (1963)). R= 0.1 MΩ, V_1= 90 Volts, V_2= 45 Volts g and h are point electrode through which the voltage drop across the test specimen was measured.

The resistivity of the liver was found to be 700 Ωcm, which yielded a difference of 18% when compared with the values reported by Schwan and Kay (840 Ωcm) (Rush et al., 1963). This difference was due to incorrect polarization correction applied as well as incorrect boundary assumptions. The heart was found to exhibit anisotropic behavior; the transverse and longitudinal resistivity values were found to be 563 Ωcm and 252 Ωcm respectively (Rush et al. (1963)). The difference with Schwan and Kay (965 Ωcm) was attributed to the electrical activity of the heart being stopped before measurements taking place. The authors noted stopping the electrical activity of the heart lead to a 25% increase in resistivity within fifteen minutes (Rush et al. (1963)).

Measurements in the lungs were taken at the extreme positions (inflation, and deflation). The results were found to be 2390 Ωcm (inflation), and 1950 Ωcm (deflation) (Rush et al. (1963)). Schwan and kay performed their measurements in closed dog chests while the current tests were conducted in an open chest thus both values may be correct for the individual measurements.

The specific resistance of blood and fat were found to be 162 Ωcm, 2500 Ωcm, respectively; additionally, the resistivity of the skeletal muscle was found to be 2300 Ωcm (transverse) and 150 Ωcm (longitudinal) respectively (Rush et al. (1963)). The resistivity values for blood and fat were found to be in agreement with other studies previously conducted. The large spread in the skeletal muscles specific resistance was due to the sensitivity of the electrode orientation.

More recently, Martinsen et al. 2010, developed a portable vascular device to aid in the location of large blood vessels and discriminate between various tissue types by measuring the electrical impedance. The test device consisted of an array of 10 needles mounted on a plastic block each separated by a distance of 3mm with the needle shaft electrically insulated (Martinsen et al. (2010)). The needles were connected through a multiplexer to an impedance analyzer. The device was inserted into the femoral artery of a 55kg pig where the initial impedance value was recorded after insertion. Subsequently, the needle was withdrawn by 3mm, and a new scan was performed until the needle was withdrawn from the animal. Performing impedance measurements every 3mm allowed the investigators to obtain impedance values of tissue at various locations. The results showed that the needle array was able to discriminate between different tissue types with artery's having the lowest electrical impedance followed by muscle and fat (Martinsen et al. (2010)).

The previous studies serve as motivation for the current thesis. If a smaller (two electrode) device were built, it could be incorporated into standard catheters (Figure **1-1**) to help nurses and physicians place the IV correctly the first time. Successfully placing the IV the first time, would reduce patient pain and save lost time associated with IV placement. This served as the inspiration for our research, which is discussed in greater detail in the chapters to follow.

3.0 MEASURMENT METHODS

This chapter describes the various measurement methods (static and transient) undertaken by the author in this project in order to successfully differentiate between subcutaneous tissue and blood.

3.1 STATIC MEASURMENT OF TISSUE RESISTANCE

Static measurement involves the set of criteria defined for instruments used to measure quantities which are mostly constant. (Basheer (2012)). The following sections describe the various static measurement methods undertaken (multimeter, Wheatstone bridge) to successfully differentiate between blood and subcutaneous tissue.

3.1.1 MULTIMETER MEASURMENT

Our initial attempt at a proof of concept was performed with a digital multimeter (**Figure *3-1***).

Figure 3-1: Digital Multimeter used to perform resistance measurements

The idea of the multimeter traces back to the invention of the galvanometers. A galvanometer is an instrument that produces a needle deflection when current is passed through its coil. The magnitude of the deflection is typically measured by balancing a Wheatstone bridge. Due to its size and slow speed of response, individual test meters were used to measure voltage and current. (Poole (2016)).

The first analog multimeter (Avometer) was invented in the early 1920's by British post office engineer Donald Macadie, and it was capable of measuring current, voltage, and resistance (Poole (2016)). Today the multimeter is the mainstay for electrical testing and is a versatile tool capable of measuring various electrical properties. For our application, the multimeter was used to measure the resistance of tissues.

Most often, a digital multimeter employs a constant current to measure the resistance (Figure ***3-2***). In the figure, a constant current (I_s) is applied to the load (R_x) to be measured, R_{Lead} is the electrode resistance, and V_m is the voltage that is measured by the multimeter.

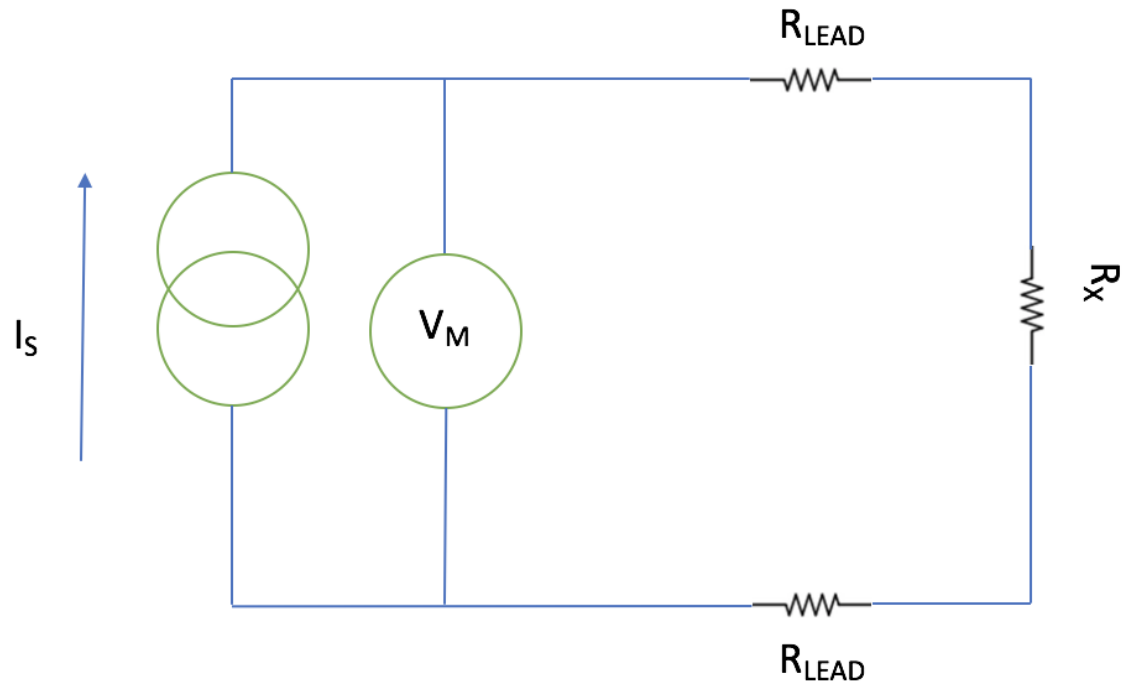

Figure 3-2: Multi-Meter resistance measurement technique (figure re-drawn from ni.com). In the figure, a constant current (I_s) is applied to the load (R_x) to be measured, R_{Lead} is the electrode resistance and V_m is the voltage that is measured by the multimeter.

The total resistance of the system is found by adding the individual resistance values (Equation 3-1). The relationship between the current (I), voltage (V), and the total resistance (R_{tot}) is described by ohms law (Equation 3-2). If the lead resistances are negligible, solving Equation 3-2 for R_x as shown by Equation 3-3 provides an expression for the unknown resistance, whose values are calculated by the multimeter and displayed for the user.

$$R_{tot} = R_{Lead} + R_{Lead} + R_x \tag{3-1}$$

$$V_M = I_s R_{tot} \tag{3-2}$$

$$R_x = \frac{V_M}{I_s} \tag{3-3}$$

3.1.1.1 MULTIMETER TESTING AND RESULTS Two sets of tests were carried out involving the digital multimeter. The tests included inserting the two electrodes (multimeter leads) separated by a distance (2 mm and 5 mm) in to various materials to measure the resistance. Materials tested were pork fat, pork muscle and Plasma-Lyte A (a commercially available liquid that has electrical properties similar to blood). Figure 3-3 shows a schematic of the test setup.

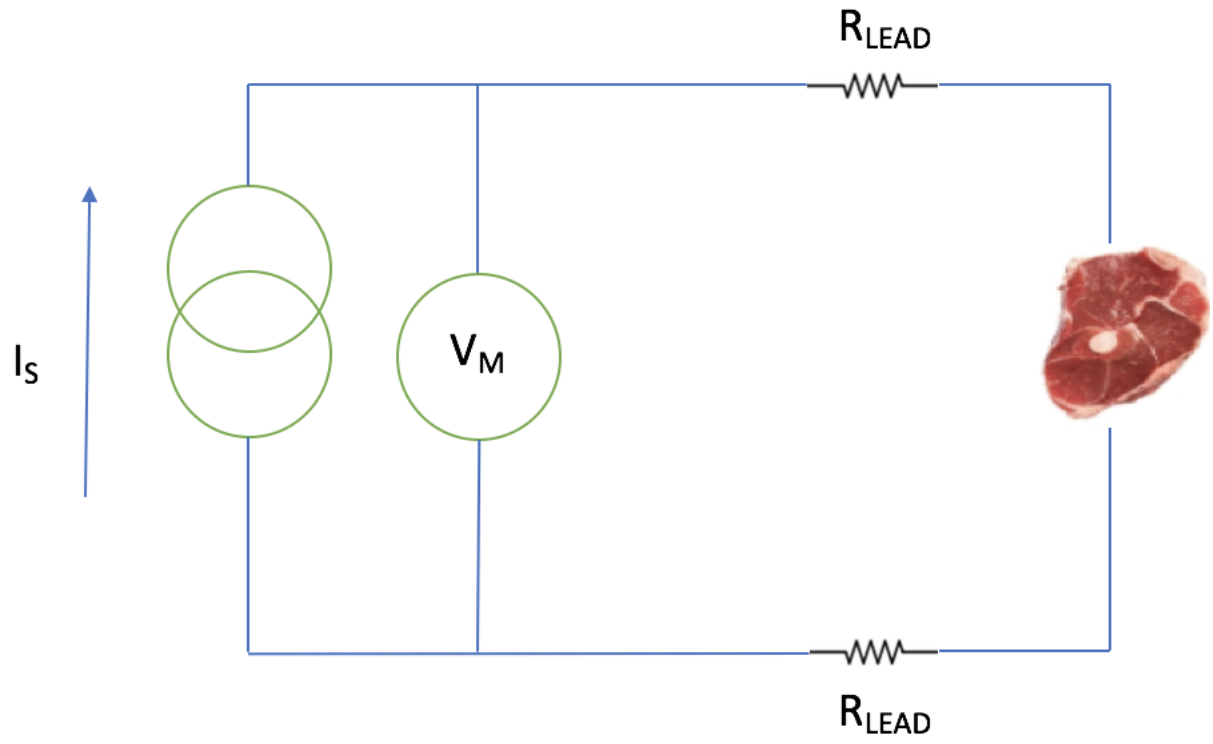

Figure 3-3: Test setup for multimeter based resistance measurement.

During the two tests, the electrodes were submerged in Plasma-Lyte A solution for one minute, and the resistance measured by the multimeter was recorded every ten seconds. Subsequently, the electrodes were used to puncture pork fat and muscle for one minute, and the output resistance displayed by the multimeter was recorded every ten seconds. In each trial, the electrodes were cleaned to avoid erroneous results from contaminated electrodes, and the data was collected for one minute to obtain the steady-state values of each material tested. Figure ***3-4***-Figure ***3-9*** display the results of these tests.

Figure ***3-4*** and Figure ***3-5*** show the measured resistance values of Plasma-Lyte A solution during six trials for 2 mm and 5 mm electrode spacing. In Figure ***3-4*** the measured resistance value starts around 50Ω-450Ω, and it reaches a final value between 150Ω-1300Ω. In Figure ***3-5*** the measured resistance value begins around 30Ω-375Ω and reaches a final value of 250Ω-275Ω.

Figure ***3-6*** and Figure ***3-7*** display the pork muscle resistance measurements for the two-electrode spacing as described above. In Figure ***3-6*** the measured resistance value of pork muscle had an initial resistance value of approximately 0.14MΩ- 0.7MΩ, and the measured resistance value increased to 1.26MΩ-3.72MΩ at sixty seconds. In Figure ***3-7*** the initial measured resistance value ranged from 0.144MΩ- 0.700MΩ. The final measured resistance values ranged from 0.8MΩ-3.7MΩ during twelve individual trials.

Figure ***3-8*** and Figure ***3-9*** display the pork fat resistance measurement for the 2 mm and 5 mm electrode spacing. In Figure ***3-8*** the measured resistance of the pork fat had an initial value of approximately 0.2MΩ- .9MΩ, and the measured resistance value increased to 0.8MΩ-1.2MΩ at sixty seconds. Figure ***3-9*** displays the pork fat resistance measurement for 5 mm electrode

spacing. Here the initial measured resistance value ranged from 0.1MΩ -2MΩ and the measured resistance value decreased to 0.7MΩ-1.2 MΩ during the twelve trials.

As can be noted from the plots, the resistance values for PlasmaLyte-A, pork fat, and muscle fluctuated and never reached steady state. All of the trials for the 2 mm and 5 mm electrode spacing were terminated after sixty seconds since the resistance of the PlasmaLyte-A, pork muscle and pork fat as measured by the multimeter continued to fluctuate and change with time without reaching a steady state value. If the plots were accepted as correct, one would conclude that muscle had a higher resistance than fat, and resistance of tissue changed with time. These conclusion would be inaccurate since fat acts as an insulator and has a resistance value that is significantly greater than that of muscle (Rush et al. (1963); Kaufman and Johnston (1943); Schwan and Kay (1956)). The error in measurement can be attributed to polarization since a direct current is applied. Applying a direct current to a biological tissue or liquid solution causes an accumulation of ions near the surface of the electrodes which leads to the polarization of the measurement electrodes (Analytical (2004); Burger and Van Dongen (1961). Thus, it is necessary to apply an alternating current or an oscillatory circuit such that the ions are forced to continuously migrate from one electrode to the other negating the effect of polarization.

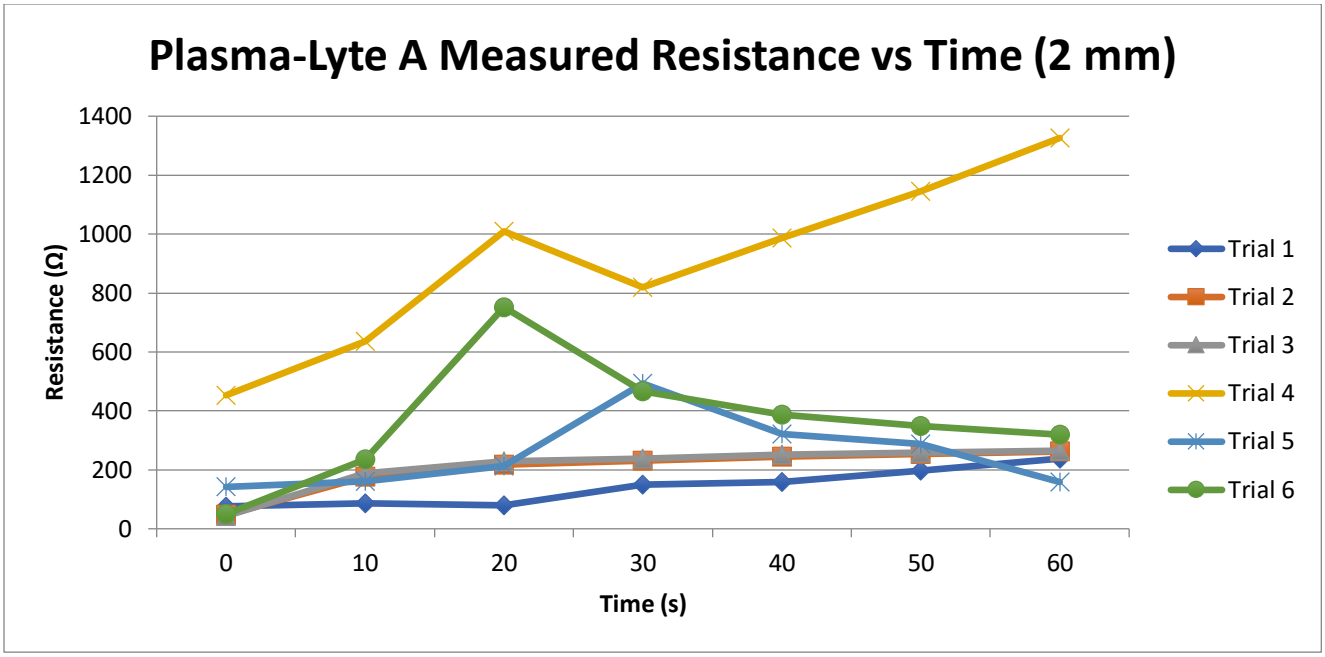

Figure 3-4: Plot of Plasma-Lyte A measured resistance vs. time for 2 mm electrode spacing through six trials using a digital multimeter.

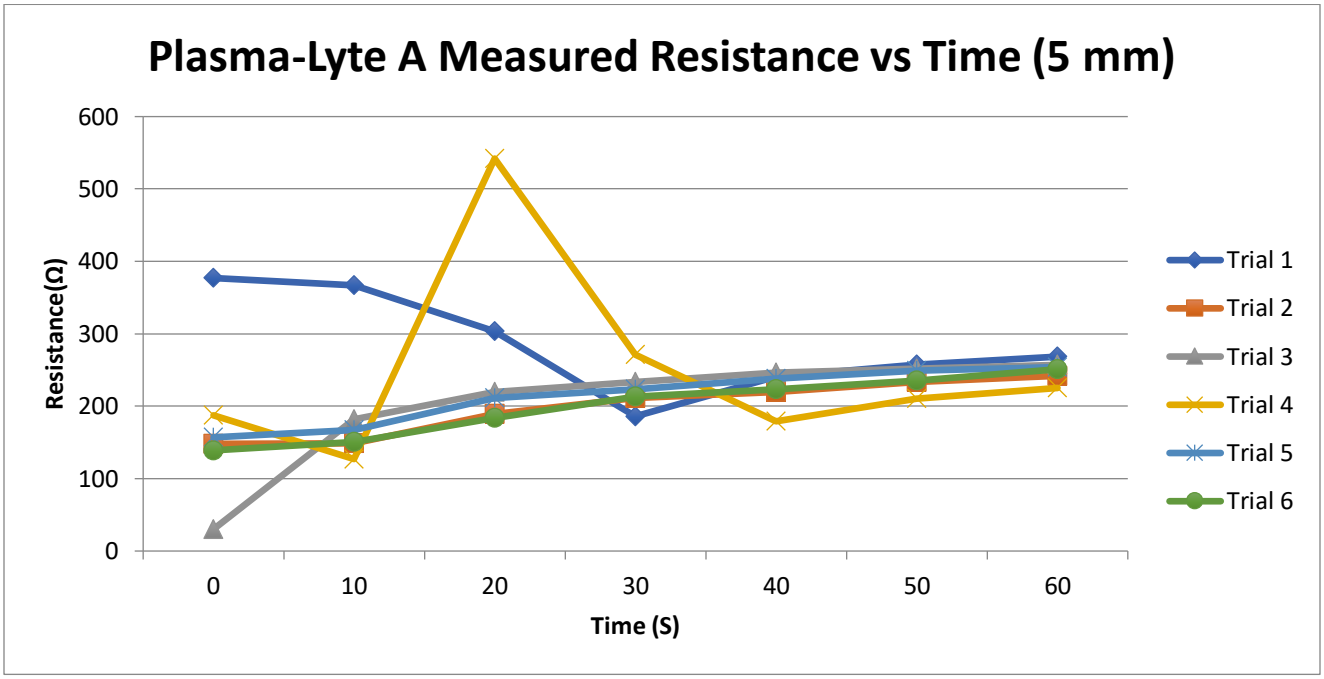

Figure 3-5: Plot of Plasma-Lyte A measured resistance vs. time for 5 mm electrode spacing through six trials using a digital multimeter.

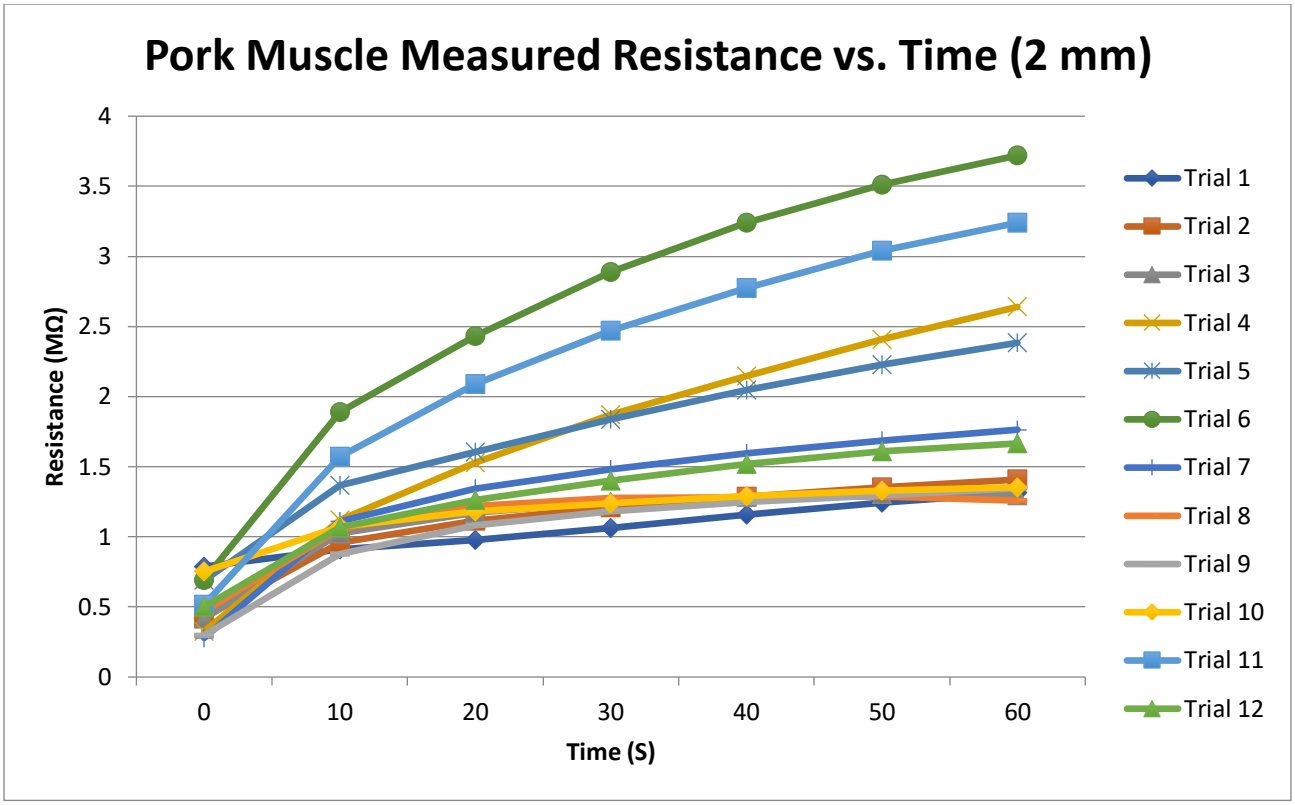

Figure 3-6: Plot of muscle measured resistance vs. time for 2 mm electrode spacing through twelve trials using a digital multimeter.

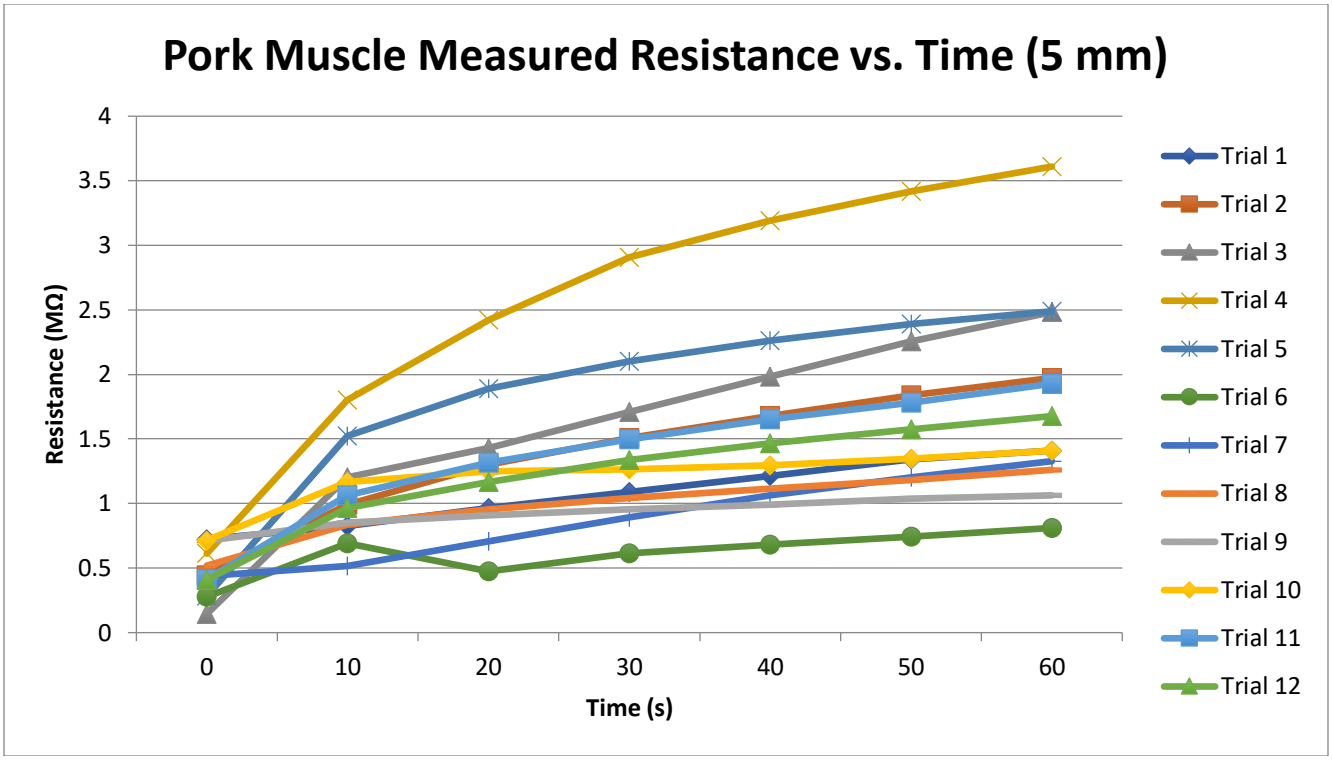

Figure 3-7: Plot of muscle measured resistance vs. time for 5mm electrode spacing through twelve trials using a digital multimeter.

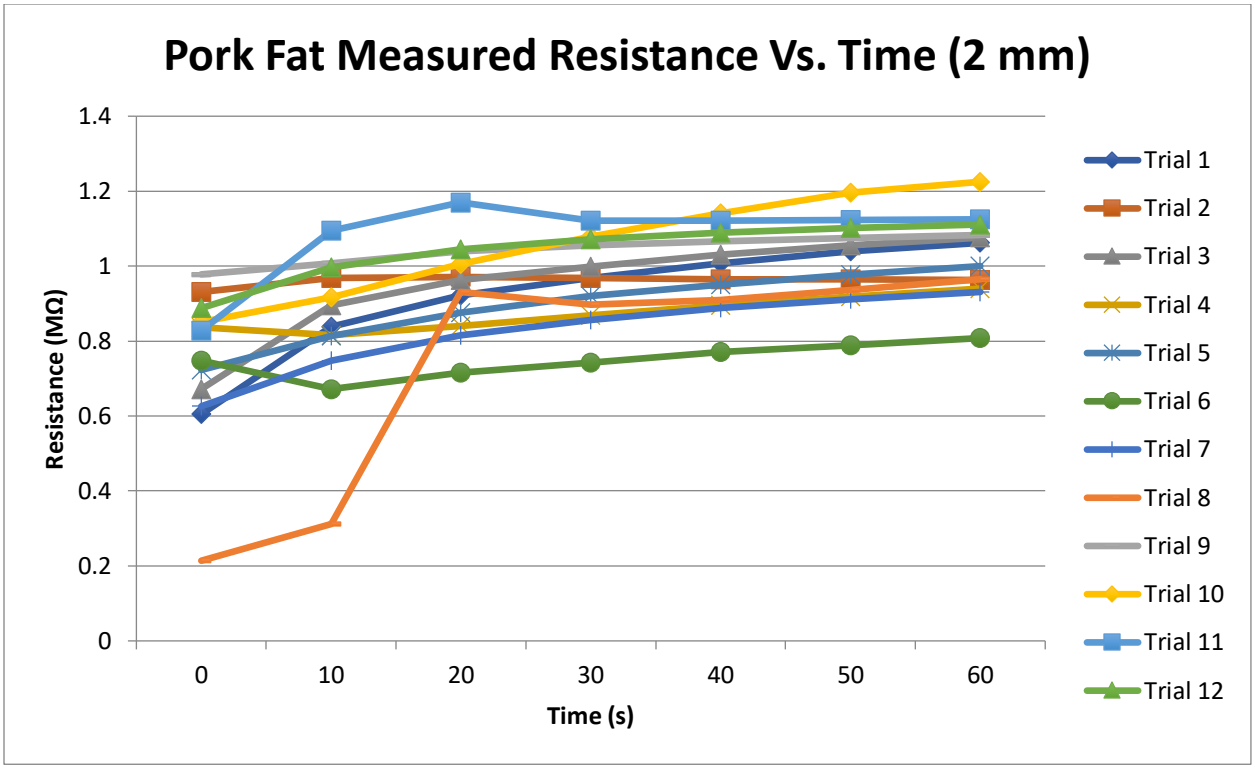

Figure 3-8: Plot of Pork Fat measured resistance vs. time for 2 mm electrode spacing through twelve trials using a digital multimeter.

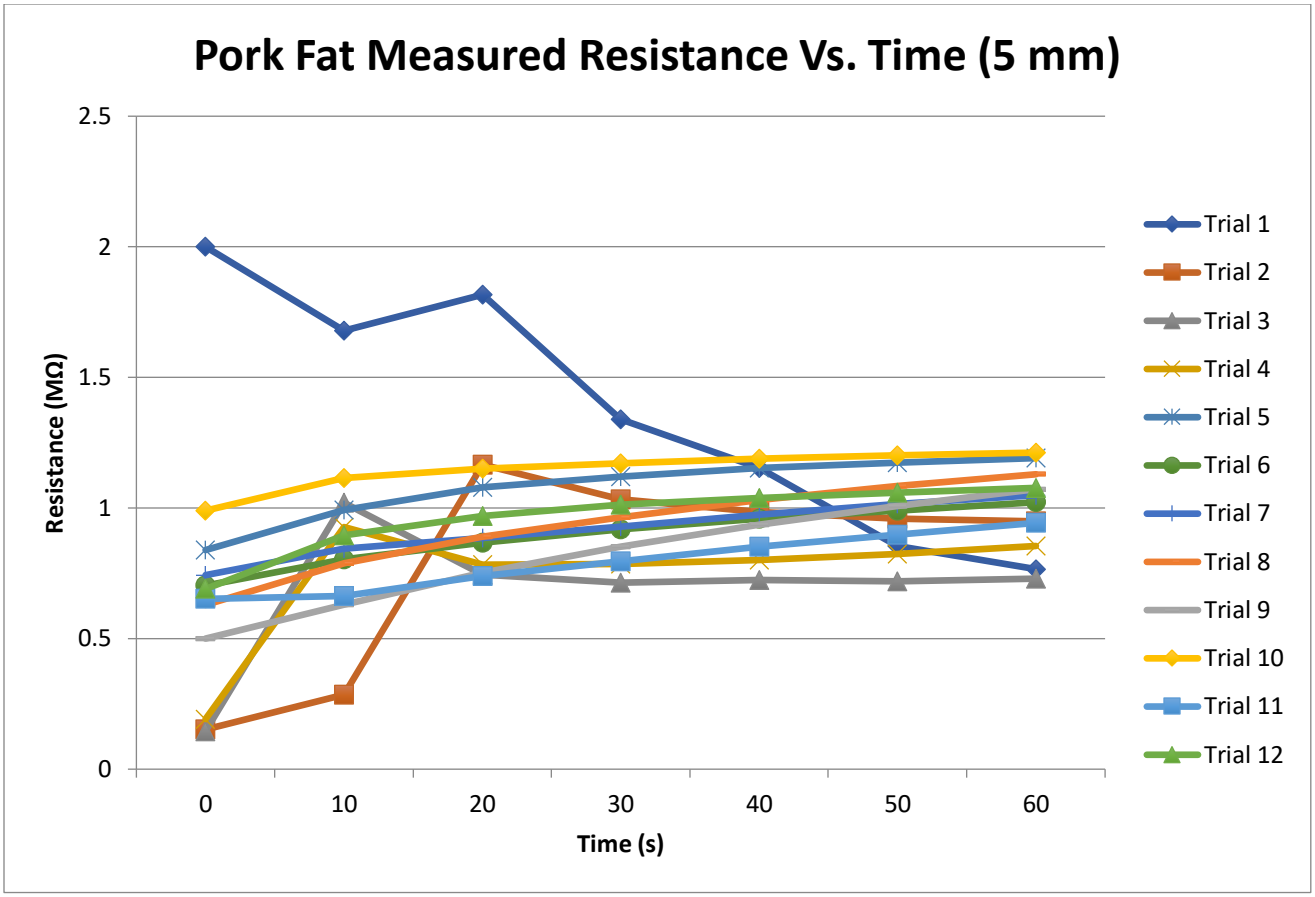

Figure 3-9: Plot of Pork Fat measured resistance vs. time for 5 mm electrode spacing through twelve trials using a digital multimeter.

3.1.2 WHEATSTONE BRIDGE MEASURMENTS

After our initial attempt with the multimeter, our subsequent endeavor involved a Wheatstone bridge. A Wheatstone bridge consists of two voltage dividers which allow for precise measurement of an unknown resistance value. It was first invented by Samuel Christie (1833) and made popular by Charles Wheatstone (Ken (2015).

For the purpose of our application, an AC bridge was used instead of DC in order to negate the effect of polarization (Section 3.1.1.2). Unlike DC bridges, where the resistance could be directly measured, AC bridges measure the impedance. Equation 3-4 displays a general expression for impedance, where R is the real component and jX is the imaginary component.

$$Z = R + jX \tag{3-4}$$

Figure ***3-10*** displays a schematic of a balanced AC Wheatstone bridge. In the figure, given an arbitrary AC voltage Z_1, Z_2, Z_3, Z_4 are the resulting impedances, and "null" indicates an output bridge voltage in the balance condition.

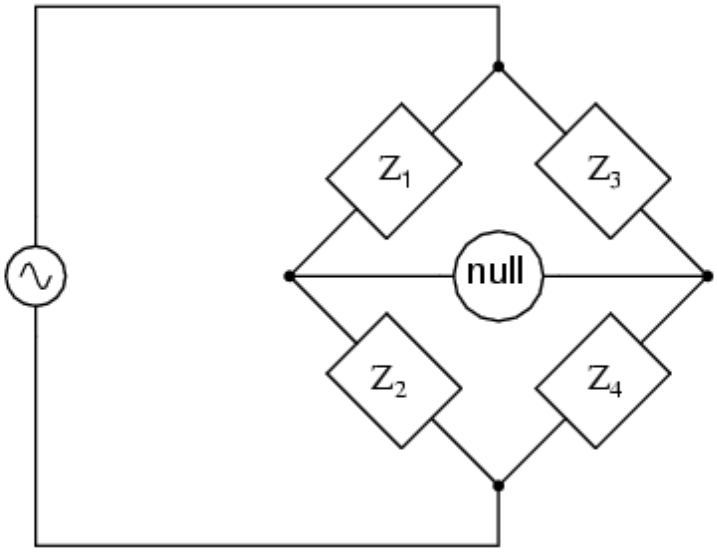

Figure 3-10: Schematic of a balanced AC Wheatstone bridge, where Z_1, Z_2, Z_3, Z_4 are the impedances, and "null" indicates an output bridge voltage in the balance condition.

The bridge circuit shown in Figure ***3-10*** works as a voltage divider when connected to a power source. A specific input voltage will result in a corresponding output voltage. A balanced condition occurs when the voltage difference and current flow between the two legs is zero (Thomas G. Beckwith (1993)). A balanced condition results in the output bridge voltage being negligible or "null". This allows for the determination of the balance condition (Equation 3-5). The relationship states that in order for the bridge to balance, the ratio of the impedances of any two adjacent arms must equal the ratio of the impedances of the remaining two arms (Thomas G. Beckwith (1993)).

$$\frac{Z_1}{Z_2} = \frac{Z_3}{Z_4} \tag{3-5}$$

In the present application, the imaginary component of the bridge is neglected and only the real portion considered since the fluid/tissue resistance is the dominant effect. Figure **3-11** shows the Schematic of a Wheatstone bridge, with impedances shown as pure resistors, in an arbitrary unbalanced condition. For a given input the output of the bridge will reflect the extent of the unbalance as, V_b is the unbalanced voltage, V_{in} is the input voltage R_a, R_b, and R_c are known resistance components, and R_x is the unknown component.

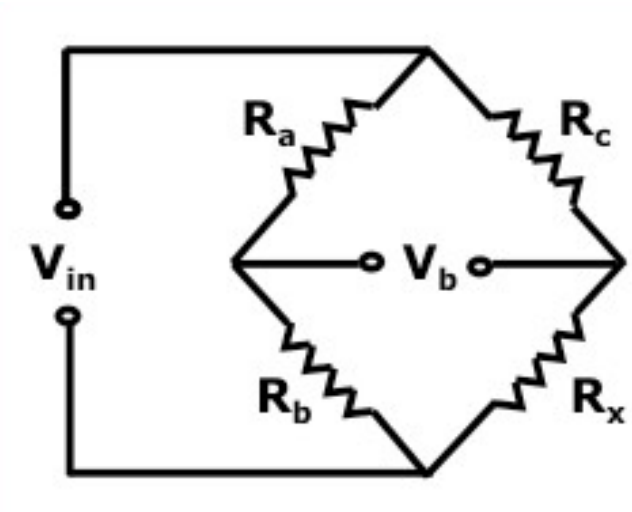

Figure 3-11: Schematic of a Wheatstone bridge, with impedances shown as pure resistors, in an arbitrary unbalanced condition, where V_b is the unbalanced voltage, V_{in} is the input voltage R_a, R_b, and R_c are known resistance components, and R_x is the unknown component.

Applying the voltage divider relationship (Equation 3-6) an expression is obtained which allows for the determination of the unbalanced voltage for a given input (Equation 3-7).

$$v_b = \frac{R_b}{R_a + R_b} v_{in} \tag{3-6}$$

$$v_b = v_{in}\left(\frac{R_x}{R_x+R_c} - \frac{R_b}{R_b+R_a}\right) \quad (3\text{-}7)$$

In the present application, the tissue/fluid being measured will take the place of the resistance value R_x, as depicted in Figure ***3-12***. Although only subcutaneous tissue is shown in the figure, it should be noted that the two electrodes encounter other materials such as blood and muscle during use in a clinical environment.

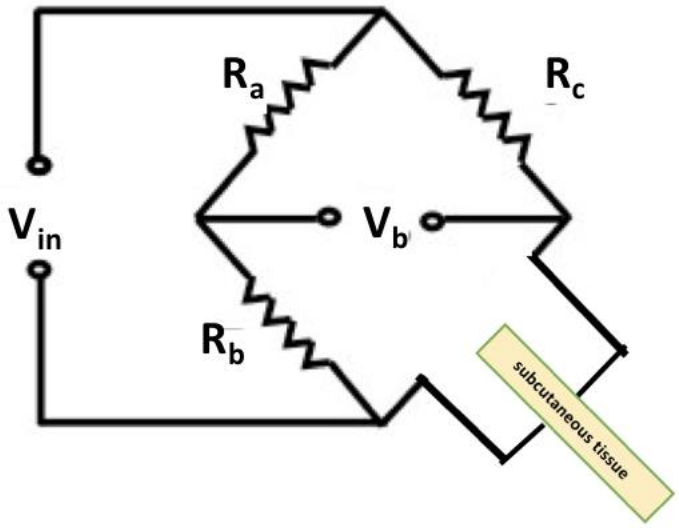

Figure 3-12: Test setup for Wheatstone bridge based resistance measurement. where V_b is the unbalanced voltage, V_{in} is the input voltage R_a, R_b, and R_c are known resistance components, and R_x is the tissue/fluid component being measured by two electrodes.

In the current arrangement, the unknown tissue/fluid resistance can be determined by using Equation 3-8 which in turn allows for the differentiation between subcutaneous tissue and blood. It is not necessary to convert the measured unbalanced bridge voltage values to their corresponding resistance values. This is possible because subcutaneous tissue and blood have

distinct output bridge voltages that can be measured allowing for differentiation between the two quantities.

$$R_x = \frac{\left(R_b R_c + \frac{V_b}{V_{in}}(R_a + R_b)\right)}{\left(R_a - \frac{V_b}{V_{in}}(R_a + R_b)\right)} \tag{3-8}$$

3.1.2.1 WHEATSTONE BRIDGE TESTING AND RESULTS Two set of tests were carried out as part of the bridge measurements. The first set of measurements were performed to calibrate the circuit with known resistor values using an AC voltage source. The second test involved measuring the resistance of biological tissue at various frequencies to identify individual quantities. PlasmaLyte–A and pork muscle were tested as part of the second experiment. **Figure** 3-13 shows the experimental setup of the first bridge test using pure resistors.

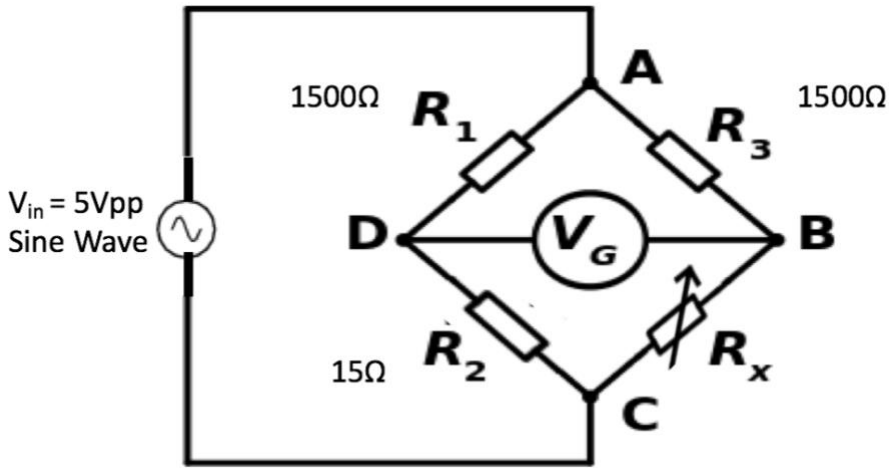

Figure 3-13: Wheatstone bridge calibration test setup using pure resistors. where Vg is the measured output voltage, V_{in} is the input waveform (sign wave, 5- volt peak-to-peak) R_1, R_3 were chosen to be 1500Ω. R_2 was set at 15Ω and the value of R_x was varied with a potentiometer.

As part of the test, an AC function generator was used to supply a 5V peak-to-peak sine wave to the bridge circuit. R_1 and R_3 were chosen to be 1500 Ω. R_2 was set at 15 Ω and the value of R_x and the frequency of the sign wave was varied. The bridge output voltage was used in conjunction with Equation 3-8 to re-calculate the value or Rx. This was done to assess the accuracy of the choice of individual resistors for the bridge.

Figure ***3-14:*** -Figure ***3-22*** display the result of the tests. From the figures, it can be noted that for higher resistance values (2.5 KΩ-534 Ω), the measured resistance begins to diverge at higher frequencies. For lower resistance values, the measured resistance converged at all frequencies. Although the measured resistance values became less accurate as the frequencies increased, the plots indicated that it is possible to identify differences between quantities such as blood and subcutaneous tissue.

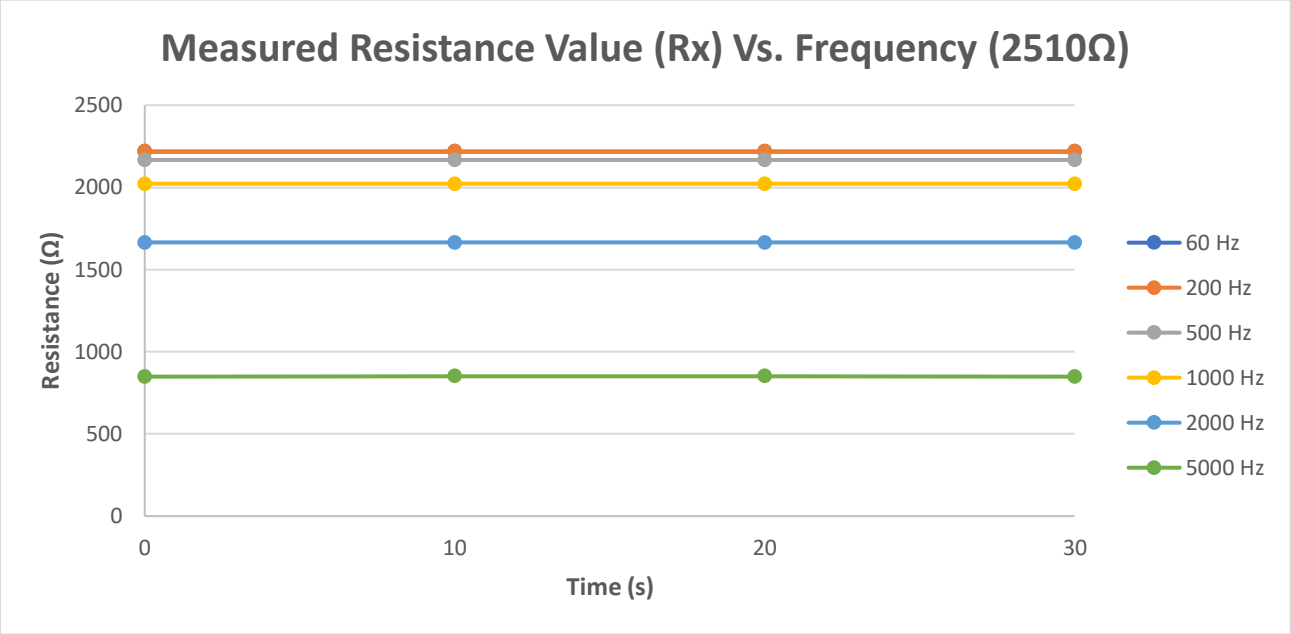

Figure 3-14: Plot of measured R_x resistance Vs. time for varying frequencies using a 2500Ω resistor.

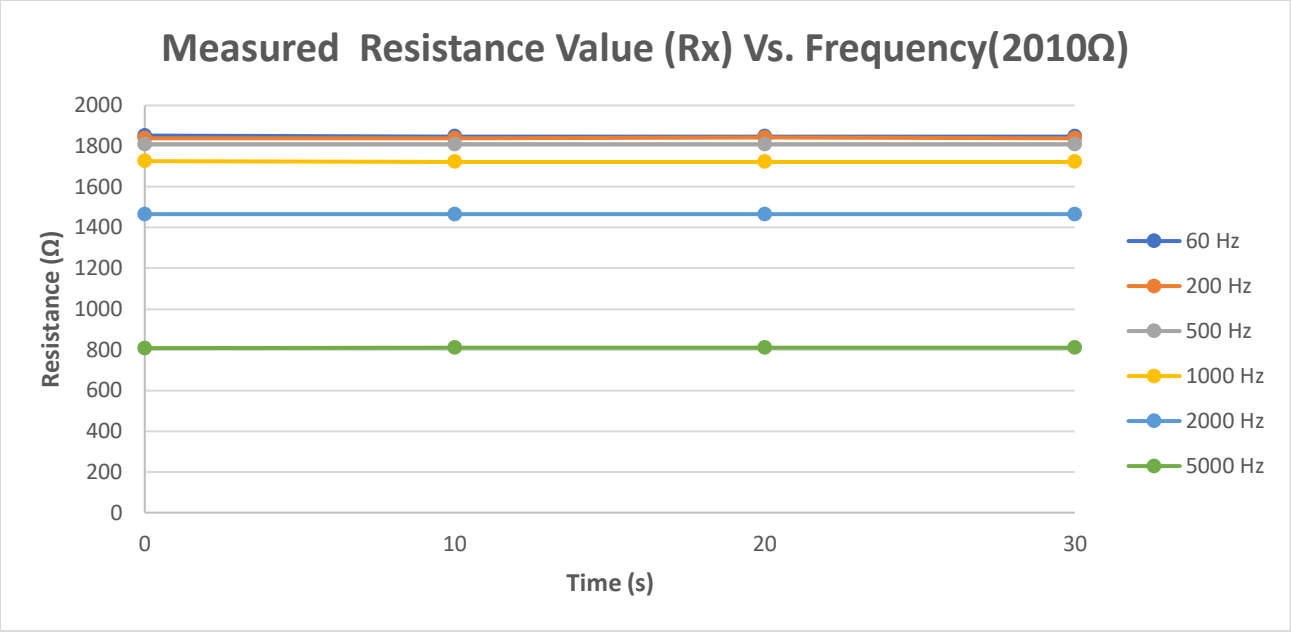

Figure 3-15: Plot of measured R_x resistance Vs. time for varying frequencies using a 2KΩ resistor.

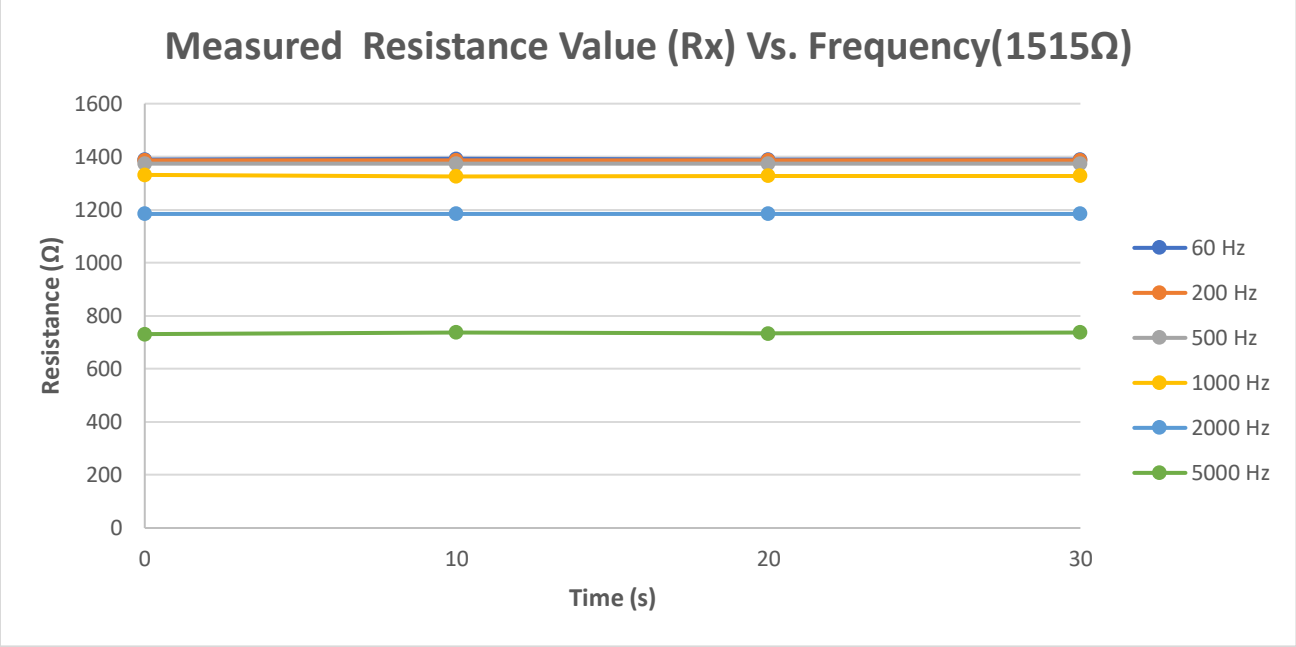

Figure 3-16: Plot of measured R_x resistance Vs. time for varying frequencies using a 1.5KΩ resistor.

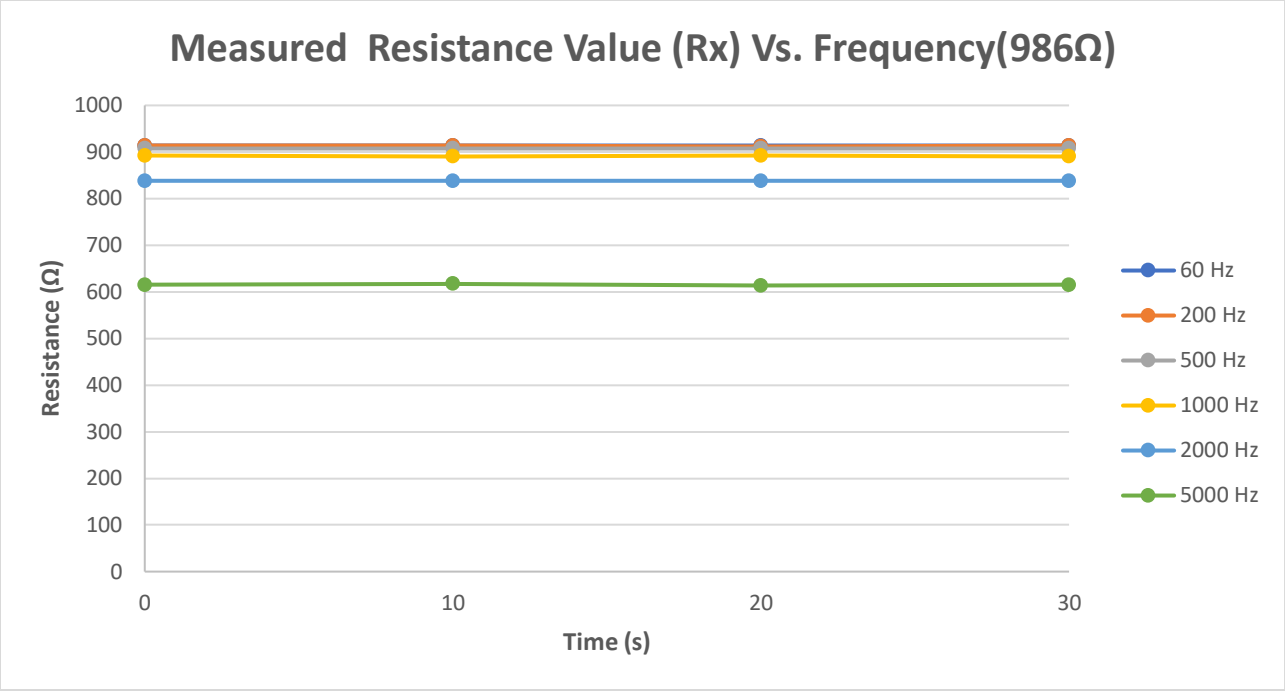

Figure 3-17: Plot of measured R_x resistance Vs. time for varying frequencies using a 1KΩ resistor.

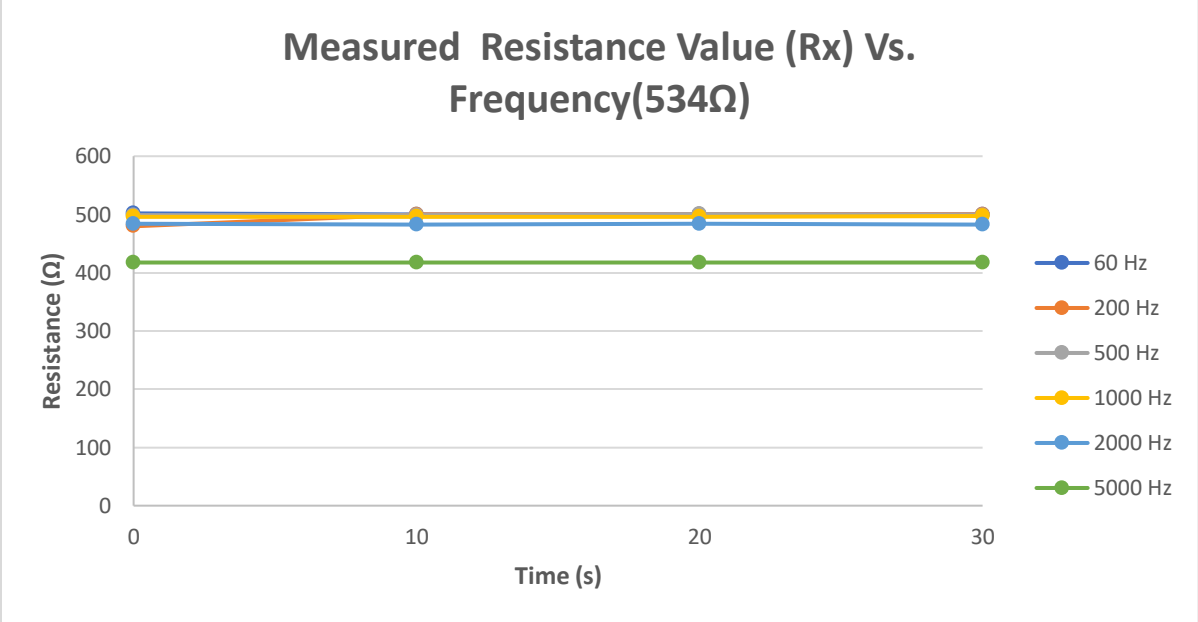

Figure 3-18: Plot of measured R_x resistance Vs. time for varying frequencies using a 500Ω resistor.

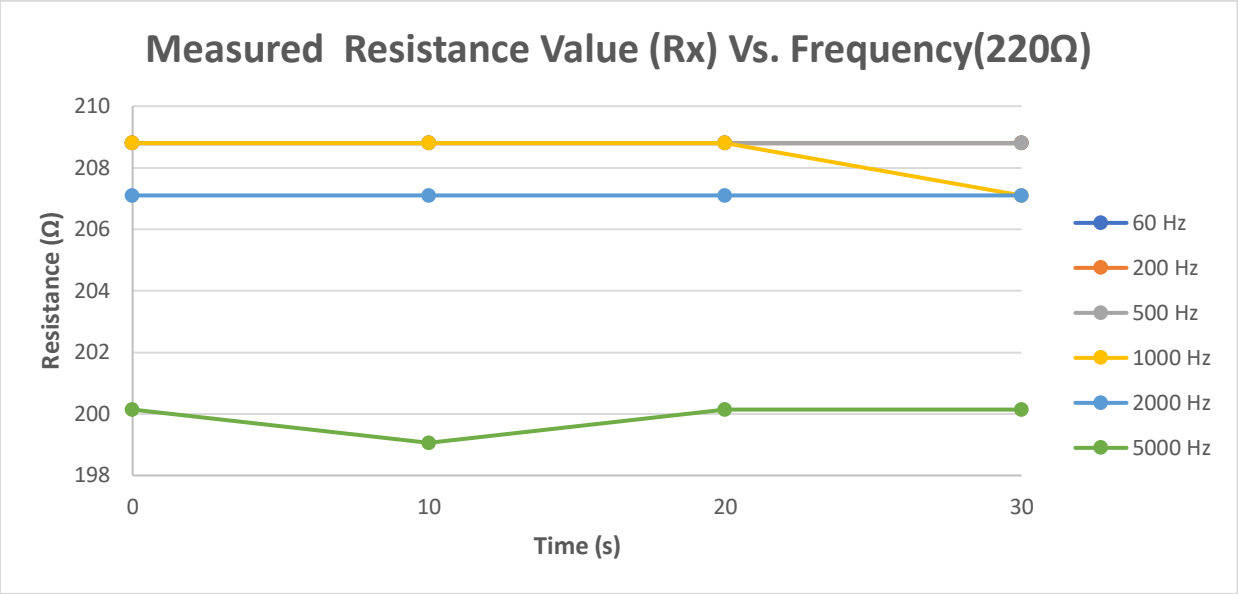

Figure 3-19: Plot of measured R_x resistance Vs. time for varying frequencies using a 220Ω resistor.

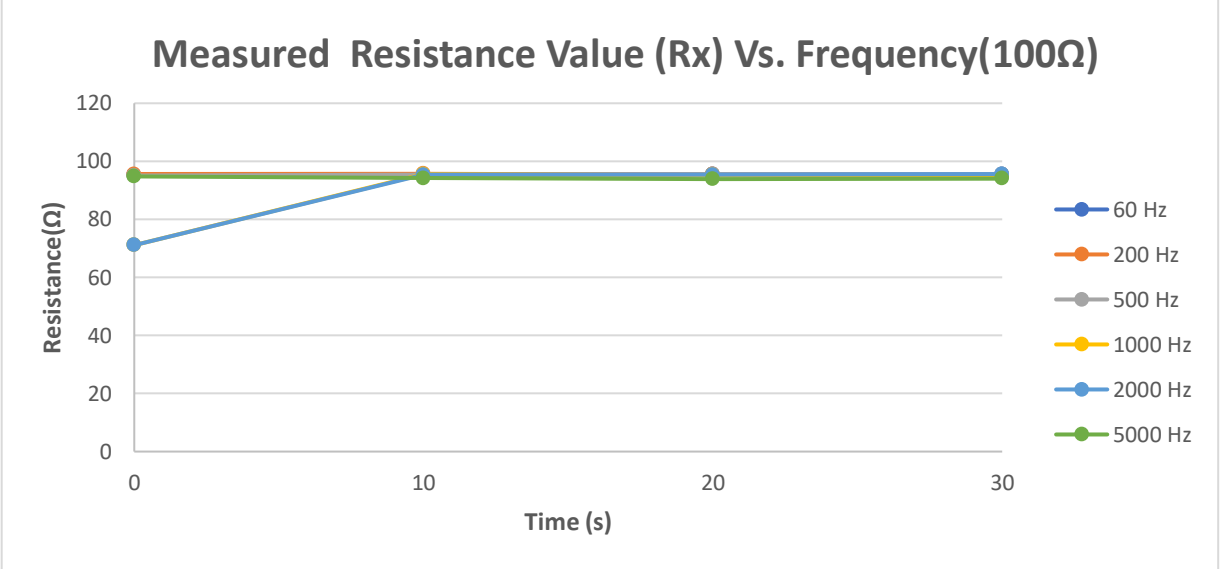

Figure 3-20: Plot of measured R_x resistance Vs. time for varying frequencies using a 100Ω resistor.

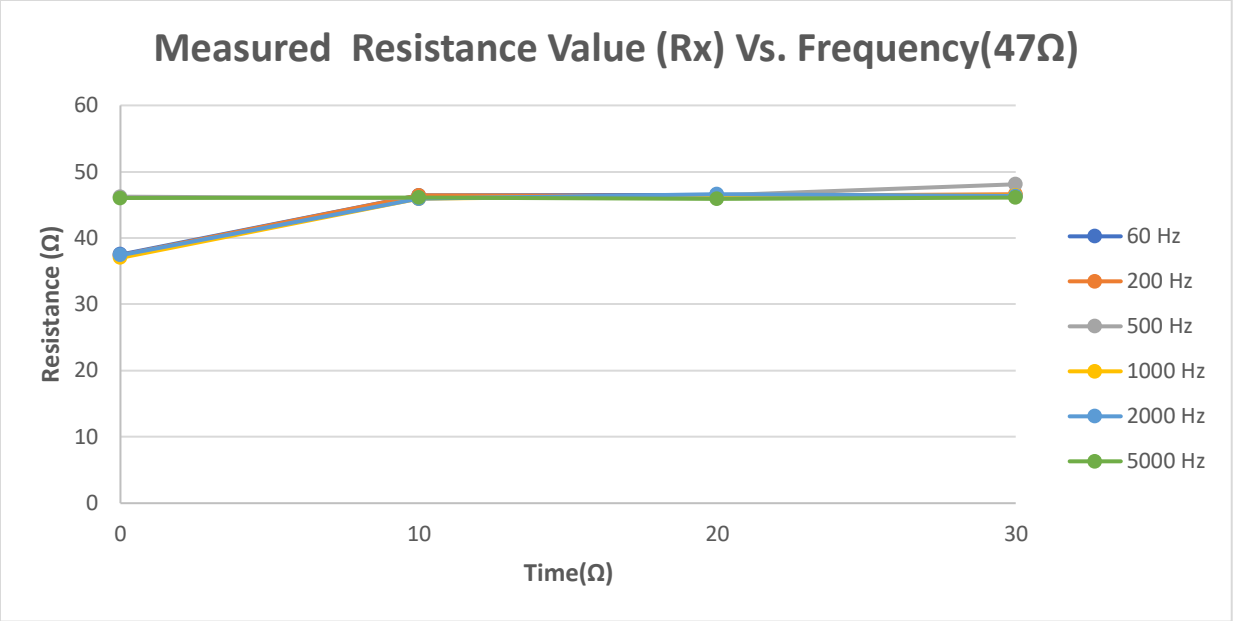

Figure 3-21: Plot of measured R_x resistance Vs. time for varying frequencies using a 45Ω resistor.

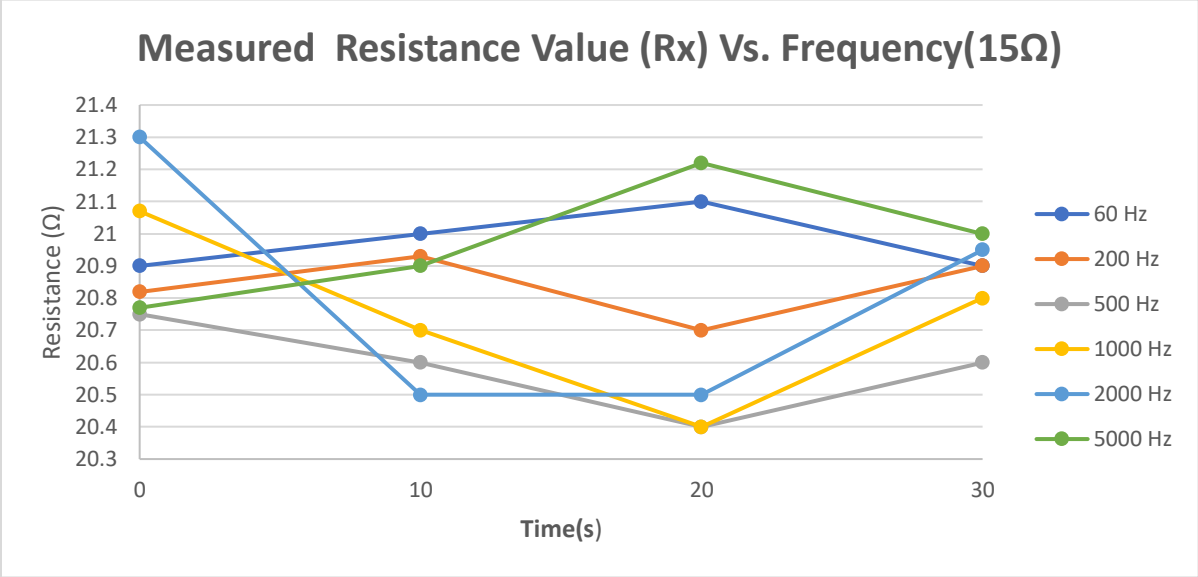

Figure 3-22: Plot of measured R_x resistance Vs. time for varying frequencies using a 15Ω resistor.

After recording the measured resistance for varying frequencies, the circuit was further tuned through trial and error (Figure ***3-23***) prior to performing the second test. As part of the second test, a 5V peak-to-peak sine wave was sent to the bridge circuit. The value of R_1 and R_3 was changed to 220 Ω and 470 Ω. R_2 was kept unchanged at 15 Ω and Rx consisted of the two electrodes used to measure the output bridge voltage of Plasma-Lyte A and pork muscle for varying frequencies. The output voltage was used in conjunction with Equation 3-8 to determine the measured resistance value of the tissue/fluid (Rx). **Figure *3-24*** and **Figure *3-25*** displays the results of these test.

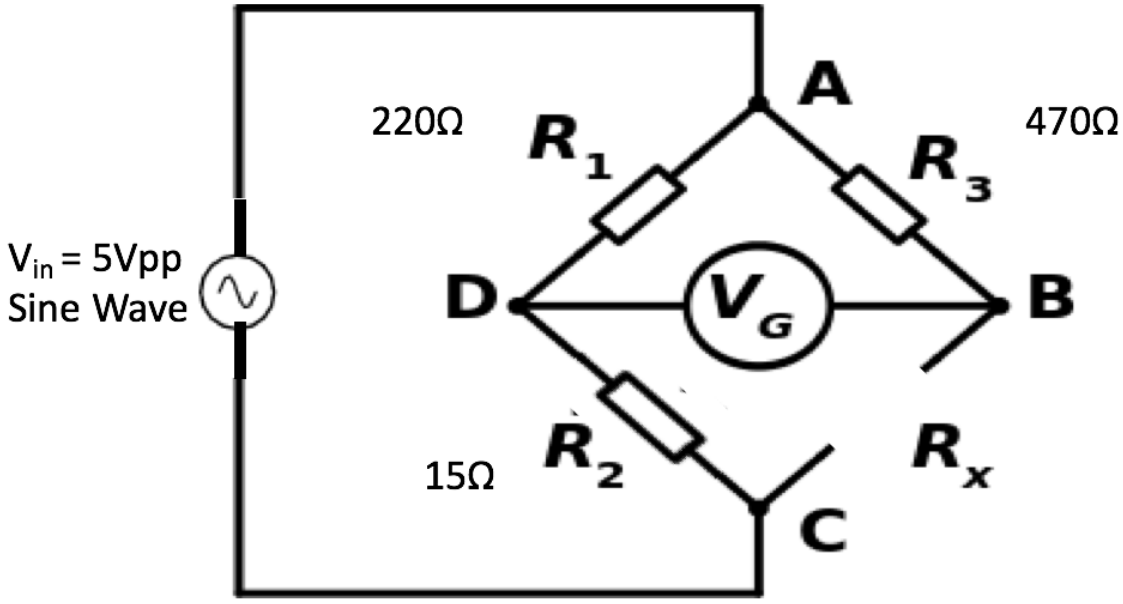

Figure 3-23: Wheatstone bridge test setup using two electrodes for an unknown tissue/fluid resistance measurement (R_x). where V_g is the measured output voltage, V_{in} is the input waveform (sign wave, 5-volt peak-to-peak) R_1, and R_3 were changed to 220Ω, and 470Ω respectively while R_2 was maintained at 15Ω.

Figure *3-24* shows the plot of PlasmaLyte –A measured resistance vs. Frequency. From the figure, it should be noted that at a frequency of 1KHz, PlasmaLyte–A had a measured resistance of 300 Ω. **Figure *3-25*** displays the measured resistance of pork muscle resistance vs frequency. It can be seen that at a frequency of 1kHz, the measured resistance of muscle was approximately 475 Ω. A frequency of 1 KHz is ideal since it produces a measurable separation between tissue/fluid quantity being measured. As the frequency is decreased, the effect of polarization increases (higher measured resistance) since we approach the DC region of operation. Although the selected resistor values produce a separation between the two quantities being measured, the resulting separation was less than desired for a potential accurate measurement technique across a wide range of applications. As a result, other methods of measurement were investigated as described in the next section.

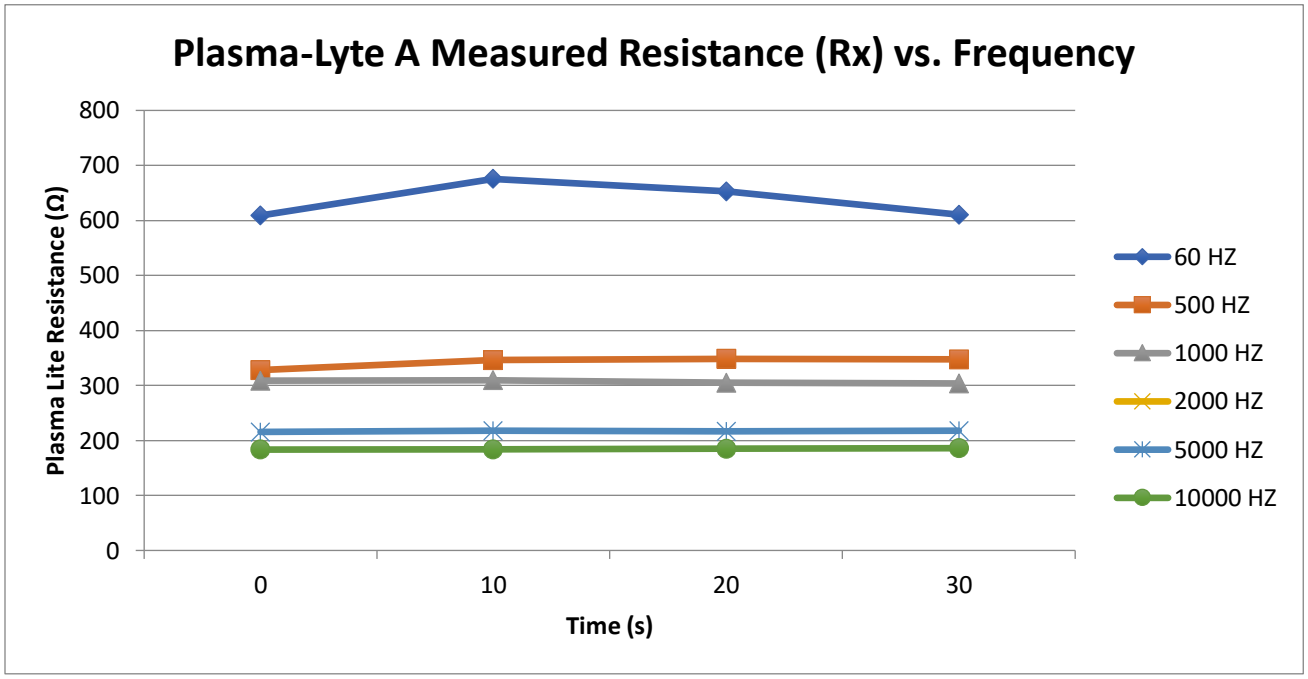

Figure 3-24: Plot of measured Plasma-Lyte A Resistance vs. time for varying frequencies.

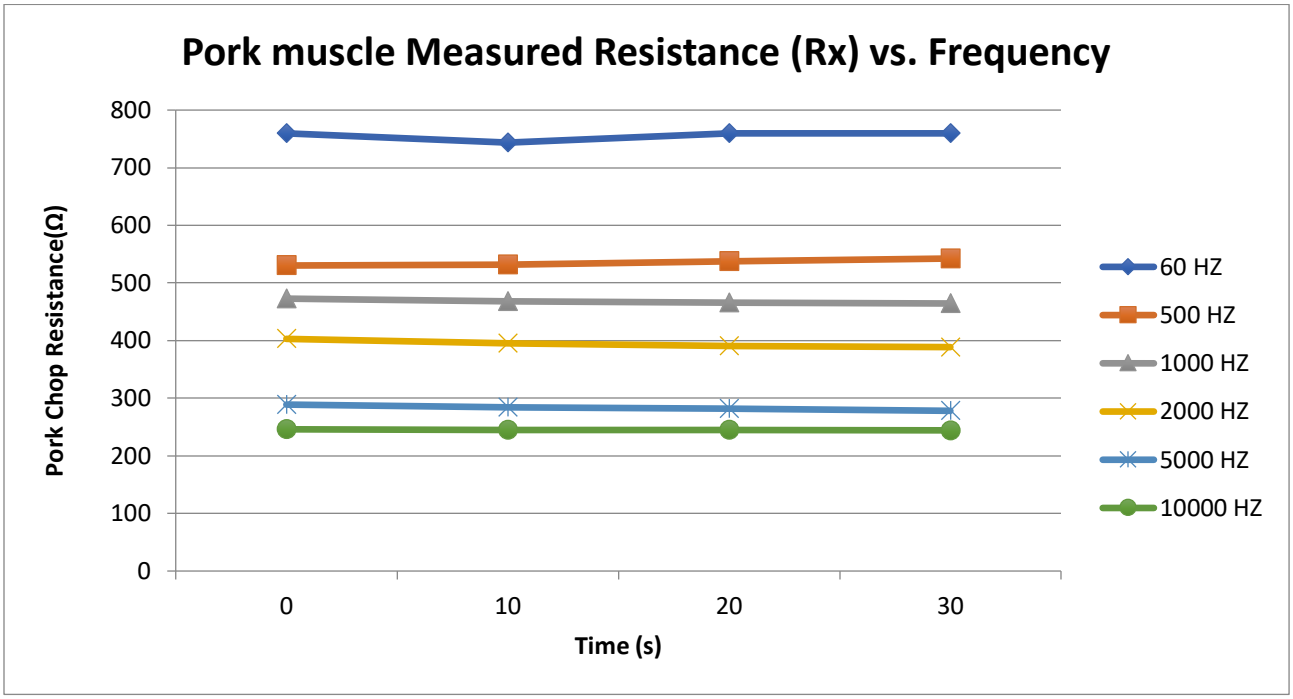

Figure 3-25: Plot of measured pork muscle Resistance vs. time for varying frequencies.

3.2 TRANSIENT MEASURMENT OF TISSUE RESISTANCE

Transient measurement involves the measurement of a time-varying current and voltage resulting from the sudden application of the source (Hambley (2008)). The following sections describe the transient measurement technique and the accompanying circuits (555 oscillator, 741 operational amplifier) used to successfully differentiate between blood and subcutaneous tissue.

3.2.1 TRANSIENT MEASURMENT USING RC TIME CONSTANT

An alternative to using static measurement methods (section 3.1) is to use the time constant of an RC circuit in conjunction with an oscillatory circuit to determine the unknown resistance. **Figure *3-26*** displays a schematic of an RC circuit consisting of a capacitor (C), resistor (R), and a DC voltage source.

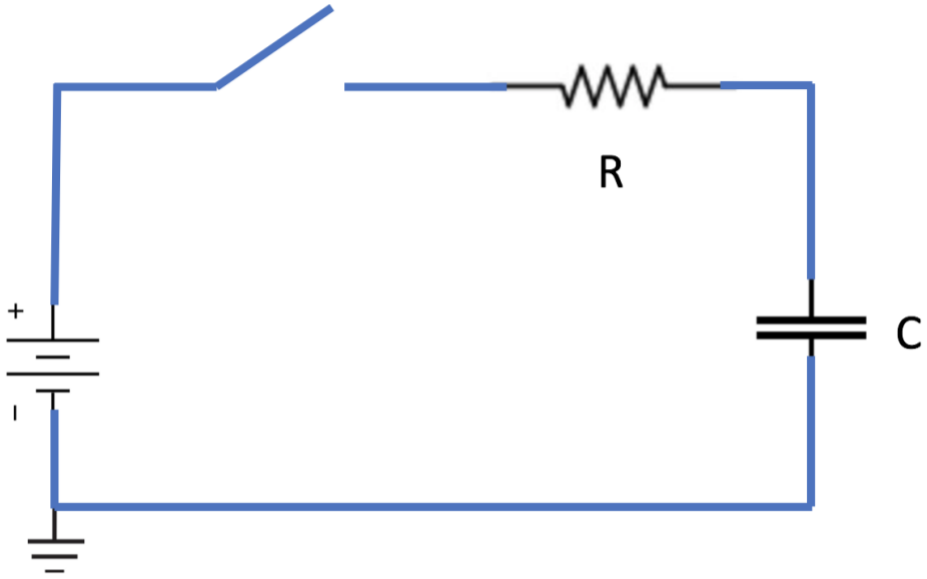

Figure 3-26: schematic of an RC charging circuit consisting of a capacitor (C), resistor (R), and a DC voltage source.

The voltage across the circuit (Equation 3-9) can be derived by using Kirchhoff's voltage law. In the equation, V_s is the source voltage, $R\big(i(t)\big)$ is the voltage across the resistor, and $V_C(t)$ is the voltage across the capacitor.

$$V_s - R\big(i(t)\big) - V_C(t) = 0 \tag{3-9}$$

When the switch in Figure ***3-26*** is initially closed at time t=0, the capacitor is initially uncharged ($V_C(t) = 0$), thus solving Equation 3-9 for $i(t)$, the charging current is found by using Equation 3-10.

$$i(t) = \frac{V_S}{R} \tag{3-10}$$

The rate of charge within the capacitor is initially high , but it slows down gradually as time progresses since the voltage in the capacitor begins to equalize with the source voltage (**Figure *3-27***).

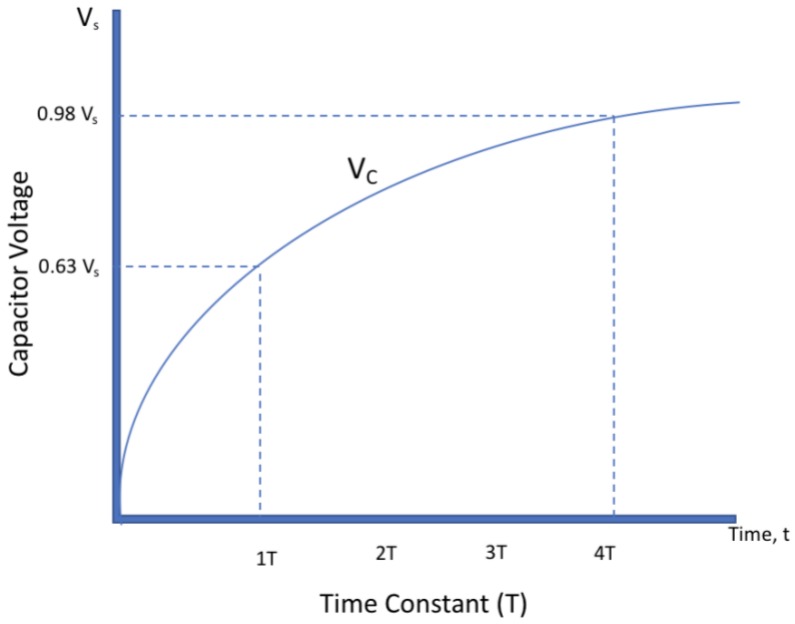

Figure 3-27: plot of capacitor voltage (Vs) vs. time for an RC charging circuit.

The voltage across the capacitor within a given time period can be found by using by Equation 3-11. In the equation, V_s is the supply voltage, V_C is the voltage across the capacitor, t is the elapsed time since the application of the supply voltage, and RC is the time constant of the charging circuit.

$$V_C = V_s(1 - e^{-t/RC}) \quad (3\text{-}11)$$

The amount of time required to charge the capacitor is determined by the time constant. One time constant is defined as the amount of time taken for the capacitor to reach 63% of its steady-state voltage (Hambley (2008). The capacitor is considered to have reached 98% of its maximum value after four time constants have passed (Hambley (2008). The time constant for the circuit in Figure ***3-26*** is determined by applying Equation 3-12. In the equation, τ is the time constant, R is resistance (Ω), and C is the capacitance.

$$\tau = R \times C \quad (3\text{-}12)$$

While the capacitor is charging, the current within the capacitor has an inverse relationship (Figure ***3-28***). Initially when the switch is closed in Figure ***3-26*** there is a significant amount of current introduced into the circuit as the voltage in the capacitor experiences the greatest increase during the first time constant (Figure ***3-27***).

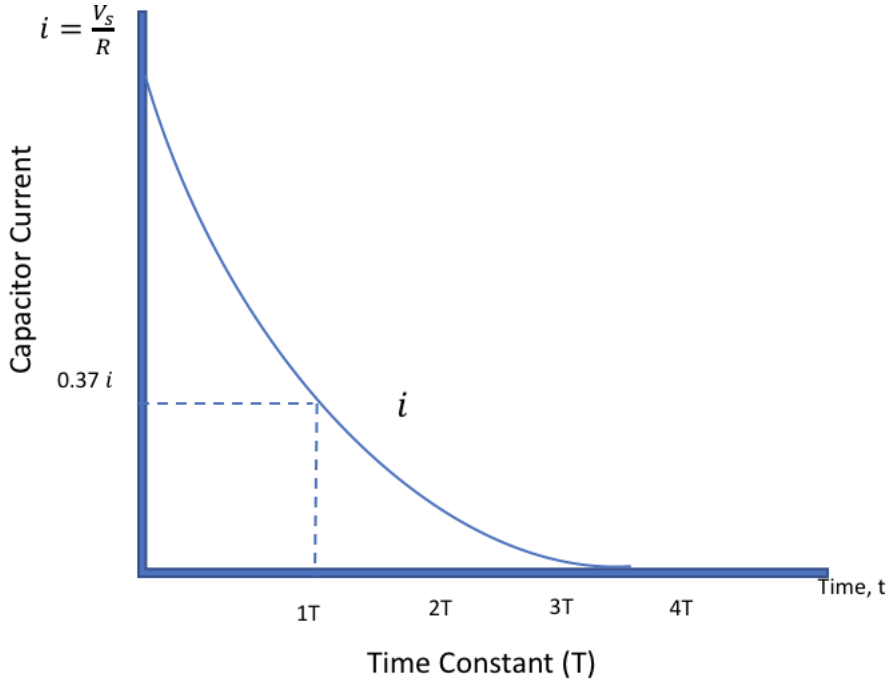

Figure 3-28: Plot of capacitor current (i) vs. time for an RC charging circuit.

The amount of current in the capacitor at any point in the charging cycle is found by applying Equation 3-13. In the equation, I_0 is the initial current found by applying Equation 3-10.

$$i(t) = I_0 e^{-\frac{t}{RC}} \tag{3-13}$$

Once the capacitor is fully charged and the voltage source is removed and replaced with a short-circuit to ground (Figure ***3-29***) the capacitor begins to discharge. The rate of discharge within the capacitor is initially high (loses 63% of its initial charge within one time constant), but it slows down gradually as time progresses (**Figure *3-30***). The capacitor is considered to have discharged 98% of its maximum value after four-time constants have passed.

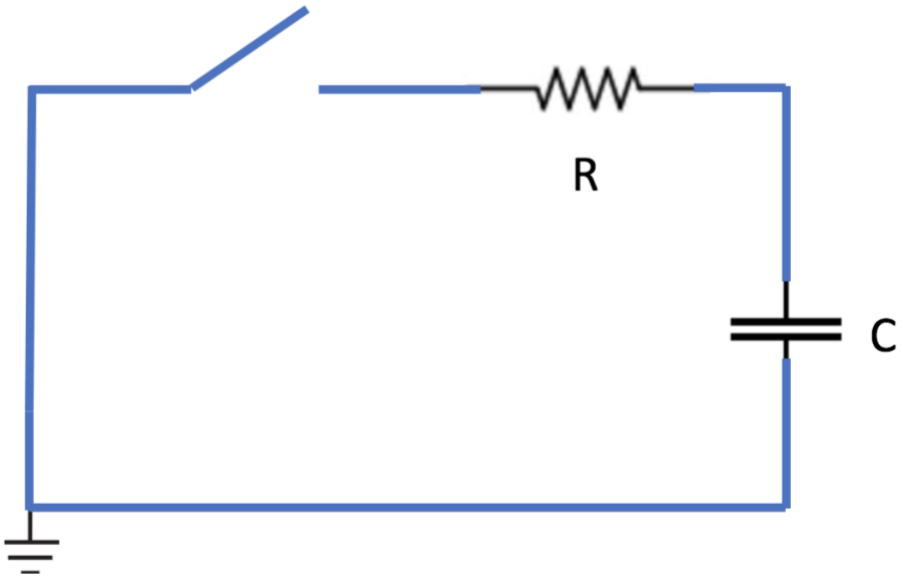

Figure 3-29: Schematic of an RC discharge circuit consisting of a capacitor (C), resistor (R).

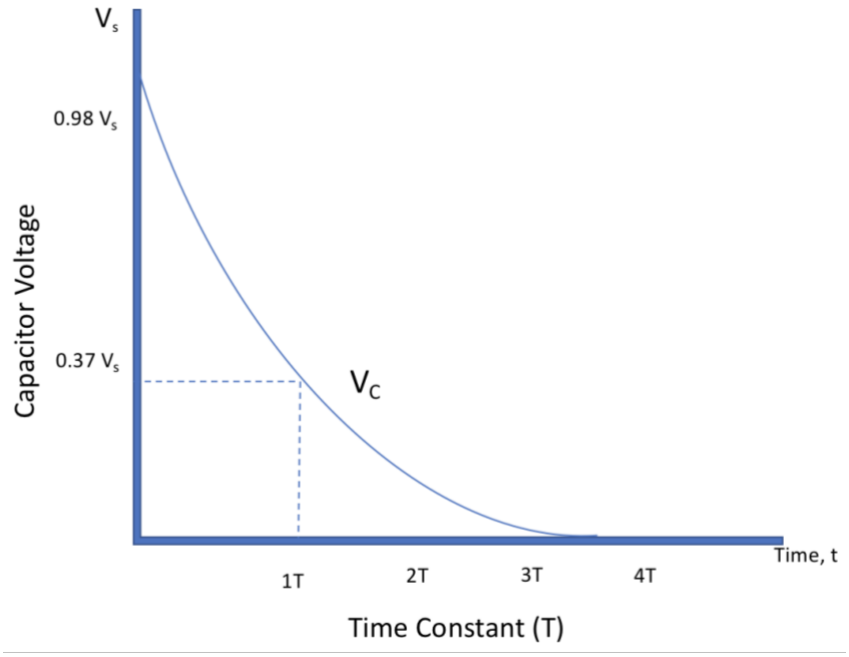

Figure 3-30: Plot of capacitor voltage (Vs) vs. time for an RC discharge circuit.

The voltage across the capacitor at any point during the discharge cycle can be found by using Equation 3-14, where V_s is the initial voltage on the charged capacitor. The amount of time required to discharge the capacitor is determined by the time constant as described by Equation 3-12.

$$V_c = V_s e^{\frac{-t}{RC}} \tag{3-14}$$

For the present application, successful differentiation between subcutaneous tissue and blood can be achieved by combining the RC charging and discharging circuit with an oscillator. An oscillatory circuit continuously charges and discharges the capacitor once initiated. Thus, by substituting the resistance with unknown biological quantities (fat, blood) it is possible to create an oscillatory circuit whose rate of oscillation changes depending on the resistance of the circuit.

There were two types of oscillatory circuits used (555 timer, and 741 op-amp). The operations of each integrated circuits (IC's) are discussed below in greater detail along with their accompanying result.

3.2.1.1 555 TIMER THEORY OF OPERATION The first oscillatory circuit employed was the 555-timer chip. The 555 timer is a monolithic timer invented by Hans R. Camenzind in 1971; following its invention, the first commercial version of the timer was subsequently released by Signetics corporation in 1972(Fuller (2012) The timer chip is most often used for timing and pulse generation circuitry. Internally, 555-timer chip (Figure 3-31) consists of three 5 KΩ resistors, two transistors, two comparators, flip-flop and an output stage.

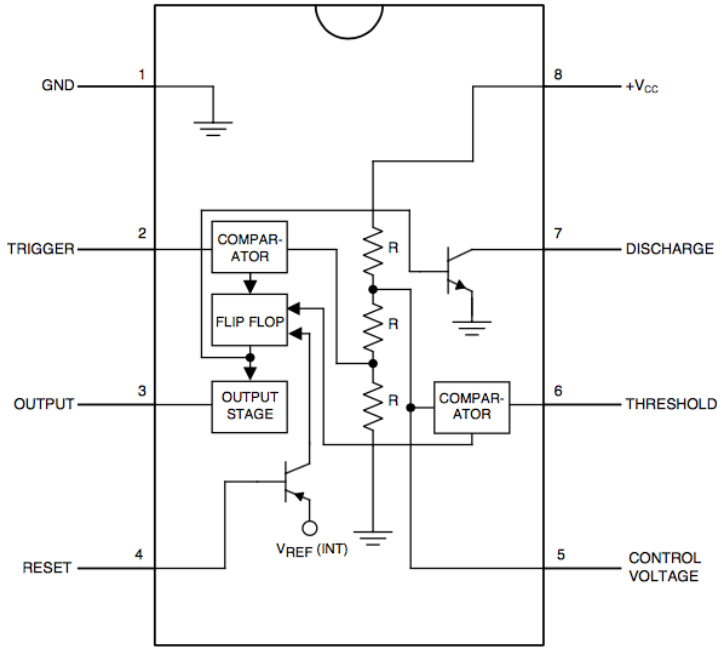

Figure 3-31: Internal circuit diagram of a 555 timer chip.

The chip has two modes of operation, mono-stable (timer) and astable (oscillator). In mono-stable mode, the timer outputs a single pulse of current for a certain length of time; often referred to as a one shot pulse (David G. Alciatore (2007)). An example of mono-stable circuit is a push button LED. Once the button is pressed, the LED lights up for a certain amount of time and turns off afterwards. On the other hand, in astable mode the timer acts as a free running oscillator that constantly produces a square wave(David G. Alciatore (2007). An example of astable oscillation is LED's blinking at a fixed rate. In our application, the timer was operated as an oscillator in astable mode to help counteract the effect of polarization. Figure ***3-32*** displays the circuit diagram of a 555-timer chip in astable mode.

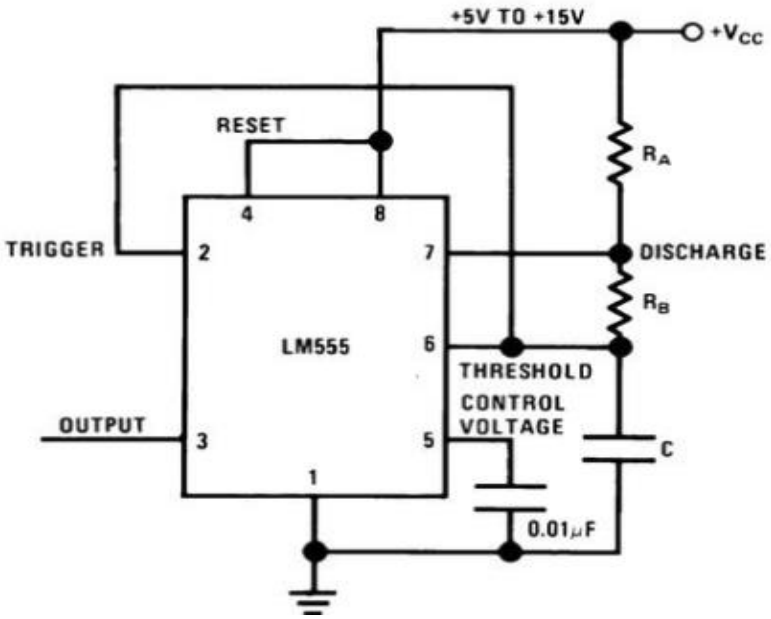

Figure 3-32: Circuit diagram of a 555 chip in astable mode.

In astable mode, a voltage (Vcc) is provided across the resistors R_A and R_B, which in turn starts charging the capacitor. The values of R_A and R_B can be adjusted to effectively alter the time constant of the system (Section 3.2.1), thereby altering the charging and discharging time of

the overall system. Once the capacitor reaches ~2/3 of the supply voltage, it discharges through the transistor in pin 7 and R_B. Once discharged the capacitor starts re-charging through resistors R_A and R_B. Each component of the 555 operation is described in the following paragraphs.

While the capacitor is charging, the first comparator inside the timer chip (Figure ***3-31***) connected to pin 2 compares the input voltage from the trigger pin to a reference voltage of 1/3 Vcc. At the same time, the second comparator compares the input voltage from the threshold pin (pin 6) to a reference voltage of 2/3 Vcc from the voltage divider(Basics (2017)).

A comparator circuit is an integrated circuit chip (IC) that is based on the fundamentals of an operational amplifier (op-amp). In this configuration the IC is used to determine whether one signal is greater than the other. The comparator consists of an op-amp circuit without a feedback, which results in the output remaining at the positive or negative voltage value (saturation) (David G. Alciatore (2007). The output of the comparator is given by Equation 3-15.

In Equation 3-15, V_{out} is the comparator output (output 1 or 2), $\pm V$ is the supply voltage of the comparator, and V_{ref} is the reference voltage to which V_{in} is being compared.

$$V_{out} = \begin{cases} +V & V_{in} > V_{ref}\ (output\ 1) \\ -V & V_{in} < V_{ref}\ (output\ 2) \end{cases} \tag{3-15}$$

When the input voltage (V_{in}) is higher than the reference voltage (V_{ref}) the comparators voltage V_{out} is equal to +V ($output\ 1$) otherwise if V_{in} is lower than the reference voltage (V_{ref}), then the comparator voltage is equal to $-V$ ($output\ 2$). In the 555 chip, the output voltage values from the comparator are equivalent to binary logic levels (logic 1 if +V, and logic 0 if -V). After the conversion, the output of the comparators are sent to the flip-flop.

A flip-flop is a sequential logic device that has the ability store and switch between two binary stages (David G. Alciatore (2007)). Figure ***3-33*** displays a fundamental RS flip-flop. In the figure, R is the reset input, S is the set input, Q and $\bar{Q}$ are the outputs where one is the inverse of the other (David G. Alciatore (2007)).

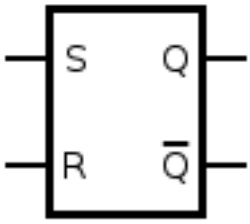

Figure 3-33: Schematic of a RS flip-flop.

Flip flops have four rules of operation that are described below.

1) The output of the flip-flop remains unchanged as long as the S and R input are both 0.

2) When S =1 and R = 0, the flip-flop is set to $Q = 1$ and $\bar{Q} = 0$.

3) when S is 0 and R is 1, the flip-flop reset to $Q = 0$ and $\bar{Q} = 1$.

4) S and R cannot be set to 1 simultaneously since the output will be unpredictable.

Thus, based on the rules of operation, the flip flop produces either a logic 1 or a logic 0 (switching states) based on the input values from the comparator. Lastly, the signal from the flip-flop travels to the output stage of the 555 chip. When the output stage receives a logic input of 0 from the flip-flop, it outputs 5V(Basics, 2017), causing the capacitor to charge. Subsequently, when the output stage receives a logic input of 1, pin 3 is connected to ground, and the transistor in pin 7 is opened allowing the capacitor to discharge (Ghassaei (2012)). This process

continuously repeats while the timer is operating in astable mode producing a clocking signal outputted via pin 3.

The frequency of the oscillating signal depends on the time constant of the attached RC circuit, which depends on the resistances in the circuit. By configuring the system such that one of the resistances is the tissue in question, the signal frequency can be measured to determine tissue or to effectively determine tissue type. In this application, the goal is to differentiate between subcutaneous tissue and blood.

Figure ***3-34*** displays a schematic of the 555 timer in astable mode. In the figure, two electrodes are used such that the material between them replaces R_B and becomes the effective resistance $R_{effective}$. In the application in this thesis, the material will be air or body tissue (e.g. subcutaneous fat, muscle, or blood).

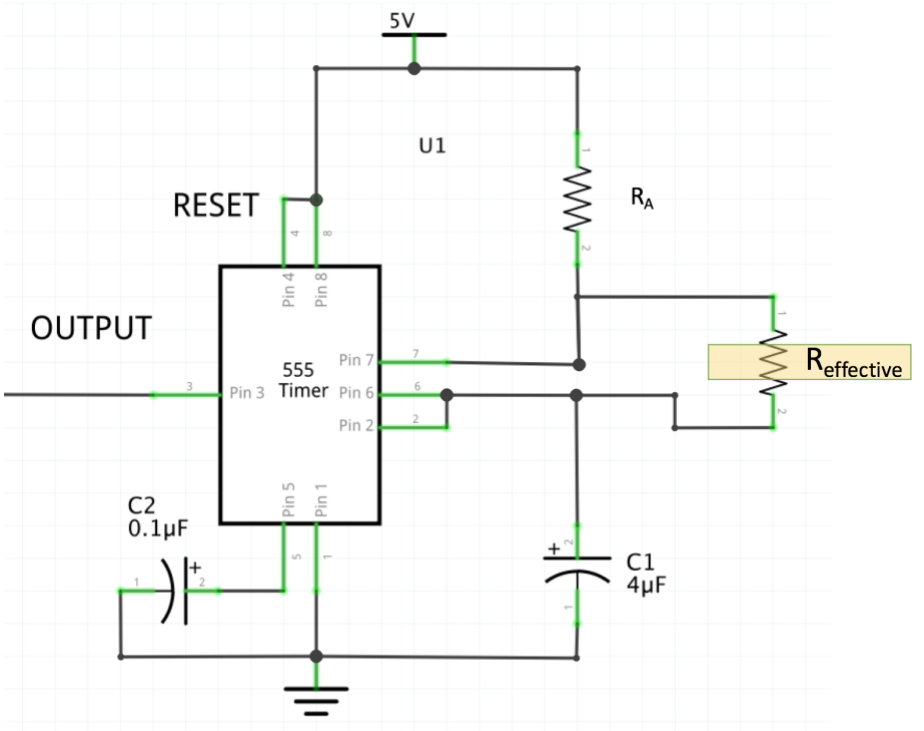

Figure 3-34: Schematic of the 555 timer in astable mode where two electrodes replaces R_B and becomes the effective resistance $R_{effective}$.

As previously mentioned, when put in astable configuration the 555 timer operates as a free running oscillator constantly charging and discharging the capacitor. Initially when the power is applied, the capacitor is uncharged. The time required to charge the capacitor to 2/3 V_{cc} (upper comparator limit) can be found by applying Equation 3-11. Applying the initial conditions of the circuit (capacitor voltage $V_0 = 0$), we obtain Equation 3-16. In the equation, R_A and $R_{effective}$ are resistors (Ω) in series with the capacitor C (farads), t is the time in seconds required to charge the capacitor. V_0 is the initial voltage across the capacitor and V_{cc} is the voltage applied to the system.

$$\frac{2}{3}V_{CC} = (V_{cc} - V_0)\left(1 - e^{\frac{-t}{(R_A+R_{effective})C}}\right) \tag{3-16}$$

Solving for t the time required to charge the capacitor to 2/3 V_{cc} when the power is turned on is given by Equation 3-17. Since the voltage V_0 across the capacitor is initially 0, the equation further simplifies as given by Equation 3-18.

$$t = -\left(R_A + R_{effective}\right)C \times \ln\left(\frac{\frac{1}{3}V_{cc}}{(V_{cc}-V_o)}\right) \tag{3-17}$$

$$t = 1.1(\left(R_A + R_{effective}\right)C \tag{3-18}$$

When the capacitor reaches 2/3 V_{cc} the upper comparators switches in state which enables the discharge pin (pin 7) leading to the capacitor to discharge to 1/3 V_{cc} through $R_{effective}$ switching the output signal to low. The time required to discharge the capacitor to 1/3 V_{cc} is found by

applying Equation 3-14. Applying the intermediate conditions of the circuit (capacitor charged to 2/3 V_{cc}), we obtain Equation 3-19. In the equation, t_{low} is the time in seconds required to discharge the capacitor C to $\frac{1}{3}V_{cc}$ through the resistor $R_{effective}$ (Ω).

$$\frac{1}{3}V_{cap} = \frac{2}{3}V_{Cap}\left(e^{\frac{-t_{low}}{(R_{effective})C}}\right) \tag{3-19}$$

Solving Equation 3-19 for the time t_{low} yields Equation 3-20, which allows for the determination of the time required to discharge the capacitor from 2/3 V_{CC} to 1/3 V_{CC}.

$$t_{low} = 0.7R_{effective}C \tag{3-20}$$

After the capacitor is discharged to 1/3 V_{cc} the lower comparator switches states. Unlike the first cycle when power is applied to the circuit, (Equation 3-17) the capacitor never fully discharged and continuously charges and discharges between 2/3 and 1/3 $V_{cc.}$ Thus, Equation 3-21 is obtained by replacing V_0 in Equation 3-15 with 1/3 V_{cc} and solving for the time t. The amount of time the waveform spends high (t_{high}) is given by Equation 3-22.

$$t = -(R_A + R_{effective})C \times \ln\left(\frac{\frac{1}{3}V_{cc}}{\left(V_{cc}-\frac{1}{3}V_{cc}\right)}\right) \tag{3-21}$$

$$t_{high} = 0.7(R_A + R_{effective})C \tag{3-22}$$

The total period of the waveform T is found by adding the high and low time together (Equation 3-23). Thus, applying Equation 3-23, the total time period of the output waveform is given by Equation 3-24.

$$T = t_{low} + t_{high} \tag{3-23}$$

$$T = 0.7(R_A + 2R_{effective})C \tag{3-24}$$

Once the time period of the output waveform is known, the frequency of the wave can be calculated by applying Equation 3-25.

$$f = \frac{1}{T} \tag{3-25}$$

Applying Equation 3-25, the relationship between the rectangular wave frequency and the unknown resistance value ($R_{effective}$) of the tissue/fluid is described by Equation 3-26. Solving Equation 3-26 for $R_{effective}$ as shown by Equation 3-27 provides an expression for the unknown resistance as a function of the measured frequency. The nominal output frequency of the system is controlled by selecting the values of the resistor R_A and capacitor C. Choosing a large capacitor value increases the overall cycle time of the system, which in turn reduces output frequency. While increasing R_A increases the high time (the amount of time spent at the top of the rectangular wave) leaving the low time (the amount of time spent at the bottom of the rectangular wave) unaffected (Equation 3-23). Based on the chosen value of R_A and the measured value of $R_{effective}$ the duty cycle can be calculated by using Equation 3-28. The duty cycle is used to describe the percentage of time a digital signal is high during given time

interval(Ghassaei (2012)). If the duty cycle of the signal is too high, then polarization error would re-surface. Thus, the value of R_A must be chosen accordingly to avoid erroneous results.

$$f = \frac{1}{T} = \frac{1.44}{(R_A + 2R_{effective})C} \tag{3-26}$$

$$R_{effective} = \frac{1}{2}\left(\frac{1.44}{fC} - R_A\right) \tag{3-27}$$

$$Duty\ cycle = \frac{(R_A + R_{effective})}{(R_A + 2R_{effective})} * 100 \tag{3-28}$$

Testing and Results. Prior to performing in-vitro testing, the accuracy of the 555 timer in astable mode (Figure ***3-34***) was tested. For this test, R_A was varied from 240 Ω-4.6 kΩ, while the values of $R_{effective}$ and C were held constant at 99.5 Ω□, and 0.972 µF respectively. These values were determined by making measurments with a multimeter. The value for $R_{effective}$ was held constant at 99.5 Ω, since it represented the lowest resistance value (blood) the electrodes encounter. Similarly, the capacitor value was chosen to be 0.972 µF since it yielded a measured resistance value ($R_{effective}$) similar to the theoretical (Table 1). If the capacitor was increased in value, the total cycle time for the waveform increased leading to erroneous measured resistance values.

During the experiment, the output frequency due to changing values of R_A was recorded every ten seconds up to sixty seconds. These values were then substituted into Equation 3-27 to determine the equivalent resistance values of $R_{effective}$ (Figure **3-35**-*Figure* **3-36**). From the figures,

it can be seen that the measured values of $R_{effective}$ ranged from 100 Ω-110 Ω resulting in a maximum error of 10%. Theoretically, pure resistors should produce a perfect square wave.

Figure **3-37** shows an output waveform from the 555 IC. As can be seen from the figure, there is a small variation when the chip switches states from low to high which leads to the error in measurement. Thus, the error in pure resistor measurement is associated with IC manufacturing.

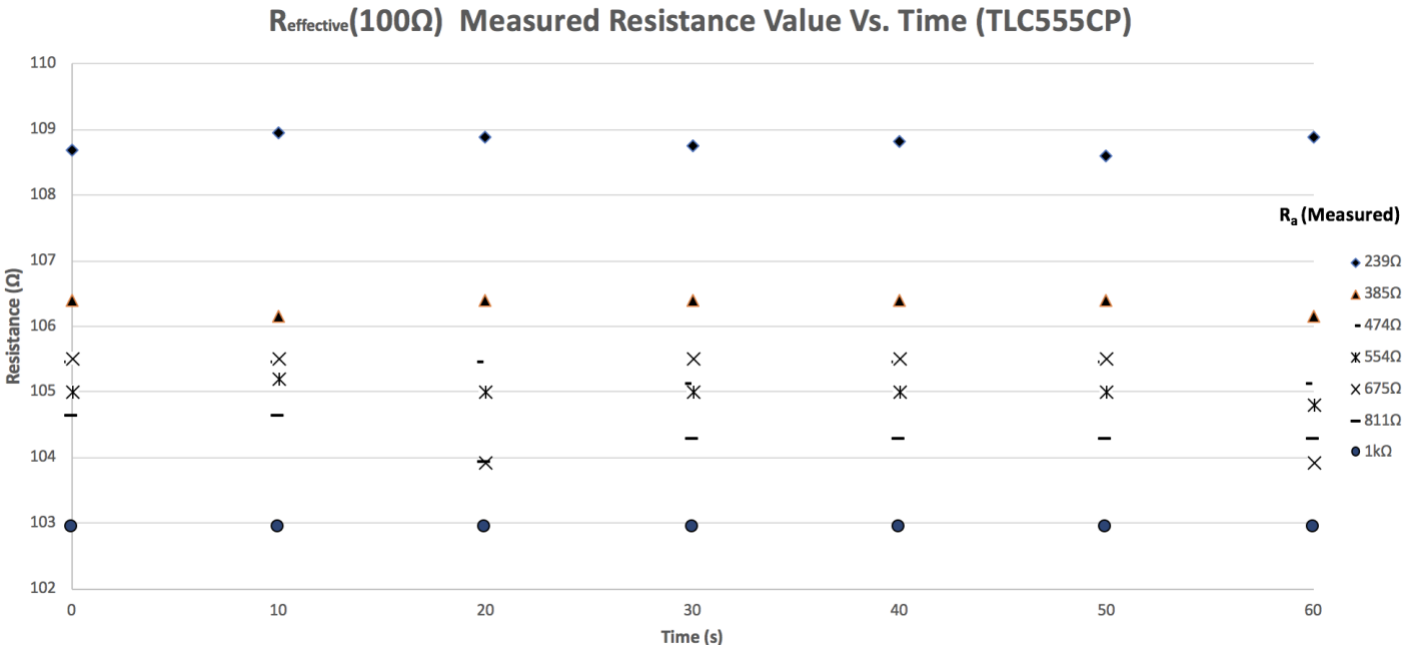

Figure 3-35: Equivalent R_b resistance value Vs. Time for R_A values varying from 239Ω-1kΩ.

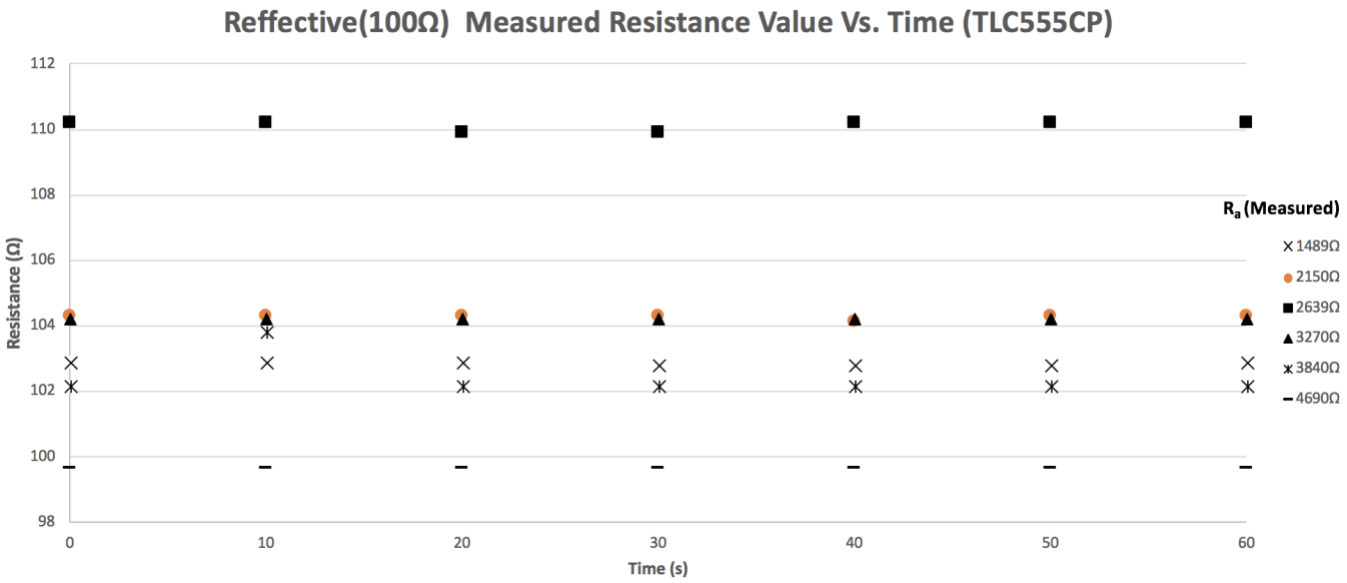

Figure 3-36: Equivalent R_b resistance value Vs. Time for $R_{A\ values}$ varying from 1489Ω-4690Ω.

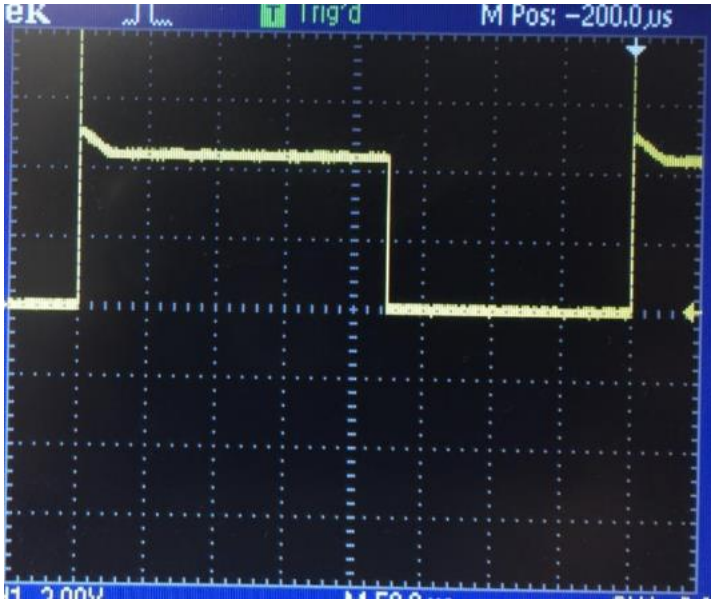

Figure 3-37: Output waveform from 555 timer in astable mode.

The corresponding duty cycle, calculated $R_{effective}$, and percent error associated with each value of R_A is shown in Table 2. From the table, it can be seen that the duty cycle goes above 90% when R_A is increased above 1kΩ. Duty cycle above 90% is not desired when the needle is in contact with tissue and blood. This is so because the effect of polarization begins to re-emerge at higher duty cycles.

Table 2: Duty cycle of 555 timer chip in astable mode for varying R_A values, while the values of R_b and C were kept constant at 99.5Ω and 1 μF respectively.

R_a (Ω Measured)	Duty Cycle %	R_b (Ω Calculated)	% error
239	72.7	108.98	9.53
385	80	106.43	6.96
470	82.8	105.45	5.98
554	84.6	105.0	5.53
675	86.9	105.53	6.06
811	88.7	104.65	5.17
984	90.4	103	3.52
1489	93.3	102.93	3.45
2150	95.3	104.33	4.85
2639	96.1	110.23	10.78
3270	96.8	104.23	4.75
3840	97.2	102.22	2.73
4690	97.7	99.68	.18

Subsequently, the circuit setup was tested by submerging two electrodes (two separate copper wires) into Plasma-Lyte A solution for the various R_A values (**Figure *3-38***). From the plot, it can be seen that as R_A increases, the measured resistance of the Plasma-Lyte A solution subsequently increases. This increase is assumed to be due to polarization error which arises due to a high duty cycle. Thus, for our experiments, a capacitor value of 1μF and a resistor value of 555Ω was chosen since these values keep the duty cycle of the overall system below 90%.

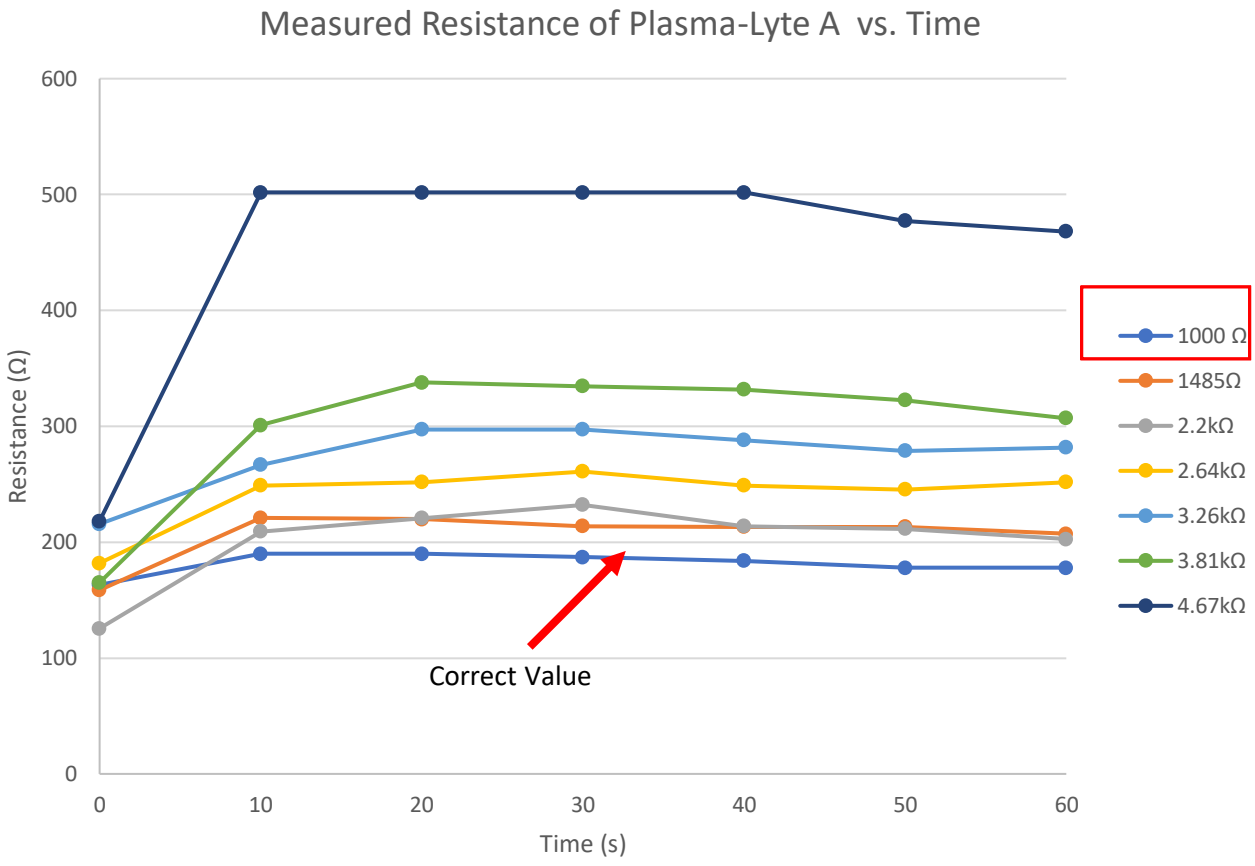

Figure 3-38: Plot of Plasma-Lyte A measured resistance vs. time for varying R_A values using 555 oscillator.

In-vitro test and results. After parameter selection, the first in-vitro test involved inserting two electrodes (two separate wires) into various materials to measure the resistance. Materials tested were pork fat, pork muscle and PlasmaLyte-A.

Although subcutaneous tissue behaves as fat, muscle was tested to account for the extreme cases such as a "blown vein" which occurs when the user advances the needle through the vein into surrounding tissue (muscle). The ability to differentiate between muscle and blood would enable the user to be notified if the needle has advanced beyond the vein.

Figure ***3-39*** shows example photos of the in-vitro test of the various materials using two electrodes, which served as proof of concept for differentiating between subcutaneous tissue and blood. During the trial, wires that made up the two electrodes were submerged in Plasma-Lyte A (Figure ***3-39***a) solution for one minute, and the frequency output of the oscillator circuit was recorded every ten seconds. Subsequently, the wires were used to puncture pork fat (Figure ***3-39***c) and muscle (Figure ***3-39***b) for one minute, and the output frequency of the oscillator circuit was recorded every ten seconds. In each trial, the data was collected for one minute to obtain the steady-state values of each material tested. The tests were repeated six times to assess consistency and repeatability of the data in each material. Between each trial, the electrodes were cleaned to avoid erroneous results from contaminated electrodes. The recorded frequency values were converted to resistance using Equation 3-27 described above. Figure ***3-40*** - Figure ***3-42*** display the results of these tests.

In Figure ***3-40*** the graph shows that the measured resistance value of the Plasma-Lyte A solution starts around 140-275Ω and it reaches a steady state value of around 300Ω in five out of the six trials. In Figure **3-41** the graph shows that the measured resistance value of the muscle (pork shoulder) had an initial value of approximately 1400-1800 Ω and the measured resistance

values reached equilibrium between 1600-2200 Ω during the six trials. Figure ***3-42*** displays the plot of the pork fat measured resistance vs. time. From the figure, it can be noted that measured resistance value of the fat had an initial value of approximately 3000-9100 Ω and the measured resistance values reached equilibrium between 3000-10000 Ω during the six trials.

Figure ***3-43*** displays a plot of the mean and standard deviation for the resulting resistance measurements of Plasma-Lyte A vs. muscle vs. fat. From the plot, it can be seen that there is a significant difference between the measured resistances of pork fat, muscle (pork shoulder), and Plasma-Lyte A and the recorded resistance values are stable for the duration of the tests. These results indicate that a timer oscillator circuit is a viable option for discerning between critical materials encountered by a needle when a catheter is placed.

a) 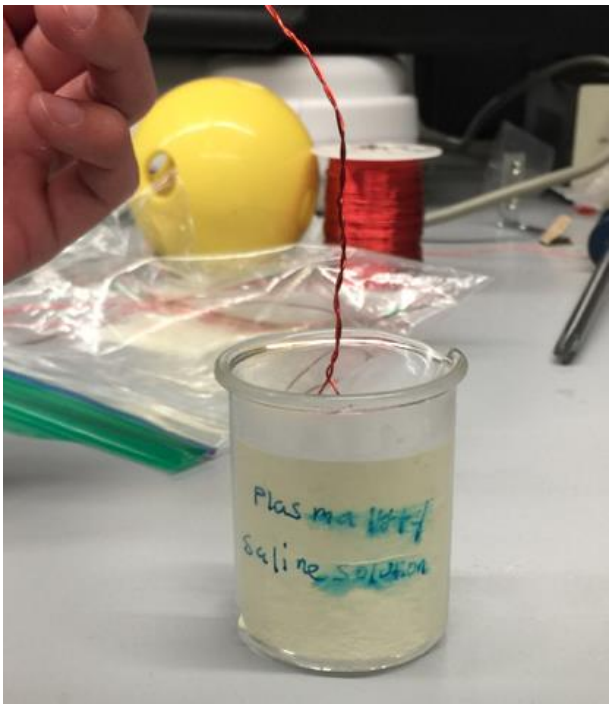

b)

c)

Figure 3-39: Test setup using two wires a) submerged in Plasma-Lyte A b) puncturing pork shoulder muscle c) puncturing pork fat.

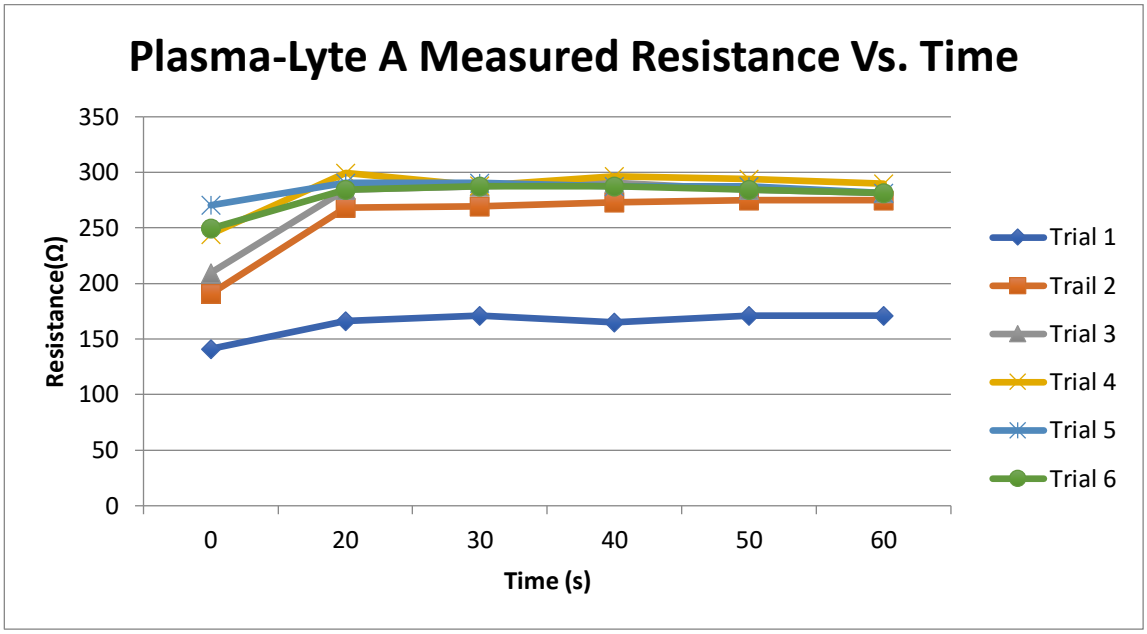

Figure 3-40: Plot of Plasma-Lyte A measured resistance vs. time through six trials using two wire electrodes and 555 oscillator.

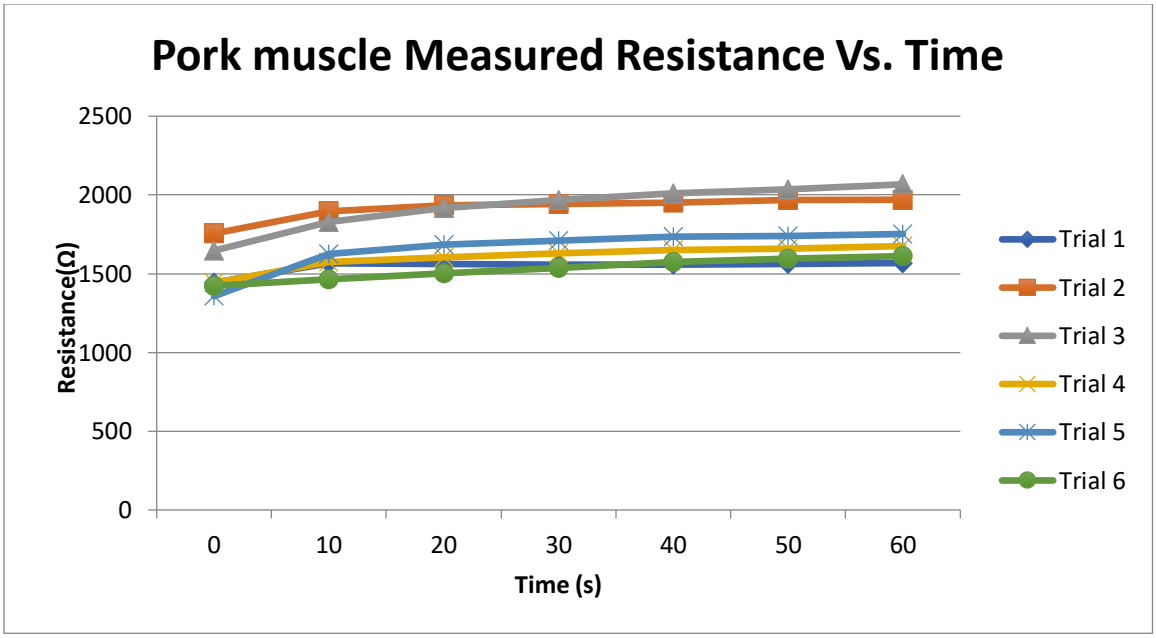

Figure 3-41: Plot of Pork muscle measured resistance vs. time through six trials using two wire electrodes and 555 oscillator.

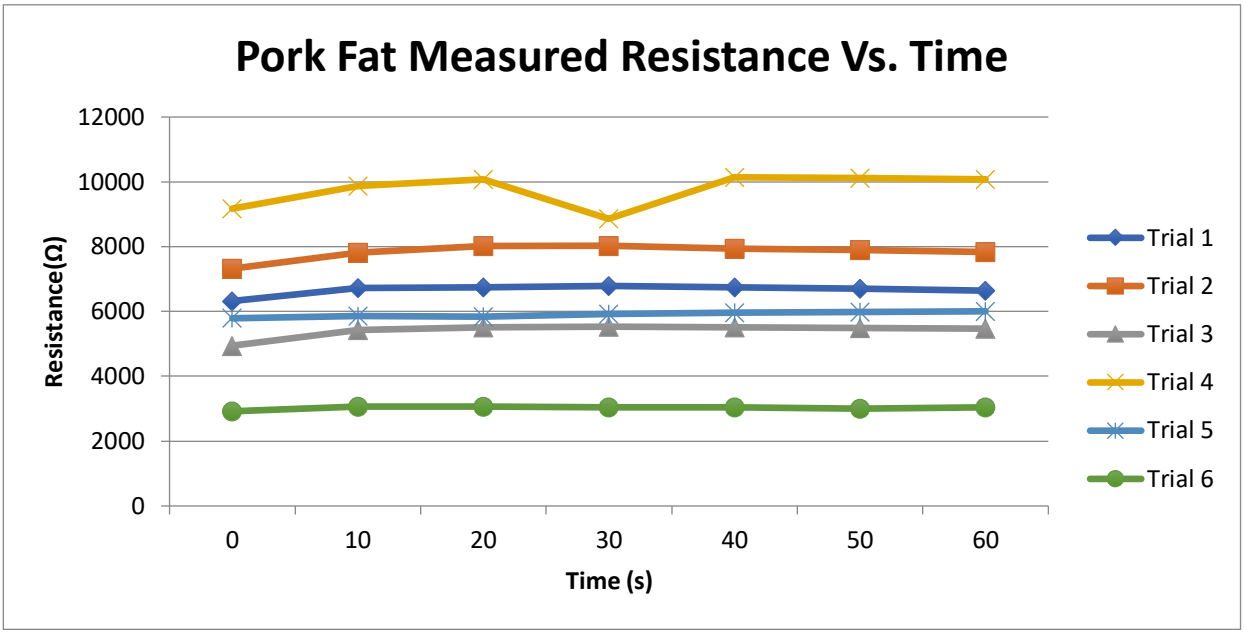

Figure 3-42: Plot of Pork Fat measured resistance vs. time through six trials using two wire electrodes and 555 oscillator.

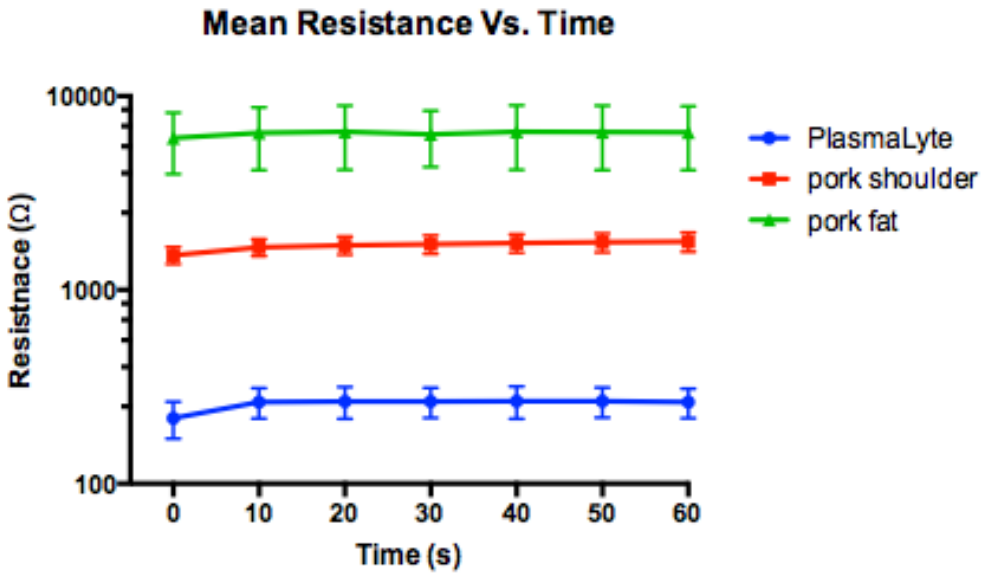

Figure 3-43: Mean and standard deviation for the resulting measured resistance measurements of Plasma-Lyte A vs. muscle vs. fat using two wire electrodes and 555 oscillator.

3.2.1.2 741 OP-AMP THEORY OF OPERATIONS. An alternative approach to the 555 timer is to use an operational amplifier. An operational amplifier (op-amp) is a common integrated circuit which can be combined with external discrete components to create a wide variety of signal processing circuits (David G. Alciatore (2007)). Op-amps serve as the basic building block for amplifiers, filters, comparators, multivibrator and etc. (David G. Alciatore (2007)). Figure *3-44* displays the electrical schematic of an op-amp which has two input terminals (inverting and noninverting) and an output terminal. The op-amp is an active electrical component that requires a connection to an external power device. Unlike standard integrated circuits, the op-amp requires a positive and negative supply voltage to operate. As shown in Figure *3-44* op-amps usually contain a feedback loop which act as a mechanism to stabilize the output; if none were present, the output would be unstable (David G. Alciatore (2007)).

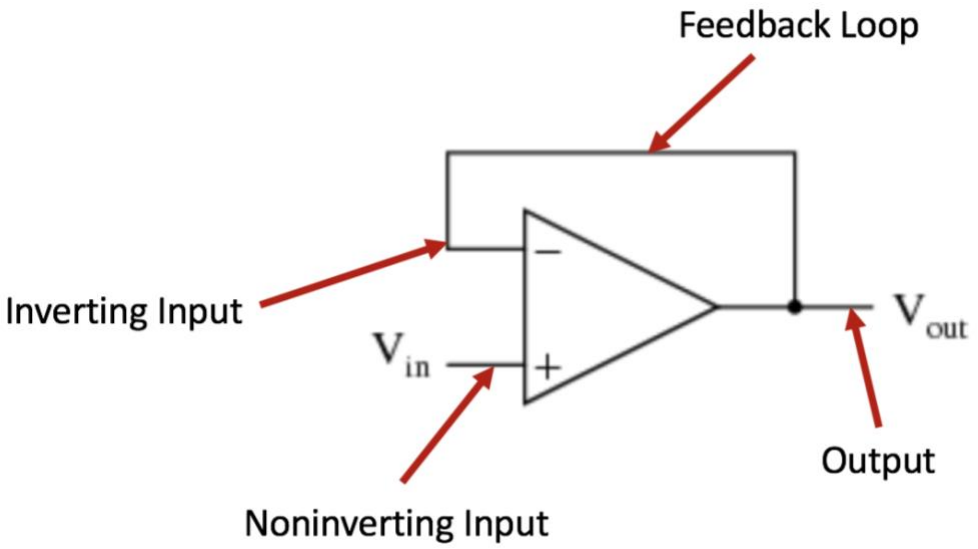

Figure 3-44: Electrical schematic of an Op-amp with a feedback loop.

Op-amps are assumed to be ideal in order to aid in circuit analysis. The ideal op-amp is based on three assumptions that are listed below (David G. Alciatore (2007)).

1) It has infinite impedance at both inputs; hence, no current is drawn from the input circuits. Thus

$$I_+ = I_- = 0$$

2) It has infinite gain. As a result the difference between the input voltages must be 0.

$$V_+ = V_-$$

3) It has zero output impedance. Therefore, the output voltage does not depend on the output current.

For the present application, the op-amp was operated as an astable multivibrator. Figure ***3-45*** displays the schematic of an op-amp as a multivibrator oscillator. The op-amp multivibrator is an astable oscillator circuit that generates a rectangular output waveform using an RC timing network. Poole (2004)

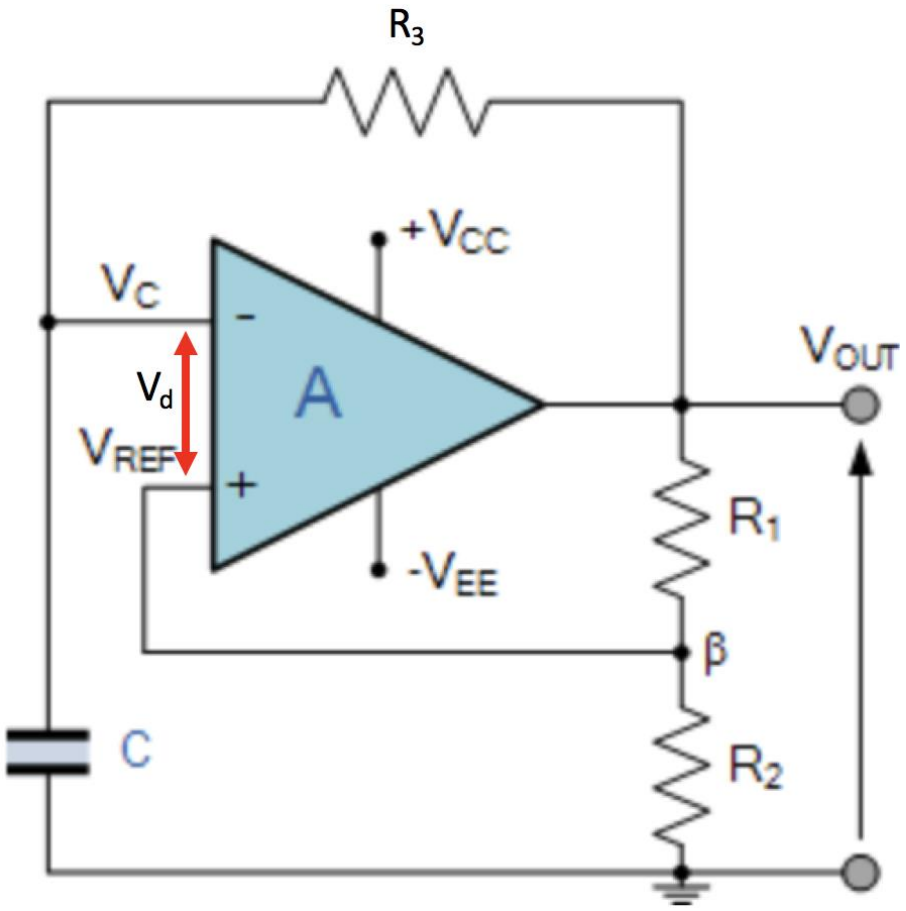

Figure 3-45: Electrical schematic of an Op-amp as a multivibrator oscillator.

The operational amplifier forces the output to operate in the saturation region. Initially when the power is applied, the capacitor is uncharged thus the voltage at the inverting input V_c=0. The reference voltage at the noninverting terminal is found by apply the voltage divider principal (Equation 3-29). In the equation, R_1 and R_2 are resistors, and V_{out} is the output voltage of the amplifier. The equation is further simplified by introducing the feedback factor β (Equation 3-30) which yields Equation 3-31.

$$V_{REF} = \frac{R_2}{R_1+R_2} V_{out} \tag{3-29}$$

$$\beta = \frac{R_2}{R_1+R_2} \tag{3-30}$$

$$V_{REF} = \beta V_{out} \tag{3-31}$$

Thus, the differential voltage (V_d) between the two nodes is given by Equation 3-32. In the equation, V_{REF} is the reference voltage at the noninverting terminal, and V_C is the capacitor voltage at the inverting terminal.

$$V_d = V_{ref} - V_C = +V_{CC} \tag{3-32}$$

When power is initially applied to the circuit, the capacitor charge from the output (positive supply rail $+V_{CC}$) through resistor R_3 to the value of the positive voltage rail ($+V_{CC}$). But before the capacitor can completely charge to $+V_{CC}$ the differential voltage (V_d) between the two terminals becomes greater than at the noninverting terminal ($V_c > V_{REF}$). This forces the op-amp to swing from the positive voltage rail to the negative voltage rail.

At that instant, the capacitor detects the negative voltage and begins to discharge its stored voltage and charge towards $-V_{EE}$. The reference voltage at the noninverting input is found by applying Equation 3-28 as stated previously with only the sign changing. Before the capacitor can completely charge up to $-V_{EE}$ the differential voltage (V_d) between the two terminals (Equation 3-33) switches once more since the capacitor voltage becomes greater than the reference. The change in differential voltage forces the op-amp to swing from negative saturation to positive.

$$V_d = V_{ref} - (-V_C) = +V_{CC} \tag{3-33}$$

Figure ***3-46*** displays the output square wave form of the op-amp. The period of the waveform can be determined from a modified version of Equation 3-13. Equation 3-13 applies when there is no charge stored in the capacitor. But in this application, there is a certain amount of charge left within the capacitor as it cycles between βV_{out} and - βV_{out}.

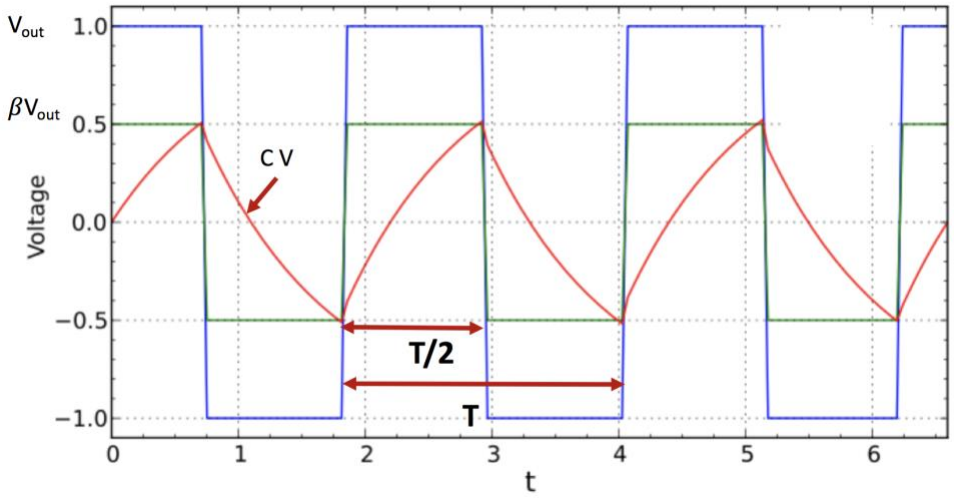

Figure 3-46: Output waveform of a 741 op-amp oscillator where V_{out} (blue) is the output voltage of the op-amp, βV_{out} (green) is the maximum value the capacitor charges to before switching states and CV (red) is the charging and discharging voltage of the capacitor.

Thus Equation 3-34 is used to determine the period of the output waveform. In the equation V_{out} is the output voltage of the op amp. V_{Cinit} is the initial voltage in the capacitor, and V_c^+ is the voltage the capacitor is charging up to.

$$V_c^+ = V_{out} + (V_{Cinit} - V_{out})e^{-t/RC} \tag{3-34}$$

When the op-amp experiences a change in state from negative saturation, the initial voltage (V_{Cinit}) within the capacitor is - βV_{out}. The capacitor wants to charge to the positive saturation value (V_{out}). V_c^+ is the value the capacitor is able to reach (βV_{out}) within the charging cycle (t/2). Substituting these values into Equation 3-34 we obtain Equation 3-35.

$$\beta V_{out} = V_{CC} + (-\beta V_{out} - V_{CC}) e^{-t/(2*R_3 C)} \tag{3-35}$$

Solving Equation 3-35, the period of the output waveform is given by Equation 3-36. The frequency of the waveform is found by taking the inverse of the time period as shown by Equation 3-37.

$$T = 2R_3 C \ ln\left(\frac{1+\beta}{1-\beta}\right) \tag{3-36}$$

$$f = \frac{1}{T} = \frac{1}{2R_3 C \ ln\left(\frac{1+\beta}{1-\beta}\right)} \tag{3-37}$$

For the purpose of this application the resistor R_2 was replaced with the material (e.g. air or tissue) between the electrodes, ultimately to differentiate between subcutaneous tissue and blood. The overall system design along with the results from the op-amp oscillator are discussed in greater detail in the chapter to follow.

4.0 SYSTEM DESIGN

Shown in Figure **4-1** is an assembly of the proposed invention which consists of a detection unit, a disposable catheter unit, and wires providing the electrical connection to the detection unit. Several design combinations have previously been presented for the detector unit (Chapter 3). The current chapter discusses the design for the disposable catheter (needle and guidewire), and the design of the overall system.

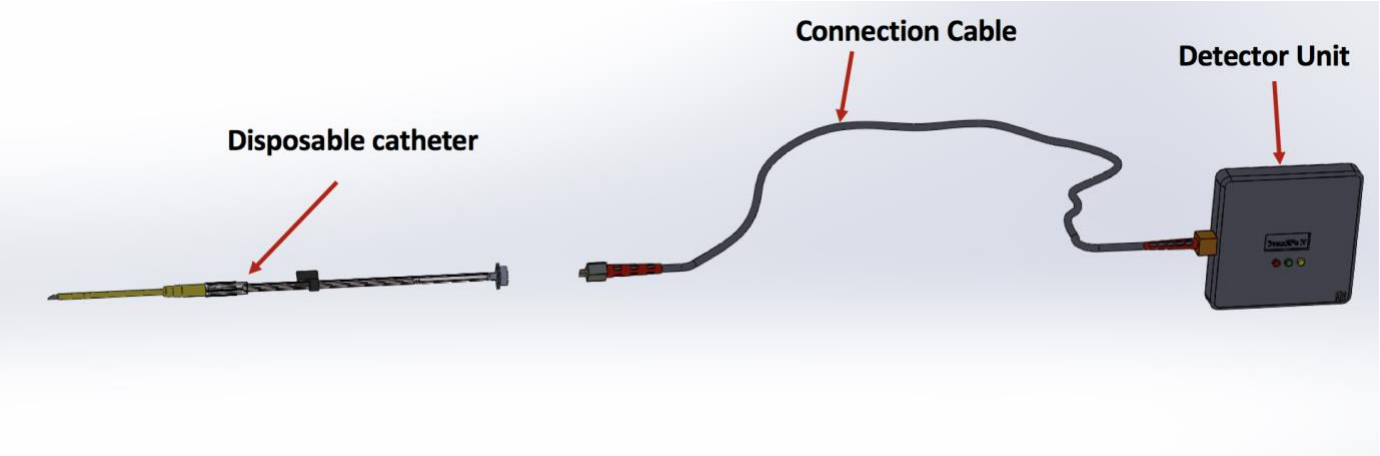

Figure 4-1: Schematic of the overall system.

The disposable catheter unit is a standard PIV modeled after an arterial catheter (Figure ***4-2***) in which a sterile guide wire inside a plastic sheath is fitted. The plastic sheath, provides a pathway for guidewire advancement.

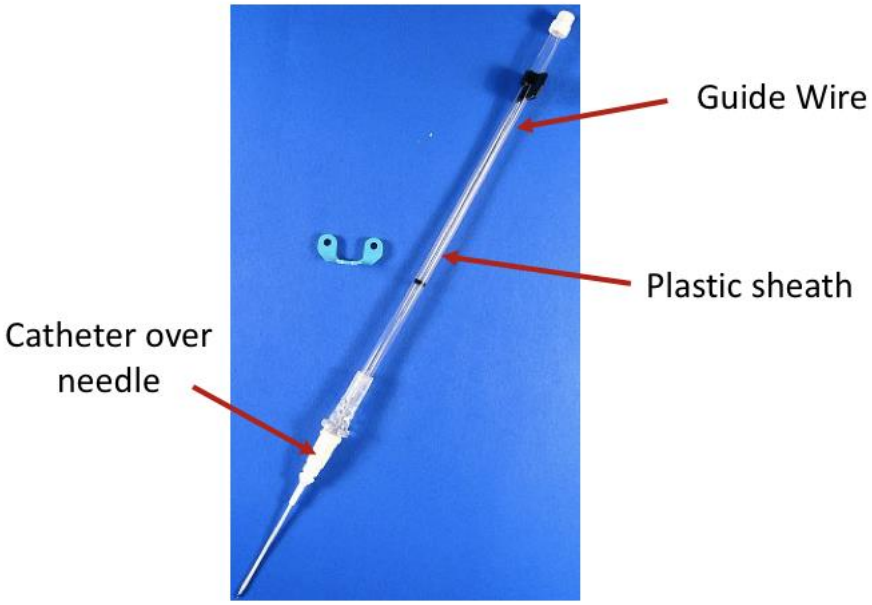

Figure 4-2: Integrated Seldinger Arterial Catheter. A sterile guidewire within a plastic sheath that fits on top of a PIV needle/catheter.

In the present application, the standard IV was modified to act as two electrodes which would allow for the resistance measurement to take place once connected to the detector unit. The IV was modified to house a guidewire that lies inside the needle with its free end located just under the bevel (Figure ***4-3***). The guidewire was chosen such that it is smaller than the inner diameter of the needle (for example a 0.0142" wire (27 gauge) for a 0.016" ID (22 gauge) needle). The tip of the needle is coated with an insulating material (Cyanoacrylate) leaving the outer portion of the needle bare, allowing for the needle housing to act as the first electrode.

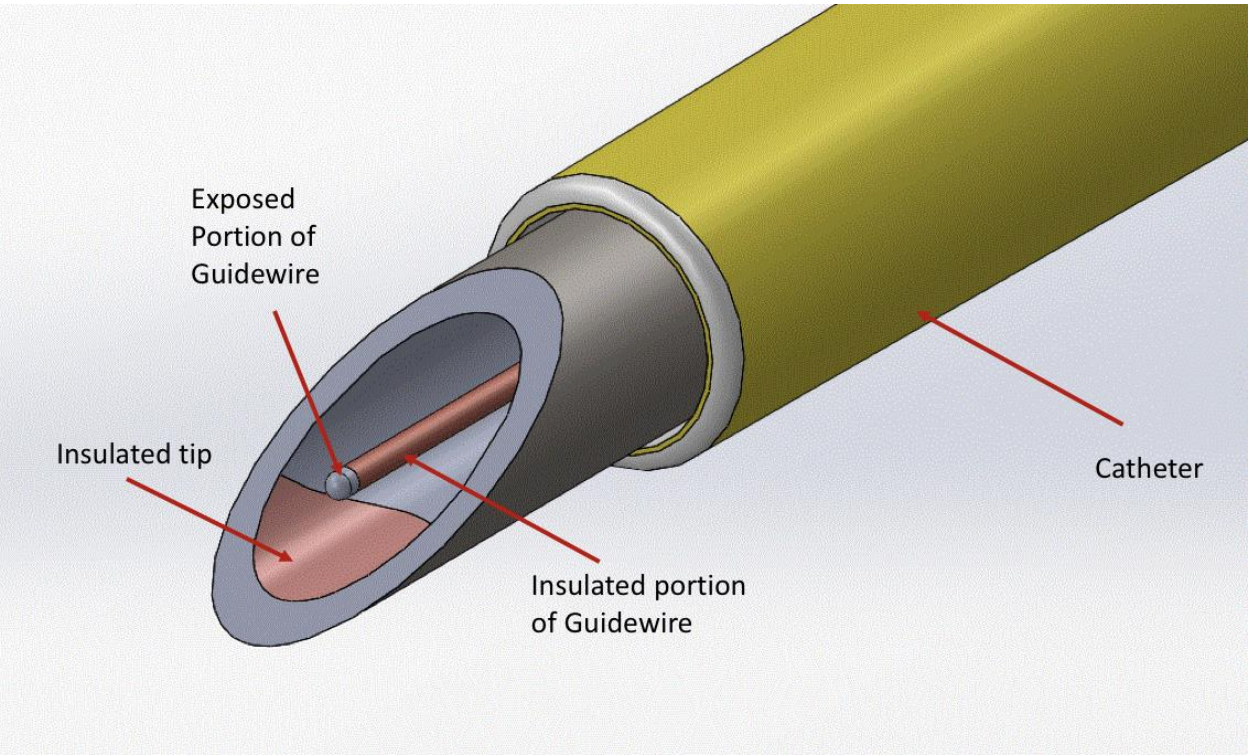

Figure 4-3: Needle and wire catheter design where the guidewire which serves as the second electrode is covered with heat shrink except at the tip. The needle is coated at the tip while the remaining surface is left bare allowing for the housing to act as the first electrode.

The guide wire inside the needle acts as the second electrode. The guide wire is covered with medical grade heat shrink tubing while the tip is left bare, as shown in Figure ***4-3***. The insulated coating on the tip of the needle and the guide wire prevents a short-circuit from occurring between the two electrodes.

The guidewire acts as a guide to facilitate catheter insertion, and it forces the vein to expand resulting in easier catheterization for tortuous vessels. Both of the electrodes are connected to an electrical connector (Figure ***4-4***) and the catheter assembly is connected to the detection unit by cable that is attached where the operator holds the unit as shown Figure **4-1**.

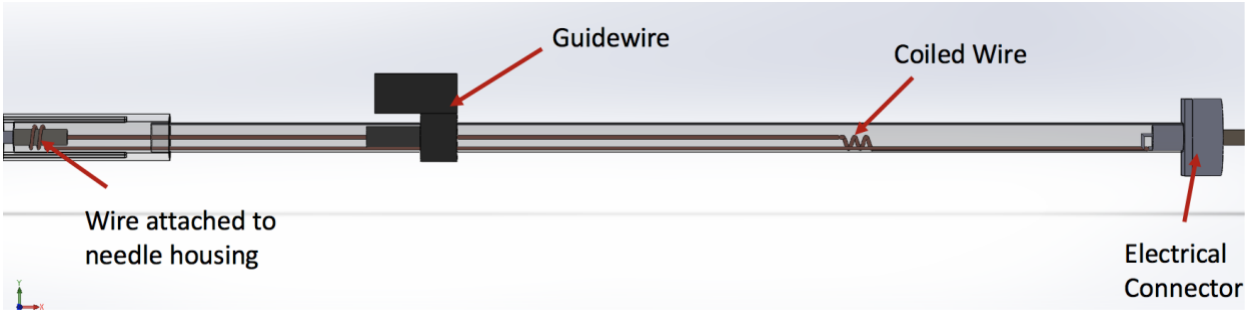

Figure 4-4: Side view of the needle and wire catheter unit.

Figure ***4-5*** displays a sketch of the modified catheter unit during various stages of use. As mentioned above, the exposed portion of the guide wire sits just under the bevel and it serves as the second electrode while the needle housing serves as the first electrode (Figure ***4-3***). In the current design (Figure ***4-4***), a wire is attached to the needle housing in order to provide an electrical signal to the detection unit via electrical connector. Furthermore, additional guidewire length is provided by coiling the wire inside the plastic tubing (or otherwise looping or arranging excess wire in other paths) as shown in Figure ***4-4***.

Shown in Figure ***4-5***a is the modified catheter assembly attached to the connector cable prior to deployment. Providing the additional guide wire length allows for the deployment of the guide wire while maintaining connection with the electrical connector as shown in Figure ***4-5***b in the catheter deployment process. Once the catheter has been advanced into the vein over the guidewire, the needle assembly is withdrawn (Figure ***4-5***c) and disconnected from the cable of the detection unit. Lastly, the catheter is left in the vein Figure ***4-5***d once the needle and guidewire assembly is withdrawn.

a)

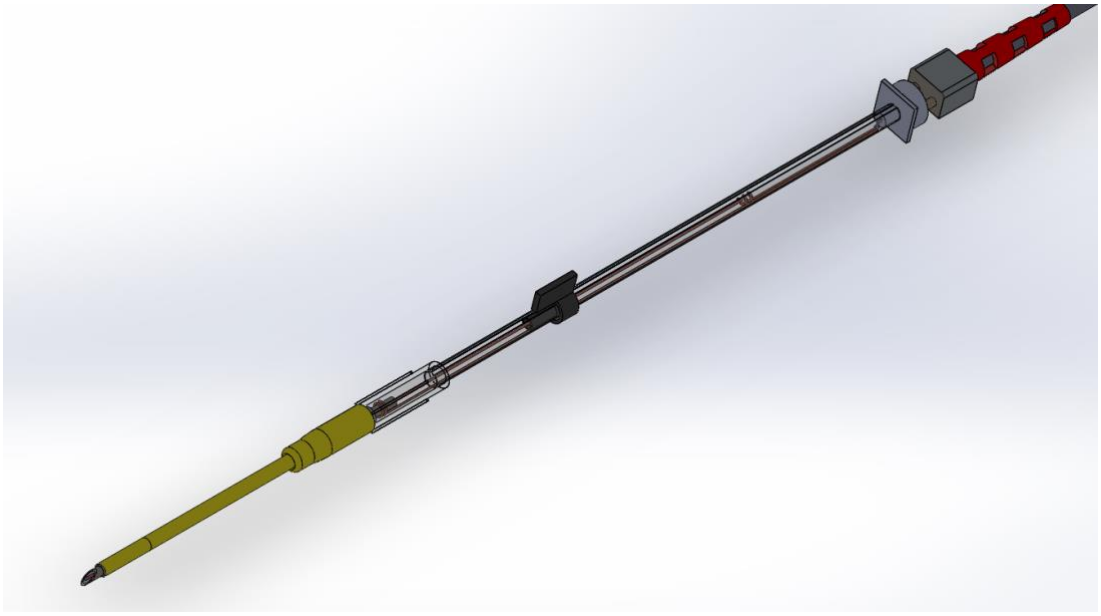

b)

c)

d)

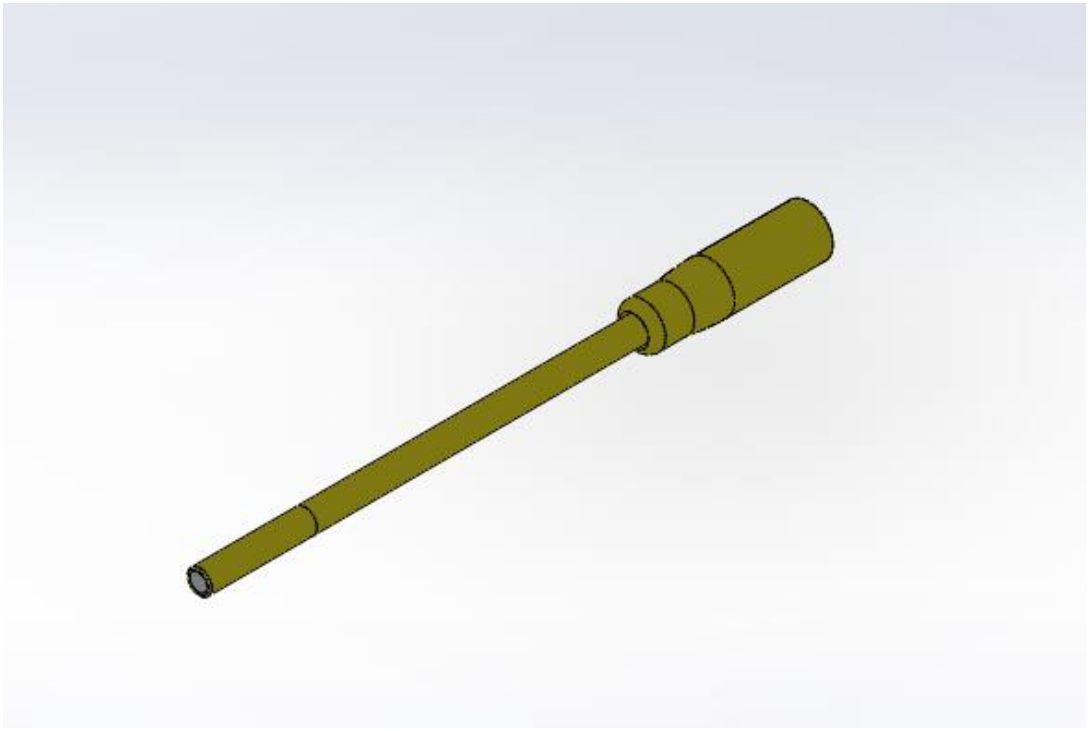

Figure 4-5: Needle and wire catheter design during various stages of use. a) disposable Catheter unit in nominal position before deployment. b) guidewire deployed c) needle and guide wire being removed once catheter is advanced into the vein d) Catheter placed in the vein once needle and guidewire removed.

4.1 555 TIMER SYSTEM DESIGN

Figure ***4-6*** displays a complete schematic of the circuit for the detector unit utilizing a 555-timer chip. In the figure, the needle and guide wire assembly serve as wires and electrodes connecting to resistance R_B, and the tissue being tested replaces R_B and becomes the effective resistance $R_{effective}$. Although only subcutaneous tissue is shown in the figure, it should be noted that the needle encounters other materials such as blood and muscle during use. The signal from the needle and guide wire interface is sent to a micro-controller, (e.g. ATmega328p) which is responsible for measuring the frequency of the signal (chapter 3.2.1.1). It is not necessary to convert the measured frequency values to resistance. This is possible because subcutaneous tissue and blood have distinctive frequencies that allow for differentiation between the two quantities and thus detection of vessel entry. Once the microcontroller has analyzed the incoming signal, the end user is alerted to vessel entry by an output interface, such as the speaker shown in the figure.

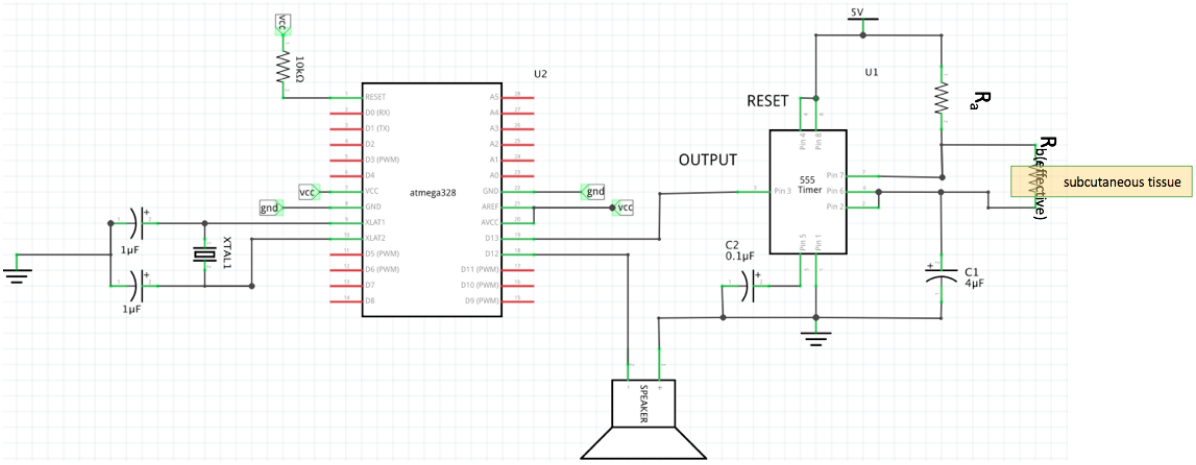

Figure 4-6: Circuit diagram of the 555 timer chip in astable mode where R_b is made up of the tissue resistance between the needle and guidewire $(R_{effective})$. The signal from the timer chip is sent to a micro controller, which measures the frequency and alerts the user to a change through an audible tone.

4.1.1 NEEDLE AND WIRE RESULTS (555 TIMER)

Two sets of tests were carried out using the needle and wire disposable catheter design mentioned above. The first tests were performed with the same materials shown in Figure ***3-39*** but with the needle-and-wire disposable catheter design. During the trial, the needle-and-wire electrodes were submerged in Plasma-Lyte A (Figure ***3-39***a) solution for one minute, and the frequency output of the oscillator circuit was recorded every ten seconds. Equation ** was used to convert the frequency readings to resistance. Subsequently, the electrodes were used to puncture pork fat (Figure ***3-39***c) and muscle (Figure ***3-39***b) for one minute each, and the output frequency of the oscillator circuit was recorded every ten seconds. In each trial, the data was collected for one minute to obtain the steady-state values of each material tested. Between each trial, the electrodes were cleaned to avoid erroneous results from contaminated electrodes. The results are shown in Figure ***4-7*** -Figure **4-9**.

In Figure ***4-7***, the graph shows that the measured resistance value of the Plasma-Lyte A solution starts around 173-325 Ω and it reaches a steady state value between 100-170 Ω in ten trials. The chart in Figure **4-8** shows that the measured resistance value of the muscle (pork shoulder) had an initial value of approximately 500-1400 Ω and the measured resistance values reached equilibrium between 540-1500 Ω during the six trials. Finally, Figure **4-9** displays the plot of the pork fat measured resistance vs. time. From the figure, it can be noted that measured resistance value of the fat had an initial value of approximately 2900-9100 Ω and the measured resistance values reached equilibrium between 3000-10000 Ω during the six trials.

Figure ***4-10*** displays a plot of the means and standard deviations for the resulting resistance measurements of Plasma-Lyte A vs. muscle vs. fat. From the plots, it can be seen that a substantial magnitude difference still exists between the measured resistances of fat, muscle, and Plasma-Lyte A and the recorded resistance values are stable when the oscillator circuit is tested with the needle and wire disposable catheter design. Thus, these results validated our disposable catheter design since the system can differentiate between critical materials encountered by the needle when a catheter is placed.

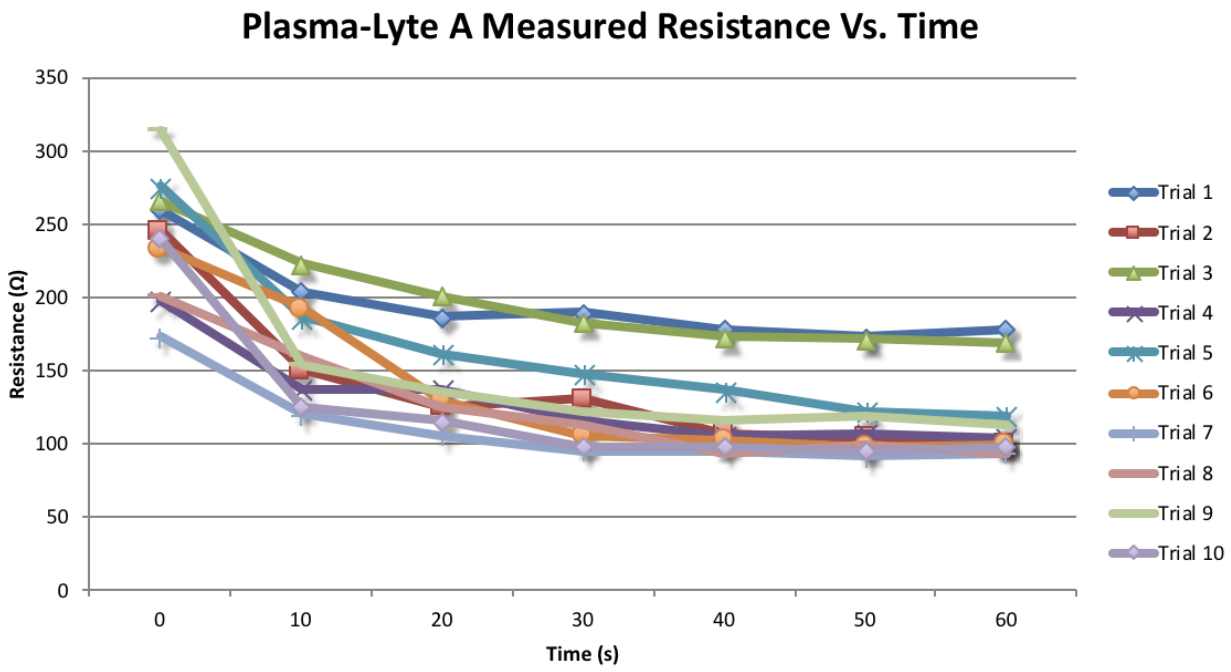

Figure 4-7: Plot of Plasma-Lyte A measured resistance vs. time through six trials using the needle-and-wire design and 555 oscillator.

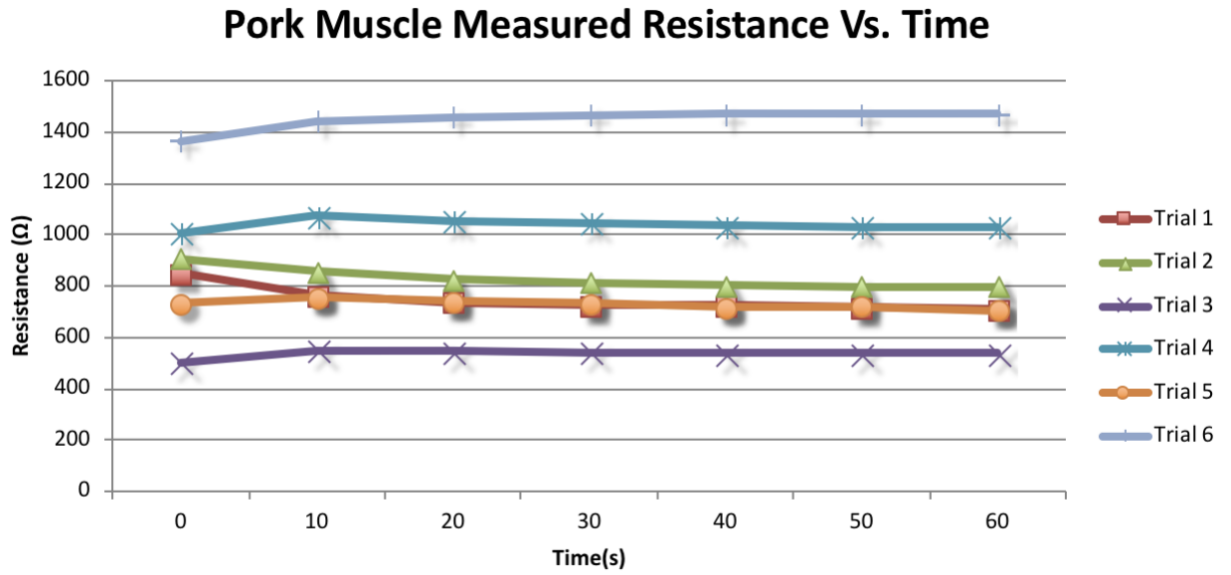

Figure 4-8: Plot of Pork Muscle measured resistance vs. time through six trials using the needle-and-wire design and 555 oscillator.

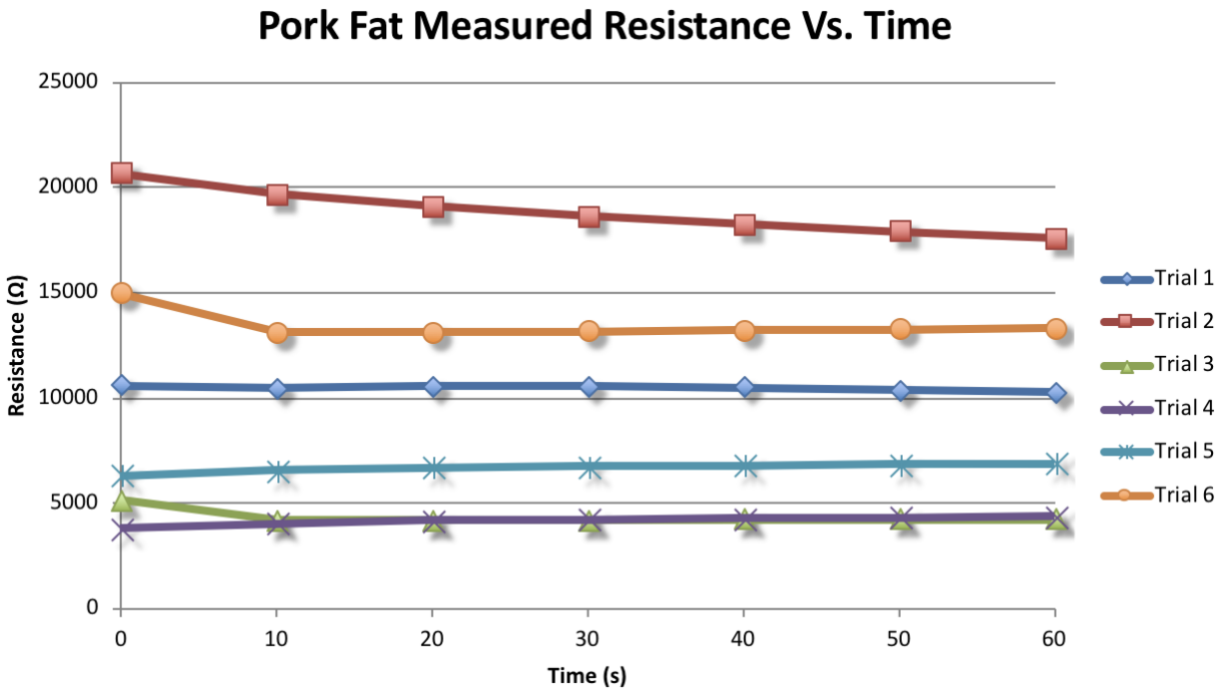

Figure 4-9: Plot of Pork Fat measured resistance vs. time through six trials using the needle-and-wire design and 555 oscillator.

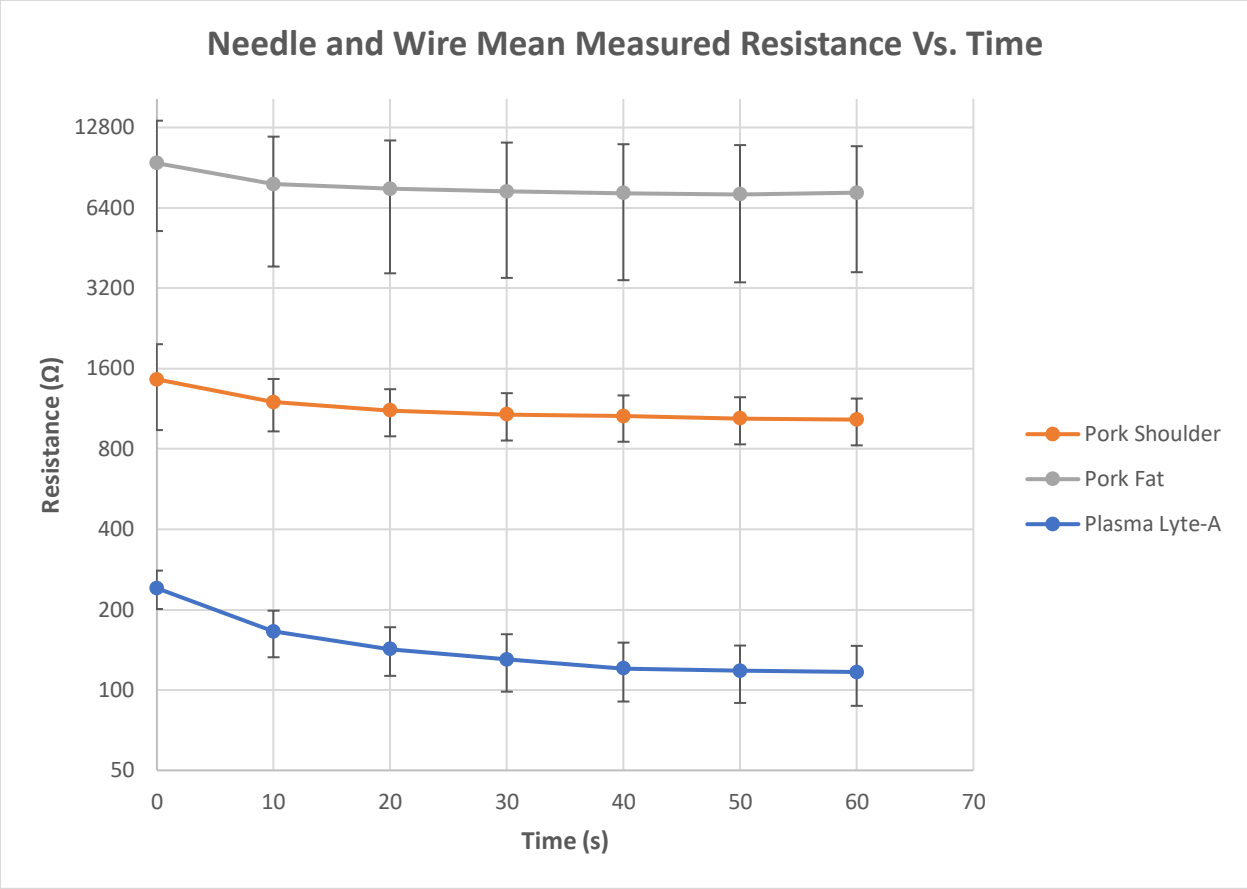

Figure 4-10: Mean and standard deviation for the resulting measured resistance of Plasma-Lyte A vs. muscle vs. fat using needle and wire electrode design and 555 oscillator.

The final test consisted of multi-layer testing where the needle-and-wire catheter assembly shown in Figure **4-11** traveled through fat before entering a Plasma-Lyte A channel to simulate the real-world scenario. The initial test was performed with a 14-gauge needle, and it was subsequently repeated with a 22-gauge needle.

Figure **4-11** shows the setup for the third test using a 14-gauge needle; this served as proof of concept for the overall design. During the trial, the needle of the needle-and-wire catheter design was used to first puncture fat for twenty-five seconds, and then it was advanced through

the layer of fat into the Plasma-Lyte A channel. During the test, the frequency output by oscillator circuit was recorded every five seconds until sixty seconds had elapsed.

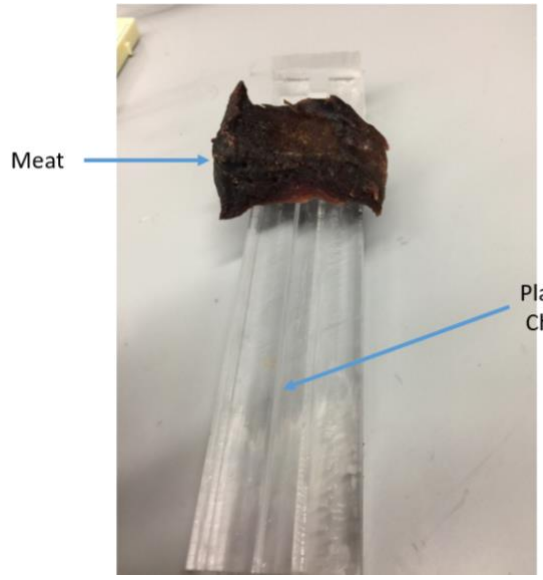

a)

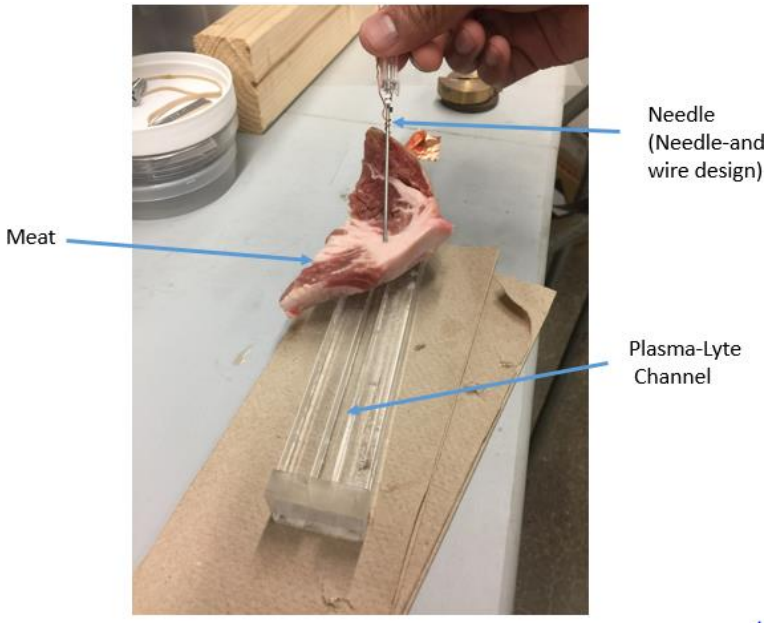

b)

Figure 4-11: Test setup using needle-and-wire catheter design. a) Pork fat sitting on top of a channel of Plasma-Lyte A b) Catheter needle connected to the detection unit puncturing the fat before entering the Plasma-Lyte A channel.

A total of twenty-four trials were conducted using the 14-gauge needle to assess consistency and repeatability of the method. A clean needle was used for each trial in order to avoid erroneous results. The results were converted to resistance using Equation 3-26 and are shown in Figure ***4-12***. From the plots, it can be noted that the measured resistance of pork fat ranged from 2400-38000 Ω. Once the needle was advanced into the Plasma-Lyte A channel the resistance value decreased significantly and ranged from 1100-275 Ω. Subsequently, the data points were plotted in a probability distribution plot as shown in Figure ***4-13***. In the plot, the data points were left in terms of frequencies to better illustrate the separation between Plasma Lyte A and pork fat. From the plot, it can be noted that the data is normally distributed and we can also make a clear distinction between the two quantities.

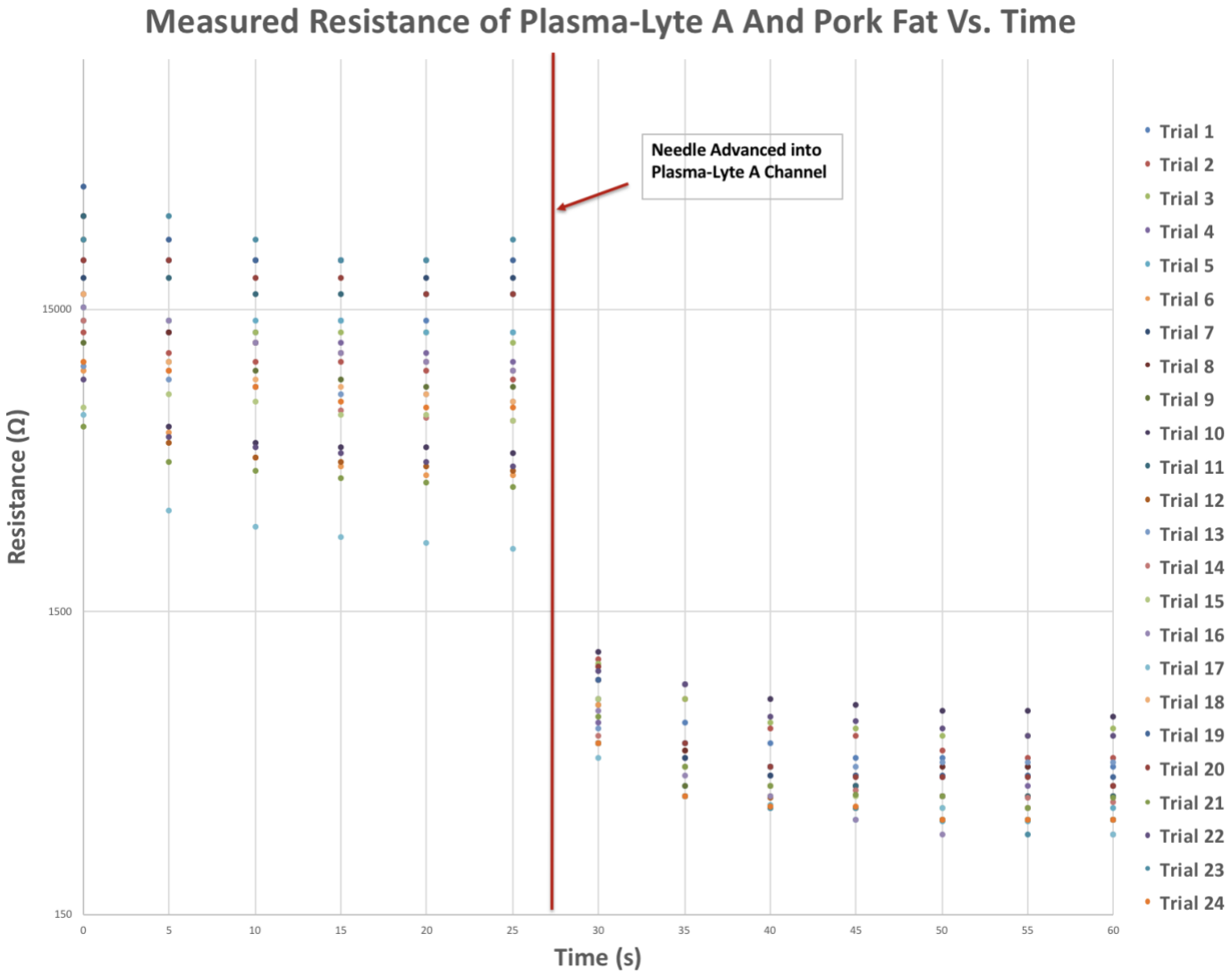

Figure 4-12: Plot of measured resistance of Plasma-Lyte A and Fat Vs. Time for twenty-four independent trials with the 14 gauge needle and wire system.

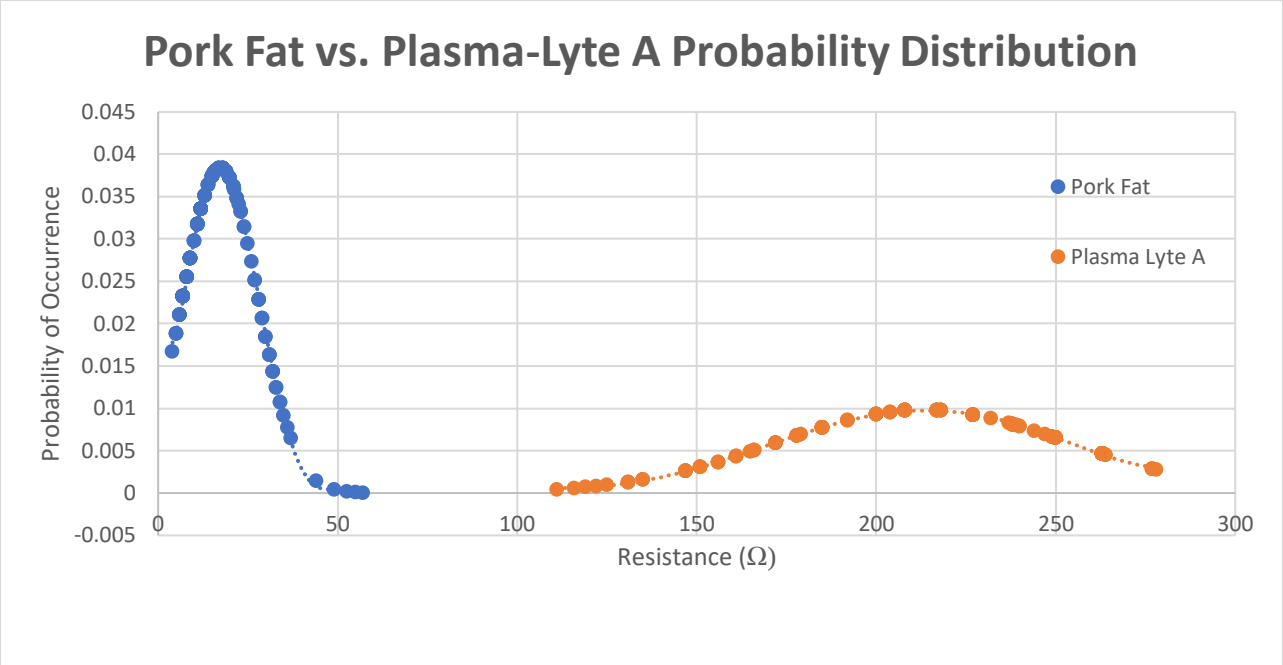

Figure 4-13: Multi-layer probability of distribution plot for the frequency of pork fat and Plasma-Lyte A for twenty-four independent trials with the 14 gauge needle and wire system.

Most often clinicians employ 18-22-gauge needles in adults to establish IV access. Therefore, the multi-layer test was repeated with a 22-gauge needle using the needle and wire design. The setup shown in Figure **4-11** was used for this test. For this test, the frequency output obtained by the oscillator circuit was recorded every five seconds until sixty seconds had elapsed. A total of seven trials were conducted using the 22-gauge needle. The results were converted to resistance using Equation 3-26. Figure ***4-14*** shows the average resistance values for pork and Plasma-Lyte A with error bars for the seven trials. From the figure, it can be seen that there is a significant difference between fat and Plasma-Lyte A once the needle was advanced into the Plasma-Lyte channel. This provides a significant margin for reliable differentiation between fatty tissues vs. blood thus allowing detection of blood vessel entry.

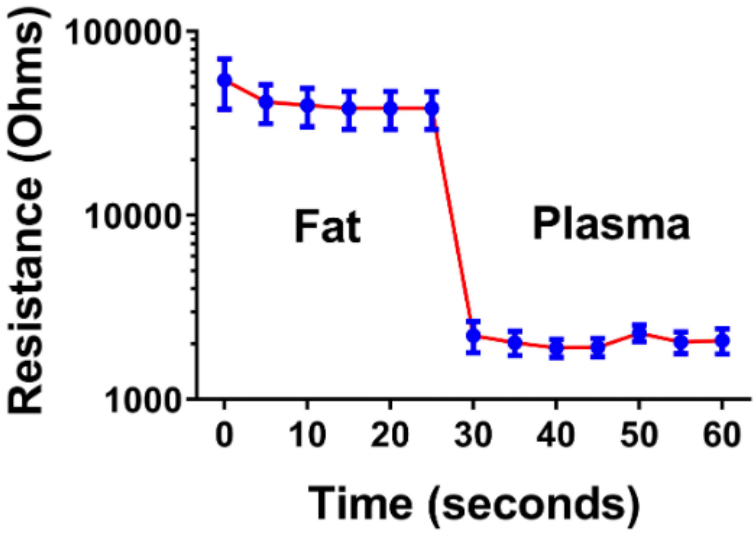

Figure 4-14: Plot of the average resistance of pork Fat and Plasma-Lyte vs. time for seven trials with the 22 gauge needle and wire system.

Figure *4-15* shown below displays the complete printed circuit board of the detector unit employing the 555 timer in astable mode. It should be noted that the circuit board shown in the figure employed LED's as output interfaces instead of a speaker as shown previously in Figure ***4-6***.Although the 555 design was successful in differentiating between subcutaneous tissue and blood, one major flaw of the system is the amount of current that is introduced into a patient's body once the skin is punctured.

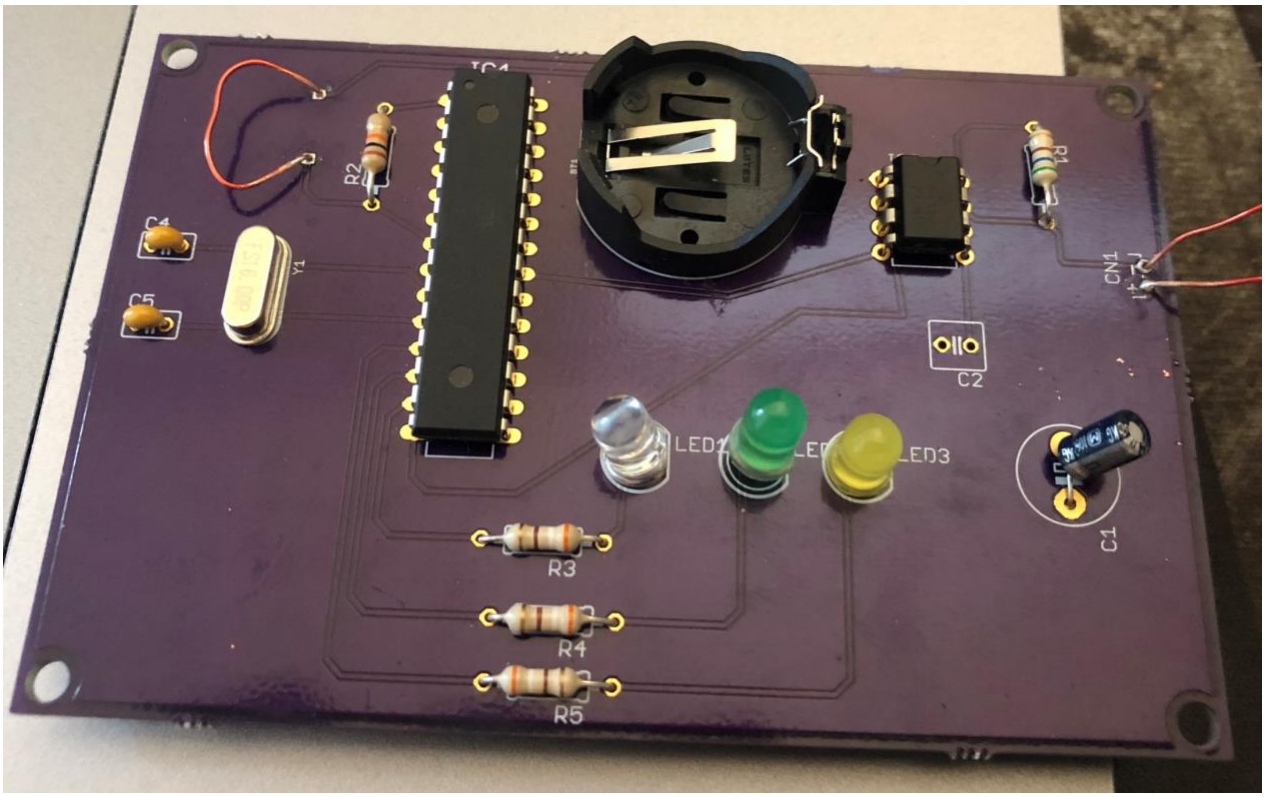

Figure 4-15: Complete printed circuit board of the detector unit employing the 555 timer in astable mode.

Recall from earlier, the needle and wire assembly takes the place of resistor R_B and R_A was set at 560K Ω in the detector circuit. From literature reviewed in chapter 2, it is known that the resistance of blood is approximately 100 Ω. Thus, utilizing the current versus time equation for an RC circuit (Equation 3-13) if 5V is applied to the circuit, the peak current introduced into the patient's body is approximately 9.2mA.

A summary of peer reviewed papers found that 1-5mA current was enough to cause significant discomfort in the patient, and 8-28 mA peak current was enough to cause muscle contractions (Bikson (2014)). One could not simply increase the value of R_A in the detector circuit since it would increase the duty cycle of the 555 timer, leading to polarization errors. Thus, it was necessary to utilize the op-Amp circuit for low current.

4.2 741 OP-AMP SYSTEM DESIGN

An alternative to the timer circuit is the op-amp based oscillator discussed in section 3.2.1.2. For the purpose of this application, the resistor R_2 in Figure ***4-16*** was replaced with two wire electrodes and intermediate tissue which becomes the effective resistance $R_{effective}$. Since it was necessary to re-design the circuit for low current, R_1 (Figure ***4-16*****)** was chosen to be 560 kΩ. Choosing a high resistor value for R_1 (e.g. 560 kΩ) ensures that the total amount of current introduced into the patient's body is below 10μA.

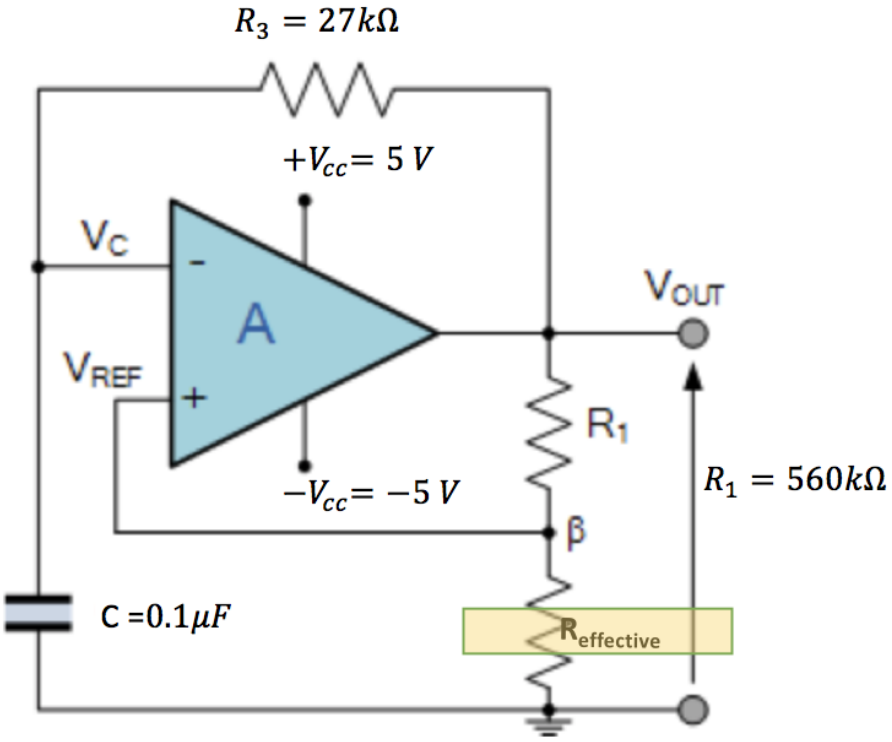

Figure 4-16: Electrical schematic of an Op-amp as a multivibrator oscillator where resistor R_2 was replaced with two wire electrodes becoming the effective resistance $R_{effective}$.

Figure *4-19* displays a complete schematic of the circuit diagram for a detector unit utilizing an oscillator circuit based on a 741 op-amp. In the figure, the needle and guide wire assembly replaces R_B and becomes the effective resistance $R_{effective}$. Figure ***4-17***a and Figure ***4-17***b

display the raw output waveform from the first op-amp for $R_{effective}$ values of 33KΩ and 100Ω resistor. From the figures it can be seen that the 33KΩ resistor produces a square wave (Figure ***4-17***a) and the 100Ω resistor produces a sign wave (Figure ***4-17***b) as the output waveform. The square wave turns into a sign wave for the 100Ω resistor since the capacitor is charging and discharging in a rapid manner. Additionally, the peak-to-peak voltage was approximately 7V with the output waveform traveling in the negative region. A microcontroller (Atmega328) is capable of processing signals between 0-5V. If the signal of Figure 4-17 were sent to the micro-controller, signal clipping or damage to the microcontroller would occur producing erroneous results. Thus, it was necessary to send the output waveform to a second op-amp.

a) 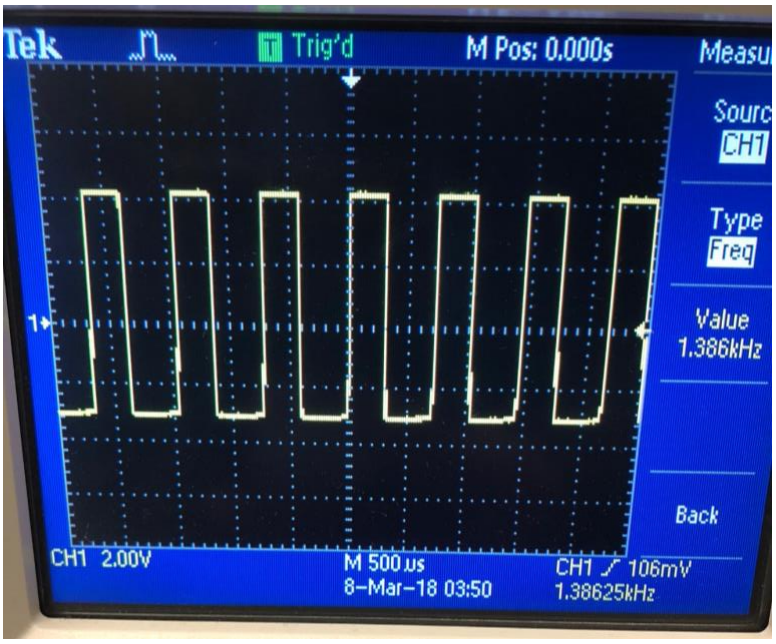

b) 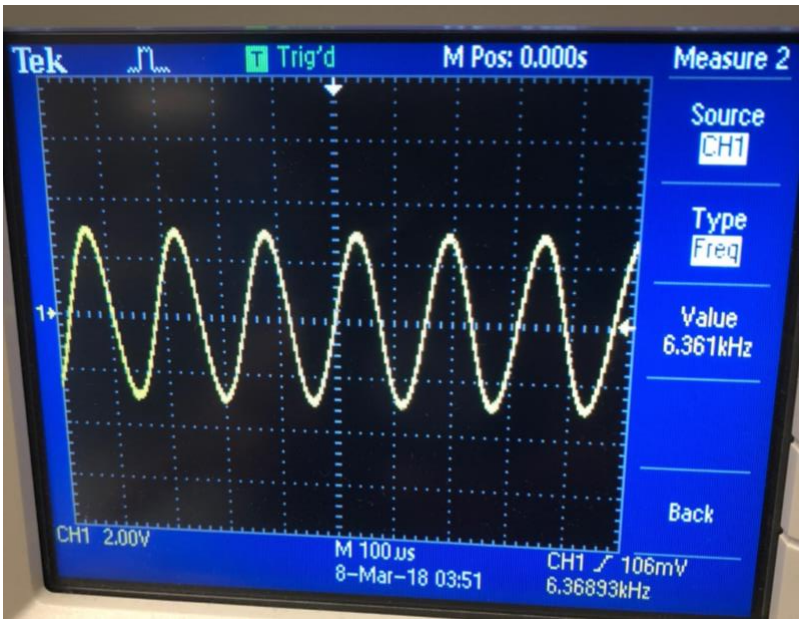

Figure 4-17: Raw output waveform for various resistor values from the op-amp based oscillator. a) $R_{effective}$ of $33K\Omega$. *b)* $R_{effective}$ of 100Ω.

Figure ***4-18***a and Figure ***4-18***b display the converted waveform from the second op-amp for $R_{effective}$ values of 33KΩ and 100Ω. The second op-amp was used to transform the sign wave into a square wave, and to shift the waveform between 0-5V. This allowed for the signals to be analyzed by a microcontroller.

a)

b)

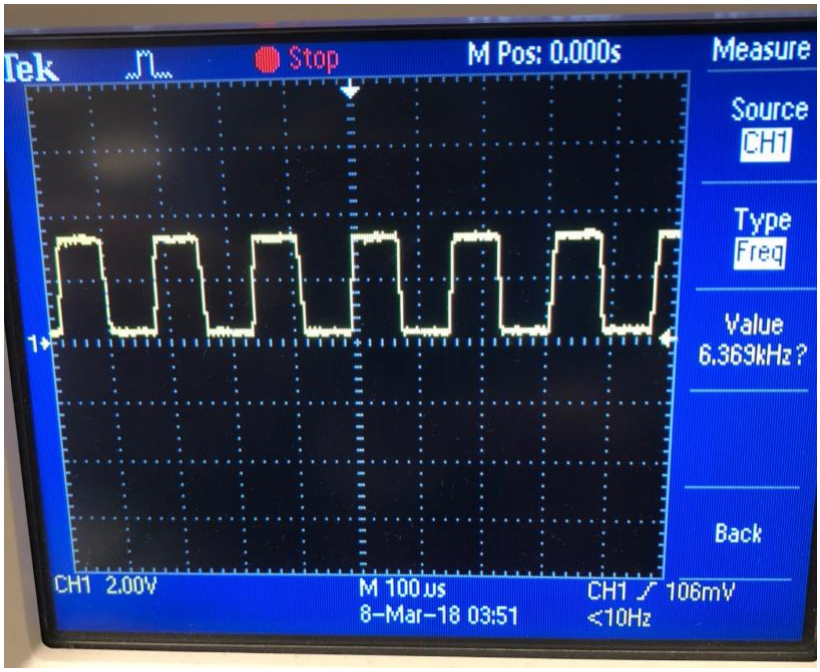

Figure 4-18: Converted output waveform for various resistor values from the second op-amp based oscillator. a) $R_{effective}$ of 33KΩ. b) $R_{effective}$ of 100Ω.

The transformed signal was subsequently sent to a micro-controller, (e.g. ATmega328p) which is responsible for measuring the frequency of the signal. It is not necessary to convert the measured frequency values to resistance. This is possible because subcutaneous tissue and blood have distinctive frequencies that allow for differentiation between the two quantities and detect vessel entry. Once the microcontroller has analyzed the incoming signal, the end user is alerted to vessel entry by an output interface, such as the speaker as shown in the figure.

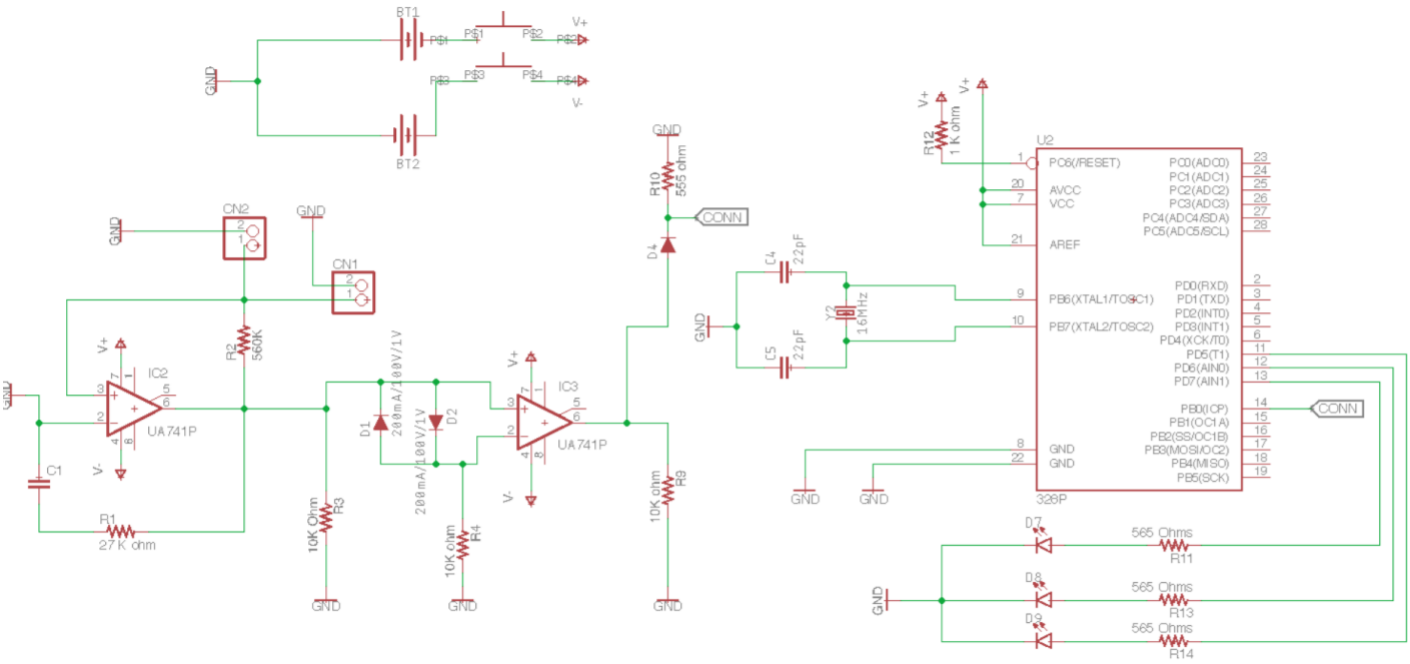

Figure 4-19: Circuit diagram of the 741 Op-amp oscillator. The signal from the first op-amp sent to a second op amp which changes the waveform into square waves. The signal from the second op amp is sent to a micro controller, which measures the frequency and alerts the user to a change through LED's.

4.2.1 NEEDLE AND WIRE RESULTS (741 OSCILLATOR)

Two set of tests were carried out involving the 741-oscillator circuit. The first test involved inserting two electrodes (two separate wires) into various materials as shown in Figure ***3-39***. Materials tested were Plasma-Lyte A and pork fat. During the trial, wires that made up the two electrodes were submerged in Plasma-Lyte A (Figure ***3-39***a) solution for one minute, and the frequency output of the oscillator circuit was recorded every ten seconds. Subsequently, the Plasma-Lyte A tests were repeated for an additional four trials, and the current across the electrodes was measured every ten seconds.

Subsequently, the wires were used to puncture pork fat (Figure ***3-39***c) for one minute, and the output frequency of the oscillator circuit was recorded every ten seconds. In each trial, the data was collected for one minute to obtain the steady-state values of each material tested. The tests were repeated five times to assess consistency and repeatability of the data in each material. Between each trial, the electrodes were cleaned to avoid erroneous results from contaminated electrodes. The results were not converted to resistance because subcutaneous tissue and blood have distinctive frequencies that allow for differentiation between the two quantities. Figure ***4-20*** - Figure ***4-22*** display the results of these tests.

In Figure ***4-20*** the graph shows that the measured frequency value of the Plasma-Lyte A solution starts around 6.02-6.05 KHz and it reaches a steady state value of around 6.04 KHz in five trials. **Figure *4-21*** displays the measured current introduced across the electrodes when the needle was submerged into the Plasma-Lyte A solution. From the plot, it can be seen the current values stayed constant at 6μA throughout the four trials.

Figure ***4-22*** displays the plot of the pork fat measured frequency vs. time. From the figure, it can be noted that measured frequency value of the fat had an initial value of approximately 1.5-4 KHz and the measured frequency values reached equilibrium between 1.7-3.8 KHz during the five trials.

Figure ***4-23*** displays a plot of the mean and standard deviation for the resulting frequency measurements of Plasma-Lyte A vs. fat. From the plot, it can be seen that there is a significant difference between the measured frequency of pork fat, and Plasma-Lyte A and the recorded frequency values are stable for the duration of the tests. These results indicate that an op-amp based oscillator circuit is a viable option for discerning between critical materials encountered by a needle when a catheter is placed.

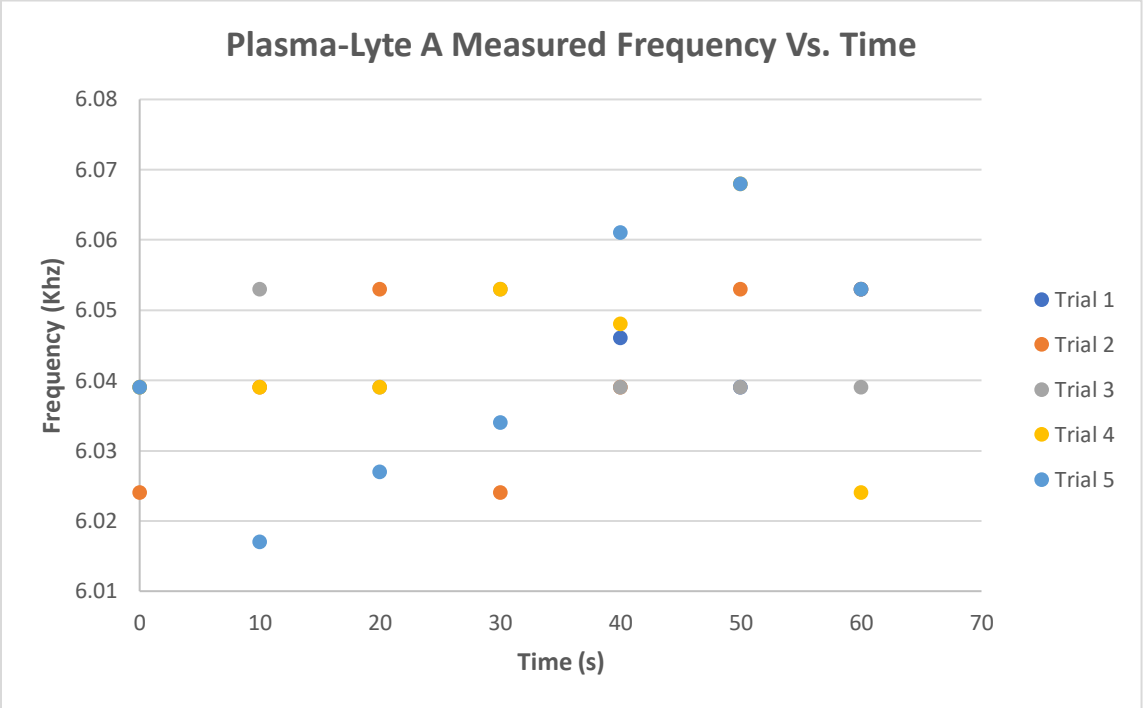

Figure 4-20: Plot of Plasma-Lyte A measured resistance vs. time through five trials using the two-wire electrode design and 741 Oscillator.

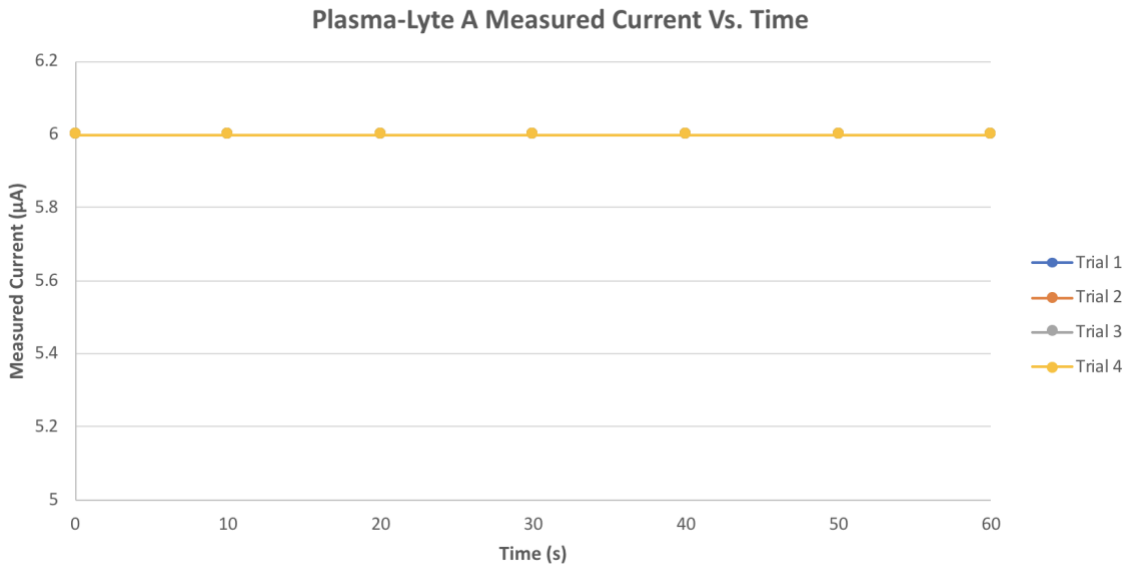

Figure 4-21: Plot of Plasma-Lyte A measured current vs. time through four trials using the two wire electrode design and 741 Oscillator.

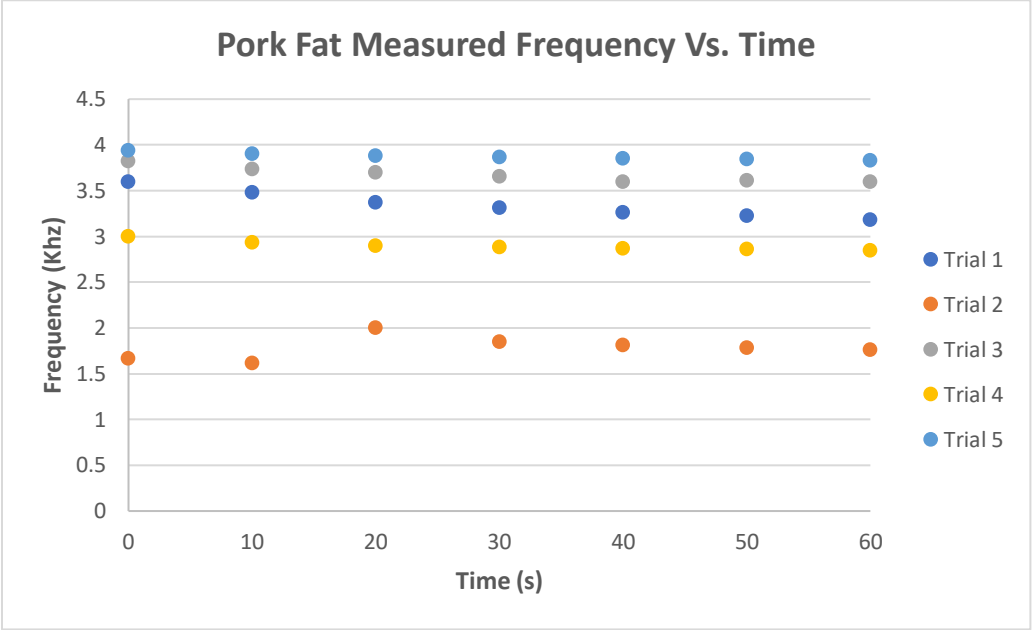

Figure 4-22: Plot of Pork Fat measured frequency vs. time through five trials using the two-wire electrode design and 741 Oscillator.

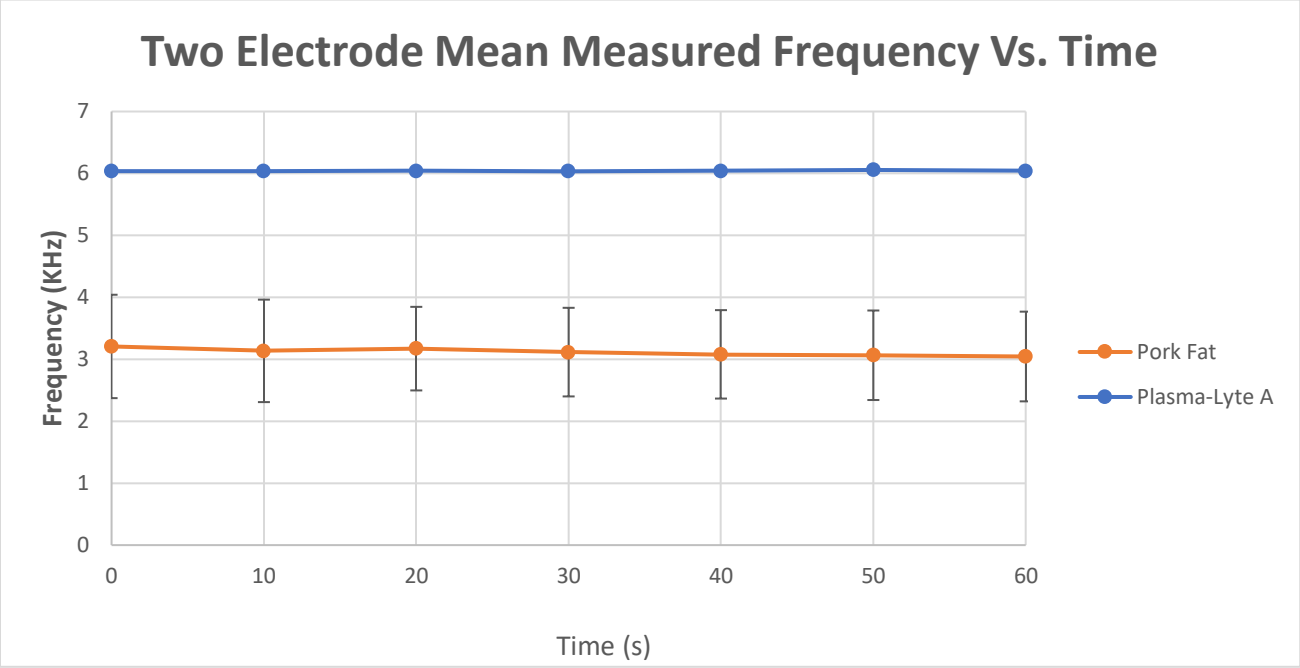

Figure 4-23: Mean and standard deviation for the resulting measured frequency of Plasma-Lyte A vs. fat using two wire electrode design and 741 Oscillator.

The final test consisted of multi-layer testing where the needle-and-wire catheter assembly shown in Figure **4-11**, coupled with an op-amp oscillator circuit, traveled through fat before entering a Plasma-Lyte A channel to simulate real-world scenario. The multi-layer trial served as proof of concept for the low current circuit. During the trial, the needle of the needle-and-wire catheter design was used to first puncture fat for twenty-five seconds, and then it was advanced through the layer of fat into the Plasma-Lyte A channel. During the test, the frequency output by the 741-oscillator circuit was recorded every five seconds until sixty seconds had elapsed. A total of twelve trials were conducted using the 22-gauge needle to assess consistency and repeatability of the method. A clean needle was used in between each trial in order to avoid erroneous results. Figure **4-24** displays the results from this experiment.

From the plots, it can be noted that the measured frequency of pork fat ranged from 1-4kHz. Once the needle was advanced into the Plasma-Lyte A channel the frequency value increased and ranged from 4.8-6.2KHz. Figure ***4-25*** displays the mean and standard deviation for the resulting frequency measurements of Plasma-Lyte A vs. fat. From the plot, it can be seen that there is a clear difference between the measured frequency of pork fat, and Plasma-Lyte A and the recorded frequency values are stable for the duration of the tests. These results indicate that an op-amp based oscillator circuit is a viable option for discerning between critical materials encountered by a needle when a catheter is placed.

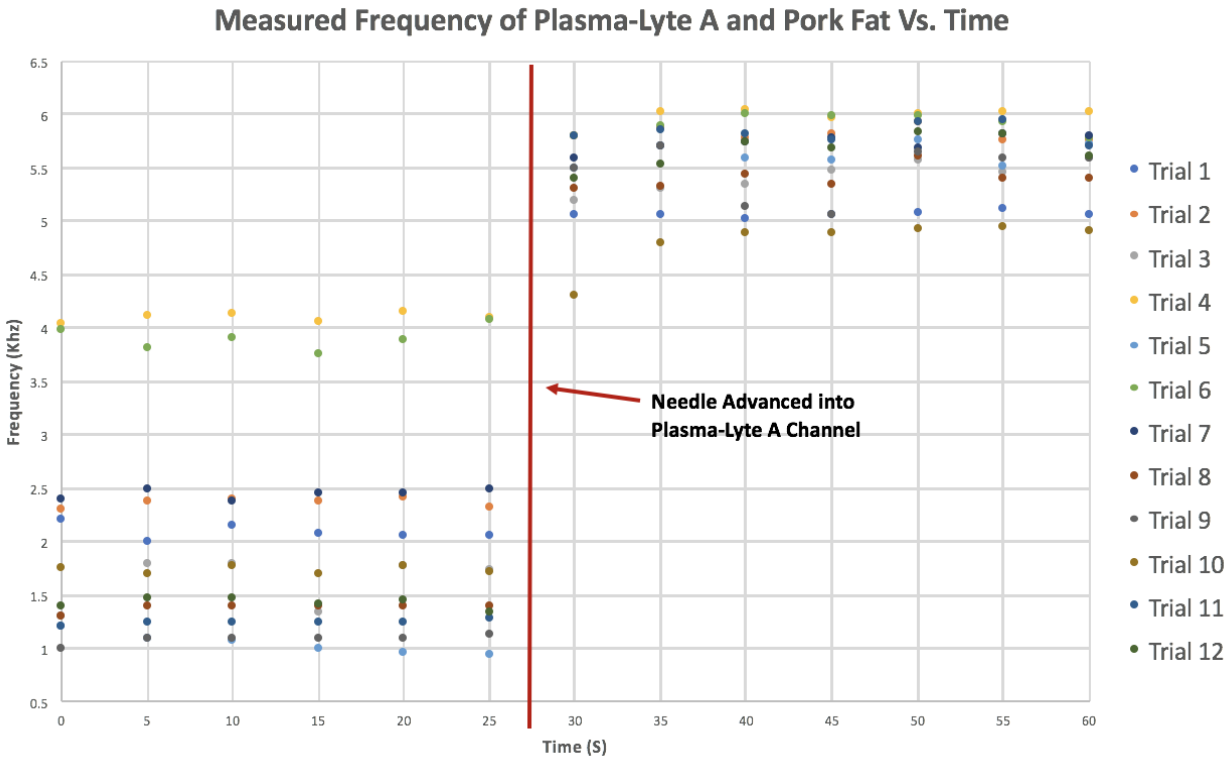

Figure 4-24: Measured frequency of Plasma-Lyte A and Fat Vs. time for twelve independent trials using needle and wire electrode design and 741 Oscillator.

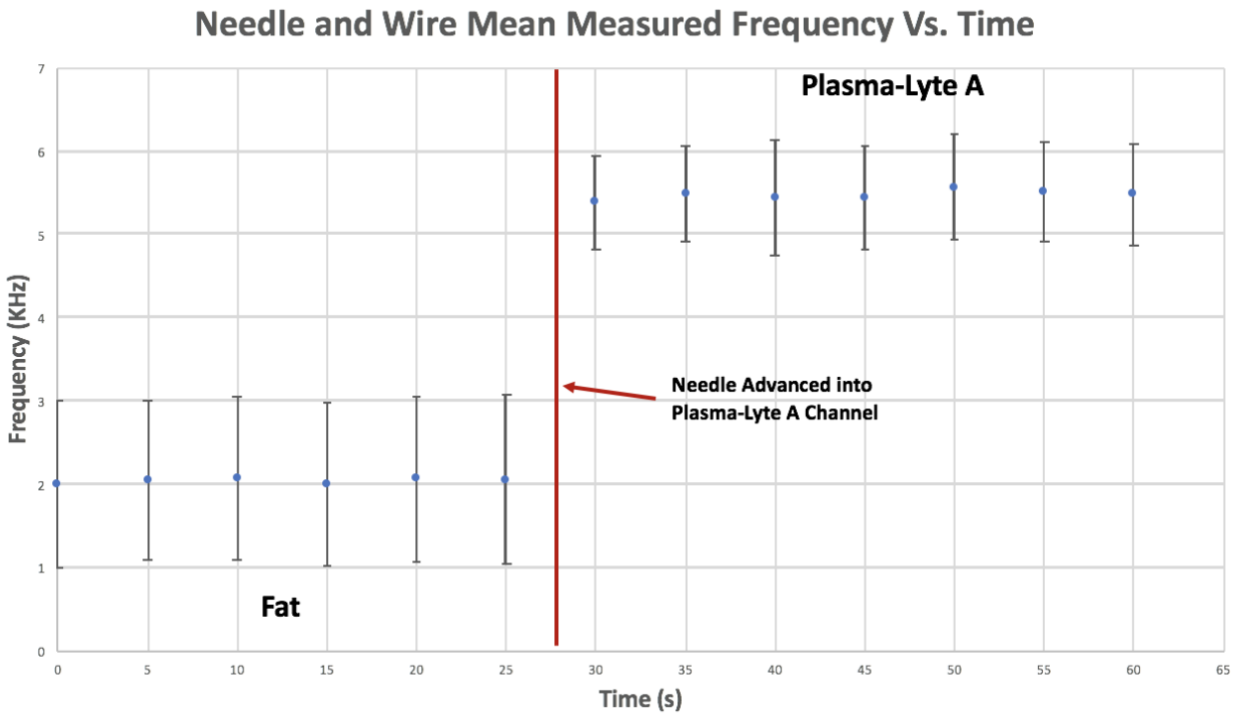

Figure 4-25: Mean and standard deviation for the measured frequency of Plasma-Lyte A vs. fat using needle and wire electrode design and 741 Oscillator.

5.0 CONCLUSION

Peripheral intravenous (PIV) line placement is one of the most common medical procedures performed by a clinician when a patient is admitted to the hospital. Although routine, approximately 25% of adults require multiple attempts in order to establish access. The current alternatives rely upon a combination of ultrasound guided PIV placement, Visual vein finders, mid line, central lines and IO placements (emergency situations) to establish IV access. Delays in establishing access leads to delayed therapy, increased patient pain, and increased institutional cost.

This thesis provided a solution to reduce the number of first time IV placement failures by measuring the resistance between subcutaneous tissue and blood. The initial measurement attempt was done with a multimeter. The measured resistance for Plasma-Lyte A, pork muscle and pork fat ranged from 200-300Ω, 1.1-3.6MΩ, and 0.8-1.2MΩ respectively. Intuitively, one can tell the measured resistance values are incorrect since the resistance of fat should be greater than that of muscle. Furthermore, the measured resistance values failed to reach steady state during the 60 second measurement period. The error in measurement occurred due to the effect of polarization.

Afterward, measurement was attempted with a Wheatstone bridge applying alternating current. In this application, the imaginary component was neglected and only the real portion considered since the fluid tissue resistance is the dominant effect. The measured resistance for Plasma-Lyte A, and pork shoulder were found to be 200Ω, and 250Ω at 10,000 Hz respectively. Unlike the multimeter measurements, the measured resistance values reached steady state during the 60 second measurement period. Although the bridge measurement produced a separation

between the two quantities being measured the resulting separation was less than desired for a potential accurate measurement technique across a wide range of applications.

Subsequently, a 555-timer oscillator circuit was employed to successfully differentiate between subcutaneous tissue and blood. The initial proof of concept test was performed with copper wires as the electrodes, and the measured resistance for Plasma-Lyte A, pork muscle and pork were 175-300 Ω, 1500-2100 Ω, and 2500-10,000 Ω. The measured resistance values reached steady state during the 60 second measurement period. The mean and standard deviation of the measured resistances showed significant differences between the three quantities being measured. These results indicated that a timer oscillator circuit was a viable option.

The delivery system was designed by modifying the standard PIV needle catheter combination to act as two separate measurement electrodes (needle and wire). The electrodes from the IV connected to a connector cable, which was then connected to the detector unit. The detector unit measures the frequency of the resulting waveform and alerts the user to vessel entry by utilizing LED's. In the future, the alerting mechanism can be modified to include auditory and vibratory signal. The needle and wire catheter design were further validated by measuring the resistance of individual components. The measured resistance for Plasma-Lyte A, pork muscle and pork fat ranged from 100-175Ω, 450-1500Ω, 5000-2000Ω respectively.

Subsequently multi-layer testing was performed where the needle and wire design traveled from fat into a PlasmaLyte channel to simulate real world scenario. The results showed a significant difference between the values of fat and Plasma-Lyte A. Although the results indicated the 555-timer oscillator is a viable option, the amount of current introduced into the body (7.5mA) exceeded the acceptable levels (0.5mA). Thus, it was necessary to re design the overall detection circuit.

The circuit was re-designed for low current use employing a 741 op-amp. Th new circuit was validated by measuring the frequency of oscillation while the electrodes were inserted into pork fat, pork muscle, and plasma-Lyte A with multi-layer tests being performed thereafter. Unlike previous measurements, the frequency values were not converted to resistance because subcutaneous tissue and blood have distinctive frequencies that allow for differentiation between the two quantities. The results showed the overall assembly is successful in detecting a change between fat and Plasma-Lyte A.

Moving forward, further testing and circuit optimization must be done in order to commercialize this technology. The design needs to be validated for safety and efficacy in animals prior to performing healthy volunteer studies. Prior to multi center studies, the circuit should be optimized in order to maximize the separation between the individual quantities being measured. If successful, the subsequent step would be conducting a multi-center study to test efficacy and to obtain user feedback in the quest to commercialize this novel device.

BIBLIOGRAPHY

Abolfotouh, M. A., Salam, M., Bani-Mustafa, A., White, D., & Balkhy, H. H. (2014). Prospective study of incidence and predictors of peripheral intravenous catheter-induced complications. *Ther Clin Risk Manag, 10*, 993-1001. doi:10.2147/TCRM.S74685

Alexandrou, E., Ray-Barruel, G., Carr, P. J., Frost, S., Inwood, S., Higgins, N., . . . Rickard, C. M. (2015). International prevalence of the use of peripheral intravenous catheters. *J Hosp Med, 10*(8), 530-533. doi:10.1002/jhm.2389

Analytical, R. (2004). Conductivity Theory and Practice. In (pp. 50).

Au, A. K., Rotte, M. J., Grzybowski, R. J., Ku, B. S., & Fields, J. M. (2012). Decrease in central venous catheter placement due to use of ultrasound guidance for peripheral intravenous catheters. *Am J Emerg Med, 30*(9), 1950-1954. doi:10.1016/j.ajem.2012.04.016

Basheer, N. (2012). STATIC & DYNAMIC CHARACTERISTICS OF MEASUREMENT SYSTEM. Retrieved from https://mediatoget.blogspot.in/2012/01/static-dynamic-characteristics-of.html

Basics, C. (2017). 555 Timer Basics - Astable Mode. Retrieved from http://www.circuitbasics.com/555-timer-basics-astable-mode/

Bikson, M. (2014). A review of hazards associated with exposure to low voltages. Department of Biomedical Engineering. The Graduate School and University Center of the City University of New York, New York, NY. In.

Brannam, L., Blaivas, M., Lyon, M., & Flake, M. (2004). Emergency nurses' utilization of ultrasound guidance for placement of peripheral intravenous lines in difficult-access patients. *Acad Emerg Med, 11*(12), 1361-1363. doi:10.1197/j.aem.2004.08.027

Burger, H. C., & Milaan, J. B. v. (1943). Measurements of the specific resistance of the human body to direct current. *Journal of Internal Medicine, 114*(6), 584-607 %@ 0954-6820.

Burger, H. C., & Van Dongen, R. (1961). Specific electric resistance of body tissues. *Physics in medicine and biology, 5*(4), 431 %@ 0031-9155.

Busti, A. J. (2015). Seldinger Technique for Central Intravenous (IV) Line Placement. Retrieved from https://www.ebmconsult.com/articles/seldinger-technique-intravenous-iv-placement

Cameron Dezfulian, W. W. C., Dennis Wist, Ehsan Qaium (2017). USA Patent No.: USPTO.

David G. Alciatore , M. B. H. (2007). *Introduction to mechatronics and measurement systems* (3rd ed.): McGraw-Hill.

de Graaff, J. C., Cuper, N. J., Mungra, R. A., Vlaardingerbroek, K., Numan, S. C., & Kalkman, C. J. (2013). Near-infrared light to aid peripheral intravenous cannulation in children: a cluster randomised clinical trial of three devices. *Anaesthesia, 68*(8), 835-845. doi:10.1111/anae.12294

Fields, J. M., Piela, N. E., Au, A. K., & Ku, B. S. (2014). Risk factors associated with difficult venous access in adult ED patients. *Am J Emerg Med, 32*(10), 1179-1182. doi:10.1016/j.ajem.2014.07.008

Fields, J. M., Piela, N. E., & Ku, B. S. (2014). Association between multiple IV attempts and perceived pain levels in the emergency department. *J Vasc Access, 15*(6), 514-518. doi:10.5301/jva.5000282

Fuller, B. (2012). Hans Camenzind, 555 timer inventor, dies. Retrieved from https://www.eetimes.com/document.asp?doc_id=1262353

Gallagher, E. J., Liebman, M., & Bijur, P. E. (2001). Prospective validation of clinically important changes in pain severity measured on a visual analog scale. *Ann Emerg Med, 38*(6), 633-638. doi:10.1067/mem.2001.118863

Ghassaei, A. (2012). 555 TIMER. Retrieved from http://www.instructables.com/id/555-Timer/

Gregg, S. C., Murthi, S. B., Sisley, A. C., Stein, D. M., & Scalea, T. M. (2010). Ultrasound-guided peripheral intravenous access in the intensive care unit. *J Crit Care, 25*(3), 514-519. doi:10.1016/j.jcrc.2009.09.003

Hadaway, L. (2007). Infiltration and extravasation. *AJN The American Journal of Nursing, 107*(8), 64-72 %@ 0002-0936X.

Haefeli, M., & Elfering, A. (2006). Pain assessment. *European Spine Journal, 15*(Suppl 1), S17-S24. doi:10.1007/s00586-005-1044-x

Hambley, A. R. (2008). *Electrical engineering: principles and applications* (4th ed.): Pearson Education.

Hartstein, B. H., & Barry, J. D. (2008). Mitigation of pain during intravenous catheter placement using a topical skin coolant in the emergency department. *Emerg Med J, 25*(5), 257-261. doi:10.1136/emj.2006.044776

Heather Brannon, M. (2017, 17,July, 2017). Subcutaneous Tissue: The Innermost Layer of Skin. Retrieved from https://www.verywell.com/subcutaneous-tissue-1068882

Hunsaker, S., & Hillis, D. (2013). Intraosseous Vascular Access for Alert Patients. *AJN The American Journal of Nursing, 113*(11), 34-39. doi:10.1097/01.naj.0000437110.65929.70

Joing, S., Strote, S., Caroon, L., Wall, C., Hess, J., Roline, C., . . . Reardon, R. (2012). Ultrasound-Guided Peripheral IV Placement. *New England Journal of Medicine, 366*(25), e38. doi:10.1056/NEJMvcm1005951 %M 22716992 %U http://www.nejm.org/doi/full/10.1056/NEJMvcm1005951

Kaufman, W., & Johnston, F. D. (1943). The electrical conductivity of the tissues near the heart and its bearing on the distribution of the cardiac action currents. *American Heart Journal, 26*(1), 42-54 %@ 0002-8703.

Ken, B. (2015). The Wheatstone Bridge. Retrieved from http://www.play-hookey.com/dc_theory/resistors/wheatstone_bridge.html

Krans, B. (2016, 05 May, 2016). Ultrasound. Retrieved from http://www.healthline.com/health/ultrasound#preparation3

Kuehnel, R. (2009). *Circuit Analysis of a Legendary Tube Amplifier: The Fender Bassman 5F6-A*: Amp Books.

Lapostolle, F., Catineau, J., Garrigue, B., Monmarteau, V., Houssaye, T., Vecci, I., . . . Adnet, F. (2007). Prospective evaluation of peripheral venous access difficulty in emergency care. *Intensive Care Med, 33*(8), 1452-1457. doi:10.1007/s00134-007-0634-y

Leigh Ann Anderson, J. S., Wolters Kluwer. (2016). Longitudinal section definition. Retrieved from https://www.drugs.com/dict/longitudinal-section.html

Martin, E. A. (2010). *Concise medical dictionary*: Oxford University Press.

Martinsen, Ø. G., Kalvøy, H., Grimnes, S., Nordbotten, B., Hol, P. K., Fosse, E., . . . Becker, L. B. (2010). Invasive electrical impedance tomography for blood vessel detection. *The open biomedical engineering journal, 4*, 135.

Oakley, E., & Wong, A. M. (2010). Ultrasound-assisted peripheral vascular access in a paediatric ED. *Emerg Med Australas, 22*(2), 166-170. doi:10.1111/j.1742-6723.2010.01281.x

P. Armstrong, C. Y., D. McKeown (1990). <Ethyl chloride and venepuncture pain- a comparison with intradermal lidocaine.pdf>. *Canadian Journal of Anesthesia, 37*, 2.

Peter Switakowski, A. M. D. M. (2003). Peripheral Intravenous Access. Retrieved from http://www.med.uottawa.ca/procedures/iv/

Poole, I. (2004). Op amp astable multivibrator oscillator circuit. Retrieved from http://www.radio-electronics.com/info/circuits/opamp_multivibrator_oscillator/op_amp_multivibrator_oscillator.php

Poole, I. (2016, 11 April, 2016). Multimeter / Test Meter Basics. Retrieved from https://www.electronics-notes.com/articles/test-methods/meters/multimeter-test-meter-basics-tutorial.php

Reades, R., Studnek, J. R., Vandeventer, S., & Garrett, J. (2011). Intraosseous versus intravenous vascular access during out-of-hospital cardiac arrest: a randomized controlled trial. *Ann Emerg Med, 58*(6), 509-516. doi:10.1016/j.annemergmed.2011.07.020

Rush, S., Abildskov, J. A., & McFee, R. (1963). Resistivity of body tissues at low frequencies. *Circulation Research, 12*(1), 40-50 %@ 0009-7330.

Schwan, H. P., & Kay, C. F. (1956). Specific resistance of body tissues. *Circulation Research, 4*(6), 664-670 %@ 0009-7330.

Sebbane, M., Claret, P. G., Lefebvre, S., Mercier, G., Rubenovitch, J., Jreige, R., . . . de La Coussaye, J. E. (2013). Predicting peripheral venous access difficulty in the emergency department using body mass index and a clinical evaluation of venous accessibility. *J Emerg Med, 44*(2), 299-305. doi:10.1016/j.jemermed.2012.07.051

Thomas G. Beckwith, R. D. M., John H. Lienhard V. (1993). *Mechanical Measurements*. Reading, MA: Prentice Hall.

Voepel-Lewis, T., Zanotti, J., Dammeyer, J. A., & Merkel, S. (2010). Reliability and validity of the face, legs, activity, cry, consolability behavioral tool in assessing acute pain in critically ill patients. *Am J Crit Care, 19*(1), 55-61; quiz 62. doi:10.4037/ajcc2010624